Emerging approaches to study cell-cell interactions

Poulcharidis, D.

Emerging Approaches
to Study Cell-Cell Interactions

PROEFSCHRIFT

ter verkrijging van
de graad van Doctor aan de Universiteit Leiden,
op gezag van Rector Magnificus prof. mr. C. J. J. M.
Stolker,
volgens het besluit van het College voor Promoties
te verdedigen op woensdag 3 juni 2020
klokke 15:00 uur

door

Δημήτριος Πουλχαρίδης
Dimitrios Poulcharidis
Geboren te Thessaloniki, Griekenland in 1989

Promotiecommissie

Promotor:	Prof.dr. A. Kros
Co-promotor:	Dr S.I. van Kasteren
Overige leden:	Prof.dr. H.S. Overkleeft (Voorzitter)
	Prof.dr. J. Brouwer (Secretaris)
	Prof.dr. J.A. Bouwstra (Universiteit Leiden)
	Dr. D. Claessen (Universiteit Leiden)
	Dr. R. Eelkema (Technische Universiteit Delft)
	Prof.dr. J.J.L.M. Cornelissen (Universiteit Twente)

Cover design: HaisonokViktoriia/Shutterstock.com

Printed by: Ipskamp Printing

Table of Contents

1

Aim and outline of this thesis

The aim of this thesis is to study cell-cell interactions and the development of an assay to explore and quantify the exchange of membrane compounds. In the first part the rate of lipid exchange was studied, during both natural cell-cell contacts and prolonged enforced contacts. In the second part lipidated coiled-coil peptides were used to study the behaviour and potential fusogenic behaviour of these compounds on cell-wall-deficient bacteria.

Chapter 2 provides a comprehensive overview of membrane component exchange in cells, as well as chemical approaches to enhance cell-cell contacts. Examples of mechanisms of intercellular transfer, biological effects of intercellular membrane component transfer and chemical strategies to enhance cell-cell contacts are described, and their strengths and limitations discussed.

Chapter 3 explores a method to quantify the amount of exchange of cholesterol and sialic acid containing compounds between cells using flow cytometry in combination with bioorthogonal and fluorescent labelling techniques. This chapter demonstrates that direct cell–cell contact is the likely mechanism of sterol exchange. Furthermore, it shows that by manipulating the contact time between cells using complementary coiled-coil peptides results in an enhanced exchange rate of membrane components between cells.

Chapter 4 provides future implications for and directions towards quantification and identification of membrane lipid exchange between immune cells. This chapter presents an adaptable strategy based on trogocytosis assays in which fluorescent and clickable lipids were used to determine the membrane component exchange between antigen-presenting cells and T cells in co-culture. A range of sterols and aliphatic acids were screened and their effect on trogocytosis was determined.

Chapter 5 presents evidence – for the first time – of surface modification of living L-form cells (cell-wall-deficient bacteria) as a first step towards L-form fusion, using cell-compatible coiled-coil peptides. These L-form variants were generated from actinomycetes, by inhibiting crucial steps in the biosynthesis pathway of the cell wall. L-form morphology is adaptable and allows cells to surpass environmental difficulties; for example, hyperosmotic stress conditions or treatment with antibiotics. Also, in this chapter L-form surface modification and viability as well as potential membrane fusion is presented using confocal microscopy and flow cytometry assays.

Chapter 6 describes the synthesis of a fluorescent alkyl phospholipid ether analogue as well as preliminary results of the *in vitro* and *in vivo* imaging testing in a zebrafish cancer model. Alkyl phospholipid ether analogues were developed for diagnostic methods due to their accumulation in cancer cells.

2

Chemical approaches to enhance cell-cell contact

2.1 Introduction to membrane component exchange in cells

Multicellular organisms form cell-cell interactions via direct interactions between cell membranes and play a vital role in cellular activity and development. Cells communicate with each other through these interactions and orchestrate the events that coordinate multicellular assembly.[1,2] Examples of cell-cell exchange include transfer via direct cell-cell contact,[3] exosome uptake[4,5] and membrane nanotubular formation.[4,6]

One particular method of cell-to-cell communication is the physical transfer of cell-surface components between adjacent cells, which plays a critical part in cellular communication responses. This was first described in the 1970s, when Bona *et al.* observed the transfer of lipopolysaccharide to lymphocytes from macrophages.[7] Recent examples have shown it to a be far more widespread phenomenon

than initially believed. In the immune system many cell-surface molecules are capable of being transferred between leukocyte subsets (Figure 1). For example, the trogocytosis[8] (from the ancient Greek word *trogo*, meaning 'gnaw') of co-stimulatory molecules of the antigen-presenting cell (APC) surface represents a key mechanism by which regulatory T cells attenuate APC function.[1,9] The trogocytosis process describes the plasma-membrane components transfer from one cell to the other. Furthermore, the same phenomenon between B-cells and lymph node-resident dendritic cells plays an important, yet poorly understood, role in the activation of humoural responses.[10,11] Membrane-component exchange is not exclusive to the immune system, with the exchange of membrane components also observed between endothelial cells and tumour cells as a further example.[12–15]

It has been shown that lipid components play an important role in cell-cell communications.[12,16,17] For example, lipid interactions were shown to be necessary for the intercellular communication between mesothelioma cells for exchanging cellular information and maintaining tumour organisation.[18,19] However, the exact role of (specific) lipids in the above-described trogocytosis events is relatively unknown.[20] In this chapter, membrane-exchange mechanisms will be discussed, as well as the chemical tools that have been developed to better study these processes.

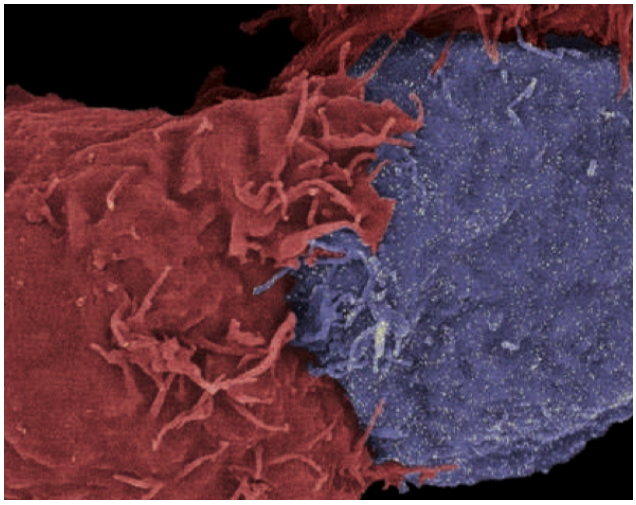

Figure 1 *Scanning electron microscopy (SEM) image shows a natural killer cell (red) grasping a target cell (blue). [Image reproduced from reference: D. M. Davis,* Nat. Rev. Immunol.*, 2009, **9**, 543–555]*

2.2 Mechanisms of intercellular transfer

The molecular mechanisms that control the transfer of membrane components remain unclear. At the cellular level, several mechanisms are thought to be responsible for facilitating the transfer of compounds between cells, such as a transfer via direct cell-cell contact, exosome exchange and nanotube formation (Figure 2).

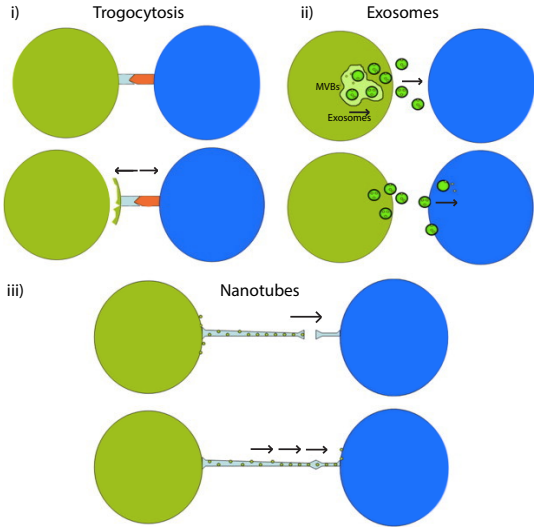

Figure 2 *Intercellular exchange of membrane components via trogocytosis transfer, exosomes and nanotubes. (i) Direct contact between cells allows the intercellular exchange of cell-surface-bound compounds. Different colours show membrane receptors that upon contact are "stealing" membrane pieces. (ii) Secreted exosomes carrying lipids, proteins and their signals can be transferred from one cell to another [where MVBs refers to multi-vesicular bodies]. (iii) Long membrane nanotubes extended between bordering cells support contact-dependent membrane component transfer from one cell to another. [Image reproduced from reference: O. Rechavi, I. Goldstein and Y. Kloog,* FEBS Lett.*, 2009,* ***583****, 1792–1799]*

Most forms of membrane component transfer appear to require cell-to-cell contact, suggested by the evidence that most transfer events are suppressed when cells are physically separated with a semi-permeable trans-well set-up.[21–23] This shows that direct contact facilitates the rapid transfer of cell-surface components (Figure 3).[24] For example, the formation of an integrin-mediated high-affinity synapse between cytotoxic T lymphocytes (CTLs) and a target cell is stabilised by the cytoskeleton.[25–27] Due to direct contact formation, membrane protein transfer between CTL and target was reported.[27]

In the immune system, this process was shown using live cell imaging. Wetzel *et al*. demonstrated that T cells, while immediately detaching from APCs, commonly acquire major histocompatibility complex (MHC) peptide complexes straight from the APC-side of the immunological synapse (IS).[28] B cells too can acquire proteins from T cells following synapse formation,[29] and even some tumour cell lines can take up patches of autologous membranes through synapse-like structures.[30] The transfer is rapid, with exchange occurring within minutes of synapse formation,[26,31] and the transferred molecules, such as lipids and proteins, commonly appear at the cell surface and are fully functional.

A different type of synapse, the 'stromal synapse', has also been reported in the immune system. It has an opposite function, namely to dampen the immune response in tissue.[32] It was observed between interstitial/stromal cells and was shown to establish close contacts. The exact role and importance of this immune dampening synapse are as yet unknown. What is known is that it can be triggered by costimulatory molecules and/or be dependent on the activation state of the donor and the acceptor (recipient) cells.[25,33,34]

Aside from the above-described trogocytic mechanisms, cells can also communicate through gap junctions (GJs). This mechanism – which is the formation of intercellular connections – allows not just the exchange of membrane components but also of cytosolic materials.[35–37] It plays a vital role in tissue maintenance and homeostasis. In the immune system, for example, it is one of the proposed mechanisms by which APCs acquire exogenous antigen.[38–40] However, it can be detrimental too, with this same gap junction-transfer between

melanoma and endothelial cells resulting in the killing of healthy neighbouring cells by autologous cytotoxic T lymphocytes.[41]

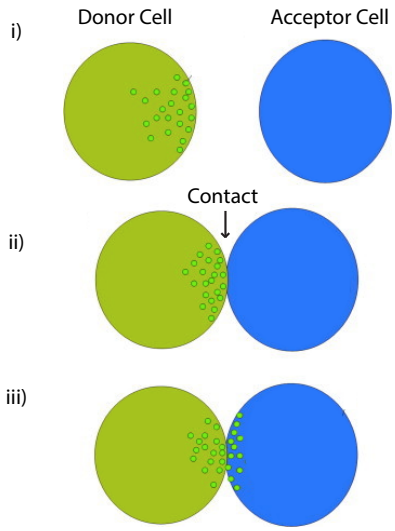

Figure 3 *Intercellular transfer of cell compounds. (i) A donor cell is expressing active compounds. (ii) The donor and the acceptor cell form a contact. (iii) During contact formation, the active membrane component is transferred to the plasma membrane of the acceptor cell from the plasma membrane of the donor cell. [Image reproduced from reference: O. Rechavi, I. Goldstein and Y. Kloog,* FEBS Lett.*, 2009,* ***583****, 1792–1799]*

A third cell-contact dependent method of membrane transfer between immune cells is through transient membrane nanotubular networks. Nanotubes are long, membranous tethers formed between cells either at the termination of the IS as the cells dissociate, or through an extension of membrane from one cell fusing to another,[42] although it is likely that these two processes are not mutually exclusive events. The formation of nanotubes has been detected in a wide variety of cells (Figure 4).[27,34,43] Rustom *et al.* have reported that membrane compounds can transfer directly between cells linked by tunnelling nanotubes.[43] In recent literature, these processes are mostly described interchangeably using the terms 'tunnelling nanotubes' (TNTs) and 'membrane nanotubes'.[34,44] Although the functional role for nanotubes is still under debate, studies have shown that nanotubes between myeloid cells can

mediate intercellular calcium alterations and thus cause phenotypic changes.[45] They can also enable the exchange of cell-surface membrane components as well as cytoplasmic content.[20,46] Studies using time-lapse imaging have shown membrane nanotube formation between B cells (B721.221) and T cells (Jurkat) following prolonged cell-cell contact, resulting in Ras-membrane protein transfer.[47]

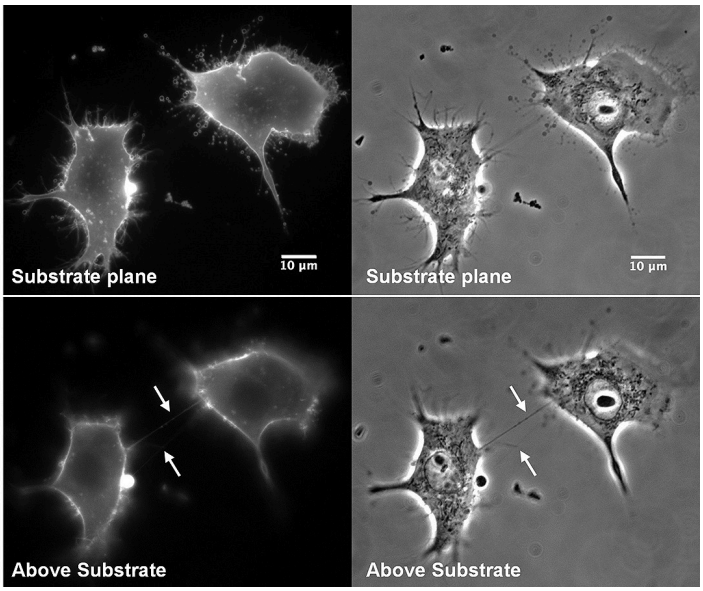

Figure 4 *Images are showing the formation of tunnelling nanotubes (TNT). The membrane of RAW/LR5 cells stained with the membrane dye FM1-43FX. The above images show cell substrates, and the lower images show the cell substrates where TNTs are formed. The arrows indicate the formed TNTs. Scale bars 10 µm. [Image reproduced from reference: K. McCoy-Simandle, S. J. Hanna and D. Cox,* Int. J. Biochem. Cell Biol.*, 2015, **71**, 44–54]*

Scanning electron microscopy (SEM) of cell-to-cell channelling showed that phaeochromocytoma (PC12) cells could form cellular TNTs[43] that provided a direct path for transporting signalling molecules between cells without escape into the extracellular milieu. The TNTs can be very long, even exceeding cellular dimensions, but their diameter is narrow (20 to 200 nm).[34] There are no known

biochemical markers for labelling tunnelling nanotubes. They can, however, be detected using high-resolution light and electron microscopy.[6]

Nanotube formation requires that cells be in close contact for a considerable length of time – if cells dissociate too quickly, nanotube formation does not occur.[48] Live cell imaging has shown that TNTs are ephemeral structures that last from minutes to hours.[49] For example, when immature neurons and astrocytes are co-cultured, after five hours, tunnelling nanotubes are formed, which disappeared after 24 hours.[49] This may reflect the amount of time required to create intercellular contacts of strong avidity which can withstand the forces required to draw out surface membranes as cells dissociate.[44] As a result, this likely eliminates the involvement of nanotubes as a mechanism for the fast transfer of membrane components between cells.

The final type of exchange mechanism that will be discussed does not rely on cell-cell contact. Instead, cells may use the secretion and uptake of exosomes to exchange material. Exosomes are tiny membrane vesicles with a diameter between 50-100 nm and are secreted by a variety of different cells.[4,50] They are formed by inward budding of endosomal membranes or multi-vesicular bodies (MVBs) within the cell and are secreted when the MVB fuses with the outer cellular membrane (Figure 5).[51] Exosome-mediated transfer is a relatively slow process but can occur over substantial distances.

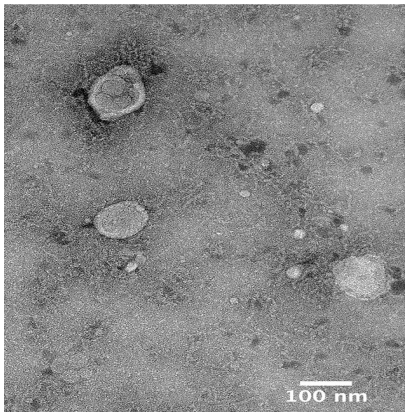

Figure 5 *Exosomes purified from mononuclear phagocytes as depicted by a transmission electron microscopy. Scale bar indicates 100 nm. [Image reproduced from reference: K. McCoy-Simandle, S. J. Hanna and D. Cox,* Int. J. Biochem. Cell Biol.*, 2015,* ***71****, 44–54]*

Exosomes can transfer membranes and encapsulating molecules that can be acquired and reprocessed by the cells that take them up.[52] For example, MHC-II-deficient dendritic cells can acquire MHC class II molecules from dendritic cell-derived exosomes, integrate these molecules into their membranes and subsequently trigger the proliferation of antigen-specific $CD4^+$ T cells *in vitro*.[53] Recently, it was demonstrated that exosomes could be secreted by T cells upon synapse formation with APCs resulting in miRNA transfer.[54]

In summary, it appears that tight junctions or intercellular nanotubes formed between two cells play an essential role in the transfer of membrane compounds, with the strength of the interaction often determining the amount of membrane transferred.[55,56] However, the exact mechanism may vary with the nature of the cells and intercellular exchange process involved.

2.3 Biological effects of intercellular membrane component transfer

The exchange of membrane components can result in biological effects either because the donor cells are stripped of molecules from their membrane or because the acceptor cells get components which they can use. In both ways, cells acquire or lose components which may alter their cell-cell interactions.[1] For instance, the regulatory activity of lymphocytes might be changed when, during cell-cell communication, cellular components are exchanged. Moreover, the exchange of highly energetic components such as lipids has been reported to affect cell proliferation.[57] Kedl *et al.* have shown that dendritic cells acquire antigenic-MHC complexes from T cells through a direct membrane-exchange mechanism affecting the T-cell maturation.[58] Moreover, the antigen-complexes exchange between dendritic cells can also reactivate memory T cells.[59] Finally, another consequence of cell-membrane component exchange has been reported by Qureshi *et al.* is the transfer of costimulatory molecules from T cells to dendritic cells which regulates the T-cell response.[60]

The exchange of lipids can also play an essential role in the development of diseases. For example, the cholesterol-glycolipids and the cholesterol from *Borrelia burgdorferi*, the causative agent of Lyme disease, are vital for bacterial life cycle and can control the interactions between the eukaryotic host's cells and the bacteria itself (Figure 6).[61] Benach *et al.* demonstrated that *B.burgdorferi* stripped off the cholesterol and cholesterol-glycolipids from the membrane of eukaryotic HeLa cells via a contact-dependent mechanism.[61] This was also shown by Norris *et al.* for *Treponema pallidum*, the agent responsible for syphilis. It may directly obtain specific membrane components from host cells, such as lipids.[62] These are important examples of lipid-exchange because neither of these bacteria can

synthesise these fatty acids.[63,64] In both examples, the two-way lipid exchange between pathogens and host cells can occur either through the release of exosomes or by direct contact between the bacteria and eukaryotic cell.

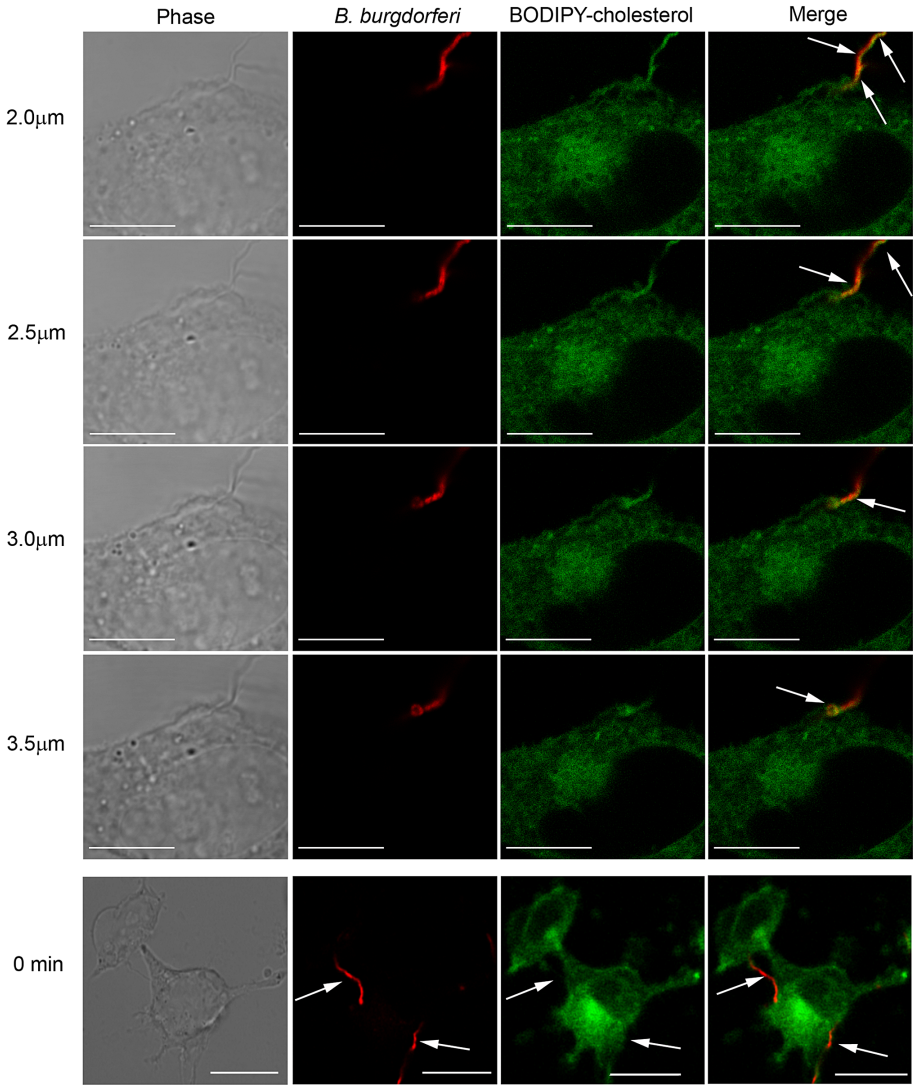

Figure 6 *Borrelia burgdorferi (red) was incubated with bodipy-cholesterol labelled HeLa cells (green). Confocal microscopy showed the co-localization (yellow, arrows) of bodipy-cholesterol (green) and Borrelia burgdorferi (red) at the point of attachment after 1 h of incubation. Scale bars = 10 μm. Confocal microscopy images taken at the beginning of the experiment, 0 mins (bottom), showed no colocalization (yellow) of*

bodipy-cholesterol (green) between labelled HeLa cells and Borrelia burgdorferi (red). The arrows point to the lack of co-localization. Scale bars = 20 µm. [Image reproduced from reference: J. T. Crowley, A. M. Toledo, T. J. LaRocca, J. L. Coleman, E. London and J. L. Benach, PLoS Pathog.*, 2013, **9**, e1003109]*

2.4 Chemical strategies to enhance cell-cell contacts

Due to the importance of cell-cell interaction and exchange in the eukaryotic life cycle, various methods to chemically control cell-to-cell contacts have been developed. These are based on approaches such as genetic engineering, chemical cell modification, metabolic engineering and many others, and will be discussed below.

Genetic modification has been used to alter cell surfaces to affect extracellular communication. For example, Mrksich *et al.* created a new specificity for the binding of the αβ integrin-receptor to the extracellular matrix (Figure 7). They created a chimeric receptor containing β1 integrin, an extracellular domain from fractalkine, and a carbonic anhydrase IV (CAIV) domain at the end (the CAIV protein binds explicitly to benzenesulfonamide (BzS) ligands in order for the whole complex to bind in an extracellular matrix).[65,66] As a result, cells expressing the modified receptor could spread and attach selectively to immobilised substrates.

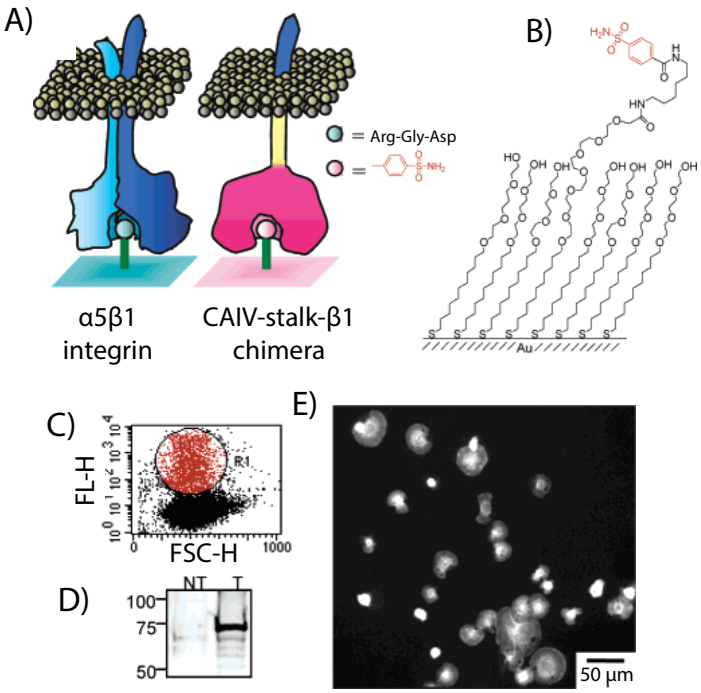

Figure 7 *Schematic illustration of the native and chimeric integrin. (A) The native α5β1 integrin (left) binds the Arg-Gly-Asp ligand. A chimeric receptor (right) was created to keep the transmembrane and intracellular domain of the β1 integrin (blue) and to contain extracellularly an enzymatic domain of carbonic anhydrase IV (CAIV) (pink) which is targeted by a benzenesulfonamide. (B) a modified gold surface presenting benzenesulfonamide. (C) A flow cytometry plot of cells expressing the chimeric receptor (red dots). (D) Western blot analysis with an anti-CAIV antibody. (E) Cells (stained with phalloidin-TexasRed) expressing the chimeric receptor attach on a modified gold surface containing benzenesulfonamide. [Image reproduced from reference: M. Kato and M. Mrksich,* J. Am. Chem. Soc.*, 2004, **126,** 6504-5]*

Chemical handles have also been introduced using a genetic engineering approach. Ting *et al.*, for example, produced cells expressing the epidermal growth factor receptor (EGFR) fused to a biotin ligase recognition sequence.[67,68] This peptide (GLNDIFEAQKIEWHE) – upon addition of a biotin ligase – could be site-specifically biotinylated, which in turn allowed a subsequent cross-linking with ligation to streptavidin.

Covalent conjugation of functional groups on the cell surface has also been used to alter cell-cell contacts. Sulfhydryl, amines, carboxyl and carbonyl groups, and carbohydrate groups have all been used for functionalisation. The chemical reactions on the cell surface should be orthogonal and performed under moderate conditions. There are a well-established and wide variety of protocols for the chemical modification of amine groups under mild conditions and with readily available linkers. For example, a popular reaction to modify primary amines is the reaction with N-hydroxysuccinimide (NHS) ester, which has been used extensively for surface modification with molecules such as PEG[69] and biotin[70,71].

The latter has been used extensively to manipulate cell-cell contacts. The cells are biotinylated with an NHS-biotin conjugate before the addition of streptavidin (Figure 8). The streptavidin serves as a ''bridge'' to connect the cells with a biotinylated ligand, thereby altering the behaviour of the cell. In this manner, cell surfaces have been functionalised with antibodies recognising epithelial growth factor receptor (EGFR)[72,73], as well as P-selectin-binding aptamers.[74,75] These surface-modified cells were then able to interact with EGFR-expressing HEK293T and HeLa cells, [72] and selectin-expressing cells *in vitro*[74], and *in vivo*[75,76]. Streptavidin has also been used to cluster and layer cells in specific orientations.[77–79]

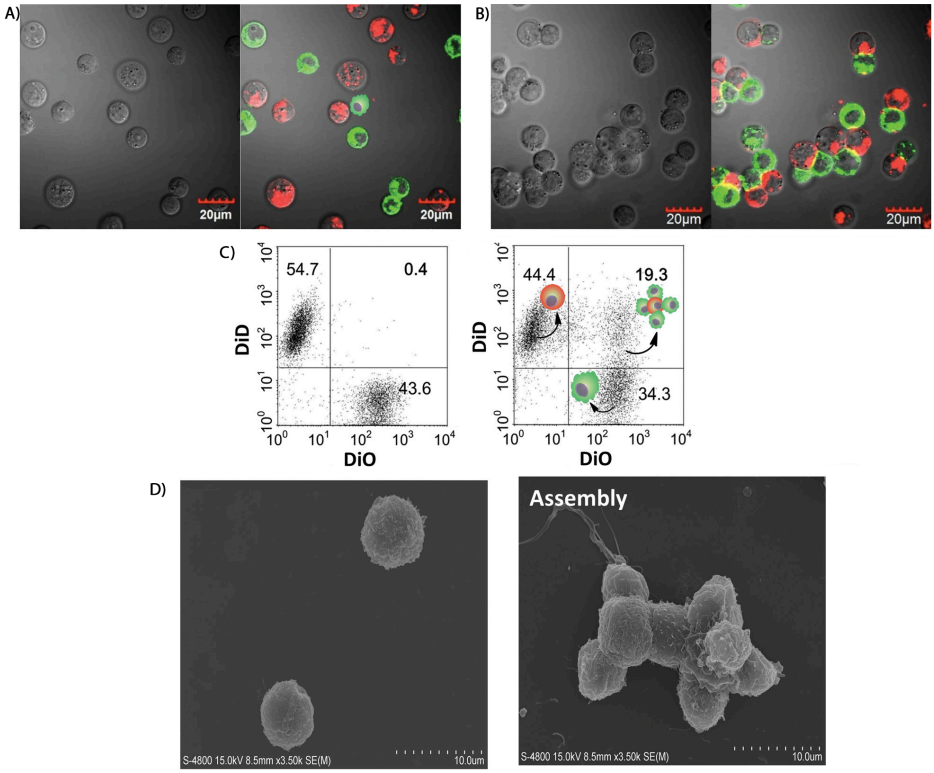

Figure 8 *Examples of surface modification using NK-streptavidin with Jurkat-biotin. Confocal laser scanning microscopy (CLSM) images of non-assembled cells (A), and of (B) assembled cells after surface modification and mixing Jurkat-biotin cells with NK-streptavidin at a 1:1 ratio. (C) Flow cytometry scatters. NK cells were labelled with DiO fluorescent dye, and Jurkat cells were labelled with DiD dye before and after modification and assembly. (D) SEM images of Jurkat-biotin cells and a multicellular cluster (mixed at a 1:1 ratio). [Image reproduced from reference: B. Wang, J. Song, H. Yuan, C. Nie, F. Lv, L. Liu and S. Wang,* Adv. Mater., *2014,* ***26****, 2371–2375]*

Although these chemical approaches are encouraging, it is still challenging to govern cell-cell interactions in time and space. To overcome these concerns, there are opportunities for enhancement by designing novel protein engineering, bioconjugation, material science and chemistry approaches for cell-surface engineering.[80–82]

One set of approaches relies on the fusion of liposomes with cells.[83–85] In order to present functional groups on the cell surface, specific liposomes containing new functional groups are incubated with cells, leading to fusion of the liposomal membrane and the cell membrane. This methodology was used, for example, to fuse biotinylated liposomes with the membrane of mesenchymal stem cells (MSC) to yield biotinylated MSCs.[76] Yousaf *et al.* used the approach to introduce a selectively ligatable handle into the cell: liposomes consisting of either O-dodecyloxyamine or dodecanone were fused with cell membranes to yield membranes carrying oxyamine or ketone functionalities, which could be ligated through oxime formation (Figure 9).[84,86]

Carbohydrates have also been used to modify the cell surface with selectively ligatable functionalities in a liposome system. Chen *et al.* used liposomes loaded with modified sugars, which are metabolically incorporated into cell-surface glycans that would allow specific modification of the surface glycans.[65,87–89]

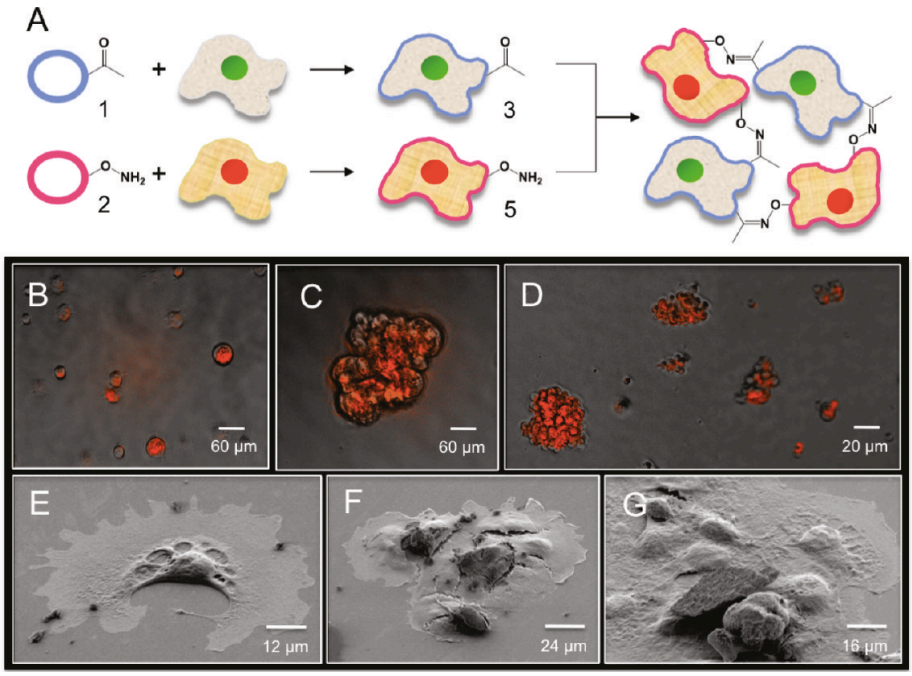

Figure 9 *Scanning electron micrographs and fluorescent images depicting the formation via liposome fusion of 3D populations. (A) Fibroblast populations were cultured separately either with ketone- (1) or oxyamine- (2) containing liposomes, resulting in membrane fusion and creation of ketone- (3) and oxyamine- (5) tethered fibroblasts. The nucleus of the oxyamine-tethered fibroblasts (5) was labelled with m-cherry, whereas the ketone-tethered fibroblasts (3) were unlabelled. After mixing these cell populations for 3 h, clusters and tissue-like forms occurred, due to oxime ligation. (B) Control experiments show the absence of cluster creation for cells which did not contain either oxyamine or ketone handles. (C and D) Images from co-cultured ketone- (3) and oxyamine- (5) tethered fibroblasts showing the formation of interconnected spheroid assemblies. (E-G) SEM images are displayed by control cells (E) and spheroid assemblies (F and G). [Image reproduced from reference: D. Dutta, A. Pulsipher, W. Luo and M. N. Yousaf,* J. Am. Chem. Soc., *2011,* ***133****, 8704–8713]*

A standard method for cell-surface modification is the treatment of cells with labelled metabolites, which are incorporated into the membrane. For example, Iwata *et al.* incubated cells with membrane lipids linked to DNA strand.[90] Introduction of a complementary strand on a second cell population created a forced interaction between the two cell types. Similarly, Gartner *et al.* manipulated the adhesive characteristics of cells using membranes modified with ssDNA oligonucleotides (Figure 10).[91] Bertozzi *et al.* also used this approach to

present synthetic glycolpolymers that mimic cell-surface glycoproteins. These are responsible for controlling cell-cell interactions.[92] The cell-assembly kinetics were controlled by adjusting the complexity of DNA sequences and enabled the formation of 3D microtissues with determined cell composition and ratio.

The glycans present on the surface of many cell types have also been used for introducing chemical functionality at the surface of cells. Bertozzi *et al.* described a method whereby they incubated cells with labelled precursors of sialic acids. These precursors containing either a ketone or azide functionality were taken by cells and incorporated to the cell surface glycome in order to get labelled.[93] This method was used by Francis *et al.* to introduce the ssDNA strands.[94,95] A modified oligonucleotide sequence (i.e. ssDNA) was first synthesised bearing a phosphine group. Via a Staudinger ligation the phosphine-ssDNA conjugation was then obtained with the azide to form the amide-link for further modification.[96]

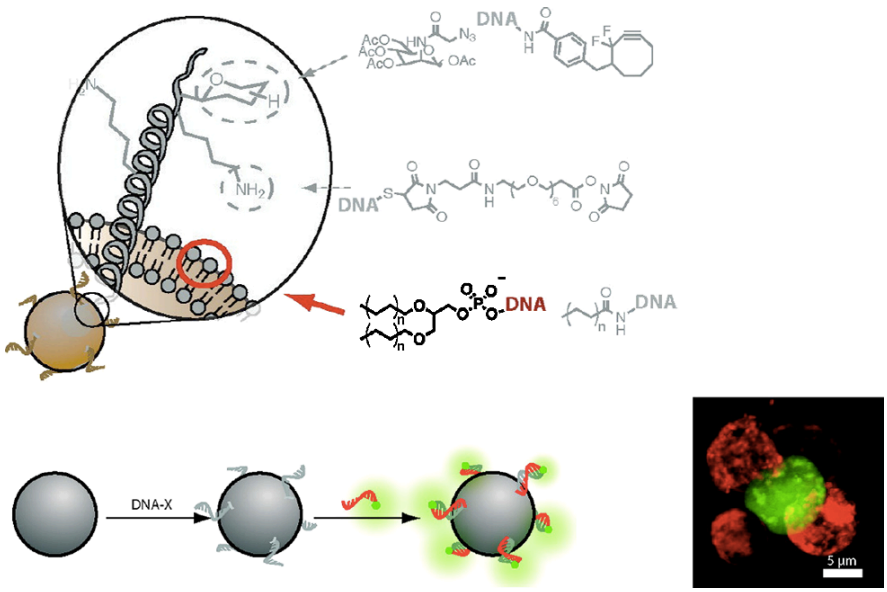

Figure 10 *Cell-surface glycans or protein lysine side chains or fatty acid amides are targeted for chemical remodelling and incorporation of oligonucleotides to cell surfaces. [Image reproduced from reference: N. S. Selden, M. E. Todhunter, N. Y. Jee, J. S. Liu, K. E. Broaders and Z. J. Gartner,* J. Am. Chem. Soc.*, 2012, **134**, 765–768]*

Sugimoto *et al.* reported a different approach: by incubating cells with methacryloyl-modified N-acetylmannosamine (ManM), they could introduce methacryloyl groups in surface sialic acid of macrophages.[97] Via a light-assisted thiolene reaction, the ManM groups were coupled with a thiol-terminated nucleic acid aptamer, targeting protein tyrosine kinase-7 (PTK7). Upon co-culture of the cells with a PTK7-positive lymphoblastic leukaemia cell line (CCRF-CEM; Figure 11), cell adhesion was observed, and the cancer cell population was reduced.[97]

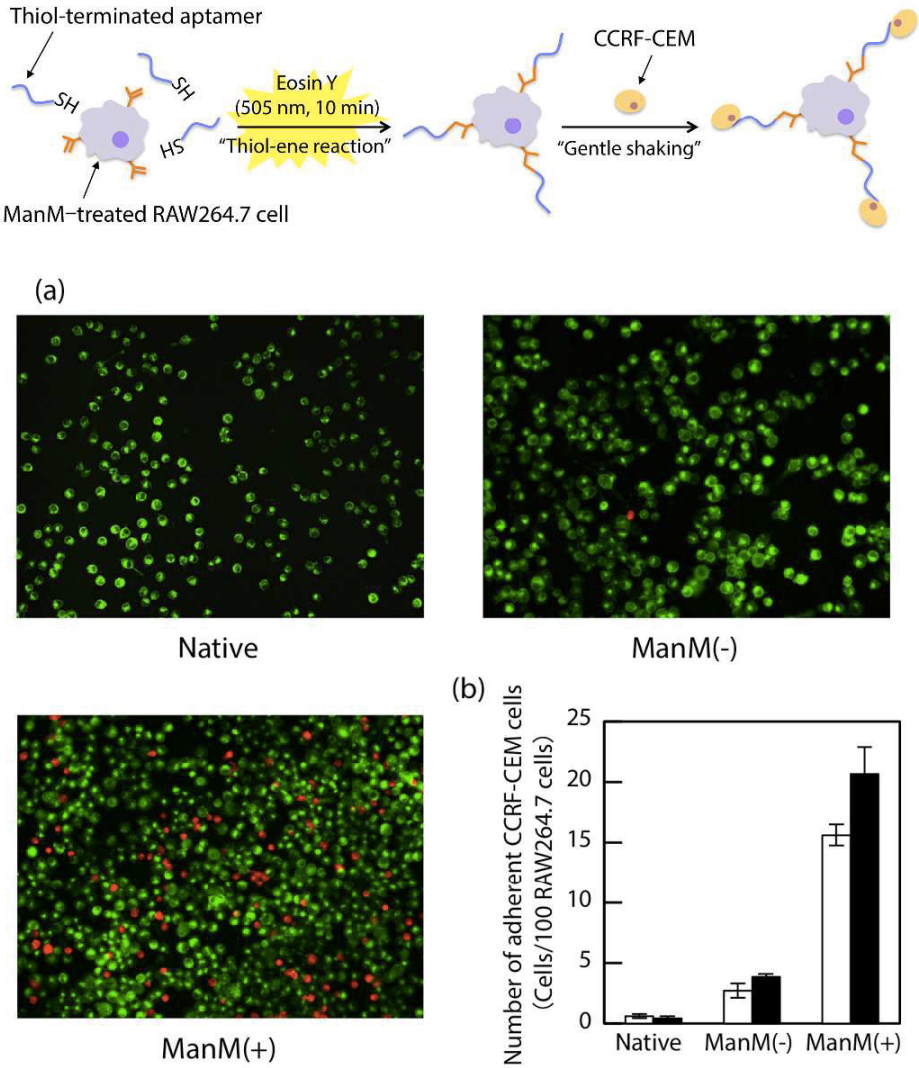

Figure 11 *The surface of RAW264.7 macrophages was modified with a nucleic acid aptamer and bound with a CCRF-CEM cancer cell. (a) Fluorescence images of co-cultured human CCRF-CEM leukaemia lymphoblasts (red) is adjacent to murine RAW264.7 macrophages (green). (b) Number of adherent T lymphoblasts on 100 macrophages. [Image reproduced from reference: S. Sugimoto, R. Moriyama, T. Mori and Y. Iwasaki,* Chem. Commun.*, 2015,* ***51****, 17428–17430]*

Supramolecular host-guest chemistry methodology has garnered widespread attention as a tool for controlling molecular recognition.[98] The aim is to create cell-cell contacts through the introduction of supramolecular interactions using host-guest motifs. Ideally, the guest molecules have a high affinity and selectivity for their host molecules and the pair make non-covalent, stable and inherent reversible supramolecular complexes in biological systems.[99] One such pair is based on phospholipidylated or cholesteryl-modified cyclodextrin. These guests could insert into phospholipid membranes and maintain the ability of the cyclodextrin group to receive guest molecules.[100-104] Alternatively, Peng Shi *et al.* modified the membrane of MCF-7 (human breast) cancer cells with β-cyclodextrin using a bioorthogonal labelling approach. Cell-cell interactions were then switched on by the addition of a divalent guest molecule that could bridge two different host molecules (Figure 12), or a cell decorated with guest molecules.[103,104] In the example mentioned above, the β-cyclodextrin decorated MCF-7 cells were co-cultured with azobenzene-decorated peripheral blood mononuclear cells (PMBCs), which resulted in the adherence of the PMBCs to the MCF-7 cells.

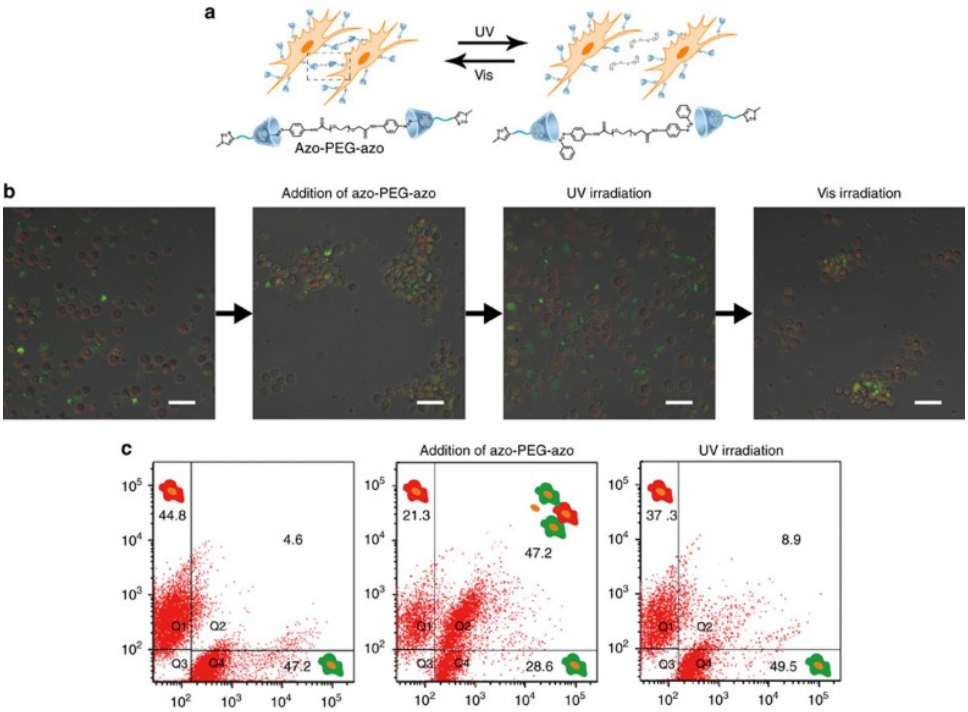

Figure 12 *(a) Schematic representation showing reversible cell-cell contacts. (b) Confocal microscopy images and (c) flow cytometry analysis of β-CD-modified cells under different conditions. Scale bars, 50 μm. [Image reproduced from reference: P. Shi, E. Ju, Z. Yan, N. Gao, J. Wang, J. Hou, Y. Zhang, J. Ren and X. Qu,* Nat. Commun.*, 2016, 7, 13088]*

Coiled-coil motifs are comprised of interacting α-helical peptides. On a subcellular level, this is one of the most common connecting motifs in nature.[105–107] These α-helices are stabilised by hydrogen bonds along the polypeptide chain due to a patterned arrangement of charged and hydrophobic residues. In nature, coiled-coil peptides present in around 10% of the eukaryotic proteome[108] and control a variety of cellular behaviours, such as transcription,[109] protein complexes assembling,[106] intracellular trafficking[110] and viral infection[111,112]. Coiled-coil motifs therefore offered a potent possible target for mediating intercellular interactions. Kros *et al.* have reported the

incorporation of lipid-modified coiled-coil forming peptides K and E (Figure 13) into eukaryotic membranes *in vitro*, but also in living zebrafish larvae.[83,113,114]

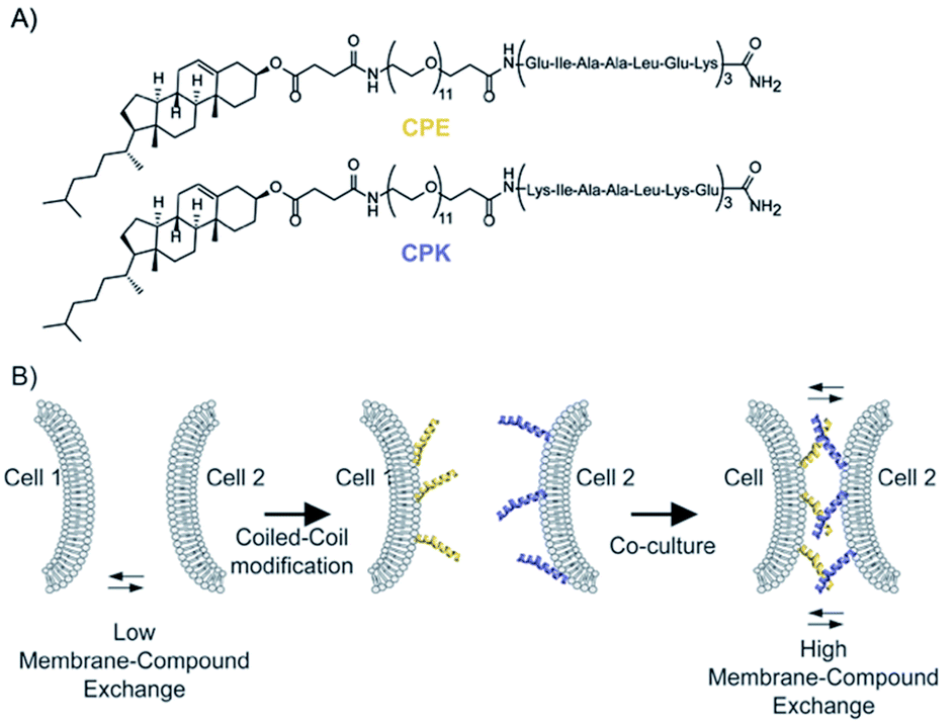

Figure 13 *(A) Structures of cholesterol-modified E_3 (CPE) and K_3 (CPK) peptides. (B) Schematic representation of coiled-coil formation and its use to prolong cell-cell contact, thus enhancing membrane component exchange.*

2.5 Conclusions

Components from the cell membrane can relocate between cells both *in vivo* and *in vitro*. This exchange of molecules plays an essential role in the regulation of cellular interactions and responses to its environment. However, the exact mechanism and functional outcome of these exchanges still remains to be elucidated in many cases.

Chemical approaches to control such cell-cell interactions have been developed, which will aid in the understanding of the role of these contact and exchange mechanisms between cells. However, in the area of cell surface engineering, many challenges remain, such as the development of mild, cell-compatible reactions and interactors. The extremely dynamic nature of the cellular membrane also complicates factors. Nonetheless, cell membrane engineering appears to be the most robust methodology to manipulate cell properties and is associated with developing beneficial present and future cell-based processes.

2.6 References

1 M. Dhainaut and M. Moser, *Front. Immunol.*, 2014, **5**, 1–4.

2 P. H. Raven and G. B. Johnson, in *Biology, 6th Edition*, 2002.

3 S. Strassburg, N. W. Hodson, P. I. Hill, S. M. Richardson and J. A. Hoyland, *PLoS One*, 2012, **7**, e33739.

4 K. A. Ahmed and J. Xiang, *J. Cell. Mol. Med.*, 2011, **15**, 1458–1473.

5 C. Théry, M. Ostrowski and E. Segura, *Nat. Rev. Immunol.*, 2009, **9**, 581–593.

6 E. Y. Plotnikov, T. G. Khryapenkova, A. K. Vasileva, M. V. Marey, S. I. Galkina, N. K. Isaev, E. V. Sheval, V. Y. Polyakov, G. T. Sukhikh and D. B. Zorov, *J. Cell. Mol. Med.*, 2008, **12**, 1622–1631.

7 C. Bona, R. Robineaux, A. Anteunis, C. Heuclin and A. Astesano, *Immunology*, 1973, **24**, 831–840.

8 E. Joly and D. Hudrisier, *Nat. Immunol.*, 2003, **4**, 815–815.

9 J. Riond, J. Elhmouzi, D. Hudrisier and J. E. Gairin, *Scand. J. Immunol.*, 2007, **66**, 441–450.

10 R. S. Allan, J. Waithman, S. Bedoui, C. M. Jones, J. A. Villadangos, Y. Zhan, A. M. Lew, K. Shortman, W. R. Heath and F. R. Carbone, *Immunity*, 2006, **25**, 153–162.

11 K. R. Wilson, H. Liu, G. Healey, V. Vuong, S. Ishido, M. J. Herold, J. A. Villadangos and J. D. Mintern, *PLoS One*, 2018, **13**, e0200540.

12 S. Rafii and D. Lyden, *Science*, 2008, **319**, 163–164.

13 D. Poulcharidis, K. Belfor, A. Kros and S. I. van Kasteren, *Chem. Sci.*, 2017, **52**, 12081–12085.

14 B. M. Lopes-Bastos, W. G. Jiang and J. Cai, *Anticancer Res.*, 2016, **36**, 1119–1126.

15 K. Hida, N. Maishi, D. A. Annan and Y. Hida, *Int. J. Mol. Sci.*, 2018, **19**.

16 D. Hudrisier and P. Bongrand, *FASEB J.*, 2002, **16**, 477–486.

17 A. Rafii, P. Mirshahi, M. Poupot, A.-M. Faussat, A. Simon, E. Ducros, E. Mery, B. Couderc, R. Lis, J. Capdet, J. Bergalet, D. Querleu, F. Dagonnet, J.-J. Fournié, J.-P. Marie, E. Pujade-Lauraine, G. Favre, J. Soria and M. Mirshahi, *PLoS One*, 2008, **3**, e3894.

18 Q.-J. Zhang, X.-L. Li, D. Wang, X.-C. Huang, J. M. Mathis, W.-M. Duan, D. Knight, R. Shi, J. Glass, D.-Q. Zhang, L. Eisenbach and W. A. Jefferies, *PLoS One*, 2008, **3**, e3097.

19 J. W. Ady, S. Desir, V. Thayanithy, R. I. Vogel, A. L. Moreira, R. J. Downey, Y. Fong, K. Manova-Todorova, M. A. S. Moore and E. Lou, *Front. Physiol.*, 2014, **5**, 1–16.

20 S. Gurke, J. F. V. Barroso and H.-H. Gerdes, *Histochem. Cell Biol.*, 2008, **129**, 539–550.

21 O. Rechavi, Y. Erlich, H. Amram, L. Flomenblit, F. V. Karginov, I. Goldstein, G. J. Hannon and Y. Kloog, *Genes Dev.*, 2009, **23**, 1971–1979.

22 M. B. Herrera, B. Bussolati, S. Bruno, V. Fonsato, G. M. Romanazzi and G. Camussi, *Int. J. Mol. Med.*, 2004, **14**, 1035–1041.

23 D. S. Game, N. J. Rogers and R. I. Lechler, *Am. J. Transplant.*, 2005, **5**, 1614–1625.

24 D. M. Davis, *Nat. Rev. Immunol.*, 2007, **7**, 238–243.

25 J. Sprent, *Sci. Signal.*, 2005, **2005**, 1–4.

26 J. F. Huang, Y. Yang, H. Sepulveda, W. Shi, I. Hwang, P. A. Peterson, M. R. Jackson, J. Sprent and Z. Cai, *Science*, 1999, **286**, 952–954.

27 J. C. Stinchcombe, G. Bossi, S. Booth and G. M. Griffiths, *Immunity*, 2001, **15**, 751–761.

28 S. A. Wetzel, T. W. McKeithan and D. C. Parker, *J. Immunol.*, 2005, **174**, 80–89.

29 F. D. Batista, D. Iber and M. S. Neuberger, *Nature*, 2001, **411**, 489–494.

30 M. Poupot and J.-J. Fournié, *J. Immunol.*, 2003, **171**, 2517–2523.

31 J. Tabiasco, E. Espinosa, D. Hudrisier, E. Joly, J.-J. Fournié and A. Vercellone, *Eur. J. Immunol.*, 2002, **32**, 1502–1508.

32 L. M. Popescu, M. Gherghiceanu, D. Cretoiu and E. Radu, *J. Cell. Mol. Med.*, **9**, 714–730.

33 G. Turturici, R. Tinnirello, G. Sconzo and F. Geraci, *Am. J. Physiol. Cell Physiol.*, 2014, **306**, 621–633.

34 B. Onfelt, S. Nedvetzki, R. K. P. Benninger, M. A. Purbhoo, S. Sowinski, A. N. Hume, M. C. Seabra, M. A. A. Neil, P. M. W. French and D. M. Davis, *J. Immunol.*, 2006, **177**, 8476–8483.

35 M. E. el-Sabban and B. U. Pauli, *Invasion Metastasis*, **14**, 164–176.

36 A. Ito, F. Katoh, T. R. Kataoka, M. Okada, N. Tsubota, H. Asada, K. Yoshikawa, S. Maeda, Y. Kitamura, H. Yamasaki and H. Nojima, *J. Clin. Invest.*, 2000, **105**, 1189–1197.

37 M. Saito-Katsuragi, H. Asada, H. Niizeki, F. Katoh, M. Masuzawa, M. Tsutsumi, H. Kuniyasu, A. Ito, H. Nojima and S. Miyagawa, *Cancer*, 2007, **110**, 1162–1172.

38 J. Neijssen, C. Herberts, J. W. Drijfhout, E. Reits, L. Janssen and J. Neefjes, *Nature*, 2005, **434**, 83–88.

39 B. Pang, J. Neijssen, X. Qiao, L. Janssen, H. Janssen, C. Lippuner and J. Neefjes, *J. Immunol.*, 2009, **183**, 1083–1090.

40 J. Neijssen, B. Pang and J. Neefjes, *Prog. Biophys. Mol. Biol.*, 2007, **94**, 207–218.

41 H. Benlalam, A. Jalil, M. Hasmim, B. Pang, R. Tamouza, M. Mitterrand, Y. Godet, N. Lamerant, C. Robert, M.-F. Avril, J. Neefjes, T. Tursz, F. Mami-Chouaib, C. Kieda and S. Chouaib, *J. Immunol.*, 2009, **182**, 2654–2664.

42 B. Onfelt, S. Nedvetzki, K. Yanagi and D. M. Davis, *J. Immunol.*, 2004, **173**, 1511–1513.

43 A. Rustom, R. Saffrich, I. Markovic, P. Walther and H.-H. Gerdes, *Science (80-.).*, 2004, **303**, 1007–1010.

44 D. M. Davis and S. Sowinski, *Nat. Rev. Mol. Cell Biol.*, 2008, **9**, 431–436.

45 S. C. Watkins and R. D. Salter, *Immunity*, 2005, **23**, 309–318.

46 H.-H. Gerdes and R. N. Carvalho, *Curr. Opin. Cell Biol.*, 2008, **20**, 470–475.

47 N. Rainy, D. Chetrit, V. Rouger, H. Vernitsky, O. Rechavi, D. Marguet, I. Goldstein, M. Ehrlich and Y. Kloog, *Cell Death Dis.*, 2013, **4**, 1–9.

48 S. Sowinski, C. Jolly, O. Berninghausen, M. A. Purbhoo, A. Chauveau, K. Köhler, S. Oddos, P. Eissmann, F. M. Brodsky, C. Hopkins, B. Önfelt, Q. Sattentau and D. M. Davis, *Nat. Cell Biol.*, 2008, **10**, 211–219.

49 H.-H. Gerdes, A. Rustom and X. Wang, *Mech. Dev.*, 2013, **130**, 381–387.

50 K. A. Ahmed, M. A. Munegowda, Y. Xie and J. Xiang, *Cell. Mol. Immunol.*, 2008, **5**, 261–269.

51 G. van Niel, I. Porto-Carreiro, S. Simoes and G. Raposo, *J. Biochem.*, 2006, **140**, 13–21.

52 A. E. Morelli, A. T. Larregina, W. J. Shufesky, M. L. G. Sullivan, D. B. Stolz, G. D. Papworth, A. F. Zahorchak, A. J. Logar, Z. Wang, S. C. Watkins, L. D. Falo and A. W. Thomson, *Blood*, 2004, **104**, 3257–3266.

53 C. Théry, L. Zitvogel and S. Amigorena, *Nat. Rev. Immunol.*, 2002, **2**, 569–579.

54 M. Mittelbrunn, C. Gutiérrez-Vázquez, C. Villarroya-Beltri, S. González, F. Sánchez-Cabo, M. Á. González, A. Bernad and F. Sánchez-Madrid, *Nat. Commun.*, 2011, **2**, 1–10.

55 I. Hwang, J. F. Huang, H. Kishimoto, A. Brunmark, P. A. Peterson, M. R. Jackson, C. D. Surh, Z. Cai and J. Sprent, *J. Exp. Med.*, 2000, **191**, 1137–48.

56 H. Sabzevari, J. Kantor, A. Jaigirdar, Y. Tagaya, M. Naramura, J. Hodge, J. Bernon and J. Schlom, *J. Immunol.*, 2001, **166**, 2505–2513.

57 H. Watson, *Essays Biochem.*, 2015, **59**, 43–69.

58 R. M. Kedl, B. C. Schaefer, J. W. Kappler and P. Marrack, *Nat. Immunol.*, 2002, **3**, 27–32.

59 L. M. Wakim and M. J. Bevan, *Nature*, 2011, **471**, 629–632.

60 O. S. Qureshi, Y. Zheng, K. Nakamura, K. Attridge, C. Manzotti, E. M. Schmidt, J. Baker, L. E. Jeffery, S. Kaur, Z. Briggs, T. Z. Hou, C. E. Futter, G. Anderson, L. S. K. Walker and D. M. Sansom, *Science*, 2011, **332**, 600–603.

61 J. T. Crowley, A. M. Toledo, T. J. LaRocca, J. L. Coleman, E. London and J. L. Benach, *PLoS Pathog.*, 2013, **9**, e1003109.

62 D. G. Edmondson, B. Hu and S. J. Norris, *MBio*, 2018, **9**, e01153-18.

63 C. M. Fraser, S. J. Norris, G. M. Weinstock, O. White, G. G. Sutton, R. Dodson, M. Gwinn, E. K. Hickey, R. Clayton, K. A. Ketchum, E. Sodergren, J. M. Hardham, M. P. McLeod, S. Salzberg, J. Peterson, H. Khalak, D. Richardson, J. K. Howell, M. Chidambaram, T. Utterback, L. McDonald, P. Artiach, C. Bowman, M. D. Cotton, C. Fujii, S. Garland, B. Hatch, K. Horst, K. Roberts, M. Sandusky, J. Weidman, H. O. Smith

and J. C. Venter, *Science*, 1998, **281**, 375–388.

64 C. M. Fraser, S. Casjens, W. M. Huang, G. G. Sutton, R. Clayton, R. Lathigra, O. White, K. A. Ketchum, R. Dodson, E. K. Hickey, M. Gwinn, B. Dougherty, J.-F. Tomb, R. D. Fleischmann, D. Richardson, J. Peterson, A. R. Kerlavage, J. Quackenbush, S. Salzberg, M. Hanson, R. van Vugt, N. Palmer, M. D. Adams, J. Gocayne, J. Weidman, T. Utterback, L. Watthey, L. McDonald, P. Artiach, C. Bowman, S. Garland, C. Fujii, M. D. Cotton, K. Horst, K. Roberts, B. Hatch, H. O. Smith and J. C. Venter, *Nature*, 1997, **390**, 580–586.

65 G. Zhu, S. Zhang, E. Song, J. Zheng, R. Hu, X. Fang and W. Tan, *Angew. Chem. Int. Ed. Engl.*, 2013, **52**, 5490–5496.

66 M. Kato and M. Mrksich, *J. Am. Chem. Soc.*, 2004, **126**, 6504–6505.

67 I. Chen, M. Howarth, W. Lin and A. Y. Ting, *Nat. Methods*, 2005, **2**, 99–104.

68 M. Howarth, K. Takao, Y. Hayashi and A. Y. Ting, *Proc. Natl. Acad. Sci.*, 2005, **102**, 7583–7588.

69 D. Y. Lee, S. J. Park, J. H. Nam and Y. Byun, *Tissue Eng.*, 2006, **12**, 615–623.

70 D. Sarkar, J. A. Spencer, J. A. Phillips, W. Zhao, S. Schafer, D P. Spelke, L. J. Mortensen, J. P. Ruiz, P. K. Vemula, R. Sridharan, S. Kumar, R. Karnik, C. P. Lin and J. M. Karp, *Blood*, 2011, **118**, 184–191.

71 B. Wang, J. Song, H. Yuan, C. Nie, F. Lv, L. Liu and S. Wang, *Adv. Mater.*, 2014, **26**, 2371–2375.

72 A. Y. Koyfman, G. B. Braun and N. O. Reich, *J. Am. Chem. Soc.*, 2009, **131**, 14237–14239.

73 K. A. Afonin, M. Viard, A. Y. Koyfman, A. N. Martins, W. K.

Kasprzak, M. Panigaj, R. Desai, A. Santhanam, W. W. Grabow, L. Jaeger, E. Heldman, J. Reiser, W. Chiu, E. O. Freed and B. A. Shapiro, *Nano Lett.*, 2014, **14**, 5662–5671.

74 M. Avadisian, S. Fletcher, B. Liu, W. Zhao, P. Yue, D. Badali, W. Xu, A. D. Schimmer, J. Turkson, C. C. Gradinaru and P. T. Gunning, *Angew. Chemie - Int. Ed.*, 2011, **50**, 6248–6253.

75 W. Zhao, S. Schafer, J. Choi, Y. J. Yamanaka, M. L. Lombardi, S. Bose, A. L. Carlson, J. A. Phillips, W. Teo, I. A. Droujinine, C. H. Cui, R. K. Jain, J. Lammerding, J. C. Love, C. P. Lin, D. Sarkar, R. Karnik and J. M. Karp, *Nat. Nanotechnol.*, 2011, **6**, 524–531.

76 D. Sarkar, P. K. Vemula, W. Zhao, A. Gupta, R. Karnik and J. M. Karp, *Biomaterials*, 2010, **31**, 5266–5274.

77 P. Gong, W. Zheng, Z. Huang, W. Zhang, D. Xiao and X. Jiang, *Adv. Funct. Mater.*, 2013, **23**, 42–46.

78 F. Wu, S. Chen, B. Chen, M. Wang, L. Min, J. Alvarenga, J. Ju, A. Khademhosseini, Y. Yao, Y. S. Zhang, J. Aizenberg and X. Hou, *Small*, 2018, **14**, 1–7.

79 V. A. Bolaños Quiñones, H. Zhu, A. A. Solovev, Y. Mei and D. H. Gracias, *Adv. Biosyst.*, 2018, **2**, 1–18.

80 M. T. Stephan and D. J. Irvine, *Nano Today*, 2011, **6**, 309–325.

81 M. T. Stephan, J. J. Moon, S. H. Um, A. Bershteyn and D. J. Irvine, *Nat. Med.*, 2010, **16**, 1035–1041.

82 H. Liu, B. Kwong and D. J. Irvine, *Angew. Chemie - Int. Ed.*, 2011, **50**, 7052–7055.

83 J. Yang, A. Bahreman, G. Daudey, J. Bussmann, R. C. L. Olsthoorn and A. Kros, *ACS Cent. Sci.*, 2016, **2**, 621–630.

84 D. Dutta, A. Pulsipher, W. Luo, H. Mak and M. N. Yousaf, *Bioconjug. Chem.*, 2011, **22**, 2423–2433.

85 N. Crone, D. Minnee, A. Kros, A. Boyle, N. S. A. Crone,

D. Minnee, A. Kros and A. L. Boyle, *Int. J. Mol. Sci.*, 2018, **19**, 2–14.

86 D. Dutta, A. Pulsipher, W. Luo and M. N. Yousaf, *J. Am. Chem. Soc.*, 2011, **133**, 8704–8713.

87 R. Xie, S. Hong, L. Feng, J. Rong and X. Chen, *J. Am. Chem. Soc.*, 2012, **134**, 9914–9917.

88 Y. Chen, L. Ding and H. Ju, *Acc. Chem. Res.*, 2018, **51**, 890–899.

89 Y. Sun, S. Hong, R. Xie, R. Huang, R. Lei, B. Cheng, D. Sun, Y. Du, C. M. Nycholat, J. C. Paulson and X. Chen, *J. Am. Chem. Soc.*, 2018, **140**, 3592–3602.

90 Y. Teramura, H. Chen, T. Kawamoto and H. Iwata, *Biomaterials*, 2010, **31**, 2229–2235.

91 N. S. Selden, M. E. Todhunter, N. Y. Jee, J. S. Liu, K. E. Broaders and Z. J. Gartner, *J. Am. Chem. Soc.*, 2012, **134**, 765–768.

92 D. Rabuka, M. B. Forstner, J. T. Groves and C. R. Bertozzi, *J. Am. Chem. Soc.*, 2008, **130**, 5947–5953.

93 Z. J. Gartner and C. R. Bertozzi, *Proc. Natl. Acad. Sci. U. S. A.*, 2009, **106**, 4606–4610.

94 R. A. Chandra, E. S. Douglas, R. A. Mathies, C. R. Bertozzi and M. B. Francis, *Angew. Chem. Int. Ed. Engl.*, 2006, **45**, 896–901.

95 W. Li, Z. Yan, J. Ren and X. Qu, *Chem. Soc. Rev.*, 2018, **47**, 8639–8684.

96 E. Saxon and C. R. Bertozzi, *Science*, 2000, **287**, 2007–2010.

97 S. Sugimoto, R. Moriyama, T. Mori and Y. Iwasaki, *Chem. Commun.*, 2015, **51**, 17428–17430.

98 X. Ma and Y. Zhao, *Chem. Rev.*, 2015, **115**, 7794–7839.

99 C. Kim, S. S. Agasti, Z. Zhu, L. Isaacs and V. M. Rotello, *Nat. Chem.*, 2010, **2**, 962–966.

100 R. Auzély-Velty, B. Perly, O. Taché, T. Zemb, P. Jéhan, P.

Guenot, J.-P. Dalbiez and F. Djedaïni-Pilard, *Carbohydr. Res.*, 1999, **318**, 82–90.

101 S. Moutard, B. Perly, P. Godé, G. Demailly and F. Djedaïni-Pilard, *J. Incl. Phenom. Macrocycl. Chem.*, 2002, **44**, 317–322.

102 M. K. Grachev, S. V. Sipin, L. O. Kononov and E. E. Nifant'ev, *Russ. Chem. Bull.*, 2009, **58**, 223–229.

103 P. Shi, E. Ju, J. Wang, Z. Yan, J. Ren and X. Qu, *Mater. Today*, 2017, **20**, 16–21.

104 P. Shi, E. Ju, Z. Yan, N. Gao, J. Wang, J. Hou, Y. Zhang, J. Ren and X. Qu, *Nat. Commun.*, 2016, **7**, 13088.

105 F. H. C. Crick, *Acta Crystallogr.*, 1953, **6**, 689–697.

106 A. Rose and I. Meier, *Cell. Mol. Life Sci.*, 2004, **61**, 1996–2009.

107 A. N. Lupas and M. Gruber, in *Advances in Protein Chemistry*, 2005, **70**, 37–38.

108 J. Liu and B. Rost, *Protein Sci.*, 2001, **10**, 1970–1979.

109 E. K. O'Shea, J. D. Klemm, P. S. Kim and T. Alber, *Science*, 1991, **254**, 539–544.

110 A. K. Gillingham and S. Munro, *Biochim. Biophys. Acta*, 2003, **1641**, 71–85.

111 C. M. Carr and P. S. Kim, *Cell*, 1993, **73**, 823–32.

112 B. Eschli, K. Quirin, A. Wepf, J. Weber, R. Zinkernagel and H. Hengartner, *J. Virol.*, 2006, **80**, 5897–5907.

113 H. R. Zope, F. Versluis, A. Ordas, J. Voskuhl, H. P. Spaink and A. Kros, *Angew. Chem. Int. Ed. Engl.*, 2013, **52**, 14247–14251.

114 E. Oude Blenke, J. Van Den Dikkenberg, B. Van Kolck, A. Kros and E. Mastrobattista, *Nanoscale*, 2016, **8**, 8955–8965.

3

A flow cytometry assay to quantify intercellular exchange of membrane components

Published as part of: Dimitrios Poulcharidis, Kimberley Belfor, Alexander Kros and Sander I. van Kasteren. Chemical Science, *2017, 8, 5585-5590*

3.1 Introduction

The ability of cells to communicate with one another is one of the most important characteristics of eukaryotic and prokaryotic cells.[1,2] Some of this communication occurs by exchange of soluble cellular components between cells, such as peptides, larger proteins, individual amino acids and nucleotides,[2] by exosome secretion,[3] or through direct exchange of membrane components upon contact between cells.[4] This direct exchange of cellular components between neighbouring eukaryotic cells remains poorly described and its

involvement in cell-cell communication between neighbouring cells requires further study.[5]

Many cell wall components are not under direct genetic control. For example, in model systems, radiolabelled or fluorescently labelled cholesterol has been shown to exchange intracellularly between organelles[6] and liposomes[7] as well as between serum and erythrocytes.[8] The rate of lipid exchange in liposomes varies depending on the solubility, the acyl-chain, the length of the fatty acid and the hydrophobicity.[7,9,10] For example, most phosphatidylcholines (PtdCho) in cells with 16 or more carbon acyl chains have a transfer half-time of 83 hours.[9–11] On the other hand, 25-hydroxylcholesterol (25OH) is more hydrophilic than cholesterol and therefore exchanges more rapidly,[9,12,13] whereas cholesteryl oleate is more hydrophobic than cholesterol and exchanges more slowly.[9] Exchange of cholesterol between host cells and bacteria (i.e. *Borrelia burgdorferi*) was also recently reported to be an important process in the pathogenesis or infectivity of pathogens.[14]

Aside from these examples of cholesterol exchange, the study of membrane component exchange is relatively underexplored,[15,16] especially in mammalian cell systems. The dynamics and kinetics of membrane compound exchange critically impacts many different biological activities in cells including cell-cell recognition, energy production, signal transduction and conversion, cell adhesion and foreign molecule identification.[17,18]

Here an adaptable strategy utilising flow cytometry is presented, in which labelled membrane components are used to quantify their exchange rates (Scheme 1) between mammalian cells in co-culture, quantify the interactions between glycans and membrane lipids, and

understand the exchange mechanism. This approach is then applied to study the exchange of fluorescently labelled cholesterol,[19] alkyne-modified cholesterol[20] as well as azide-modified sialic acids to determine any differences in exchange between these different classes of membrane components.[21] The latter two are visualised in a two-step bioorthogonal method.[22,23] Using this approach, the rate of sterol exchange was shown to be highly cell-line dependent and the rate of sialic acid-containing component exchange is significantly slower than that of the sterolic lipids. Finally, a non-exchanging cell line was forced to exchange both sterols and carbohydrates when brought into prolonged close proximity using complementary coiled-coils.[24,25] This suggests that lipid exchange mediated by direct contact is the dominant mechanism of sterol exchange in these cells.

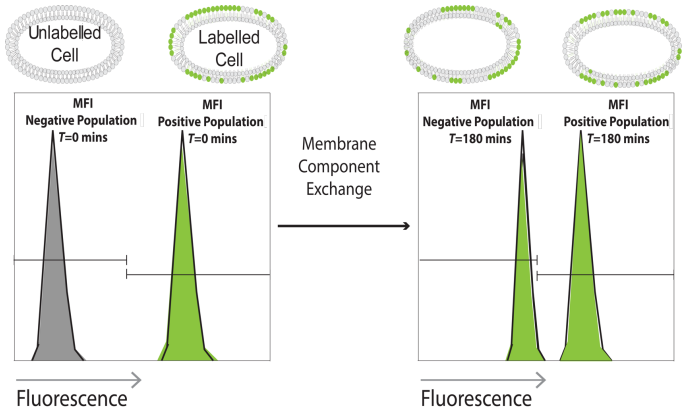

Scheme 1 *Schematic overview of the approach: cell lines are treated with fluorescently labelled sterol and/or glycan and co-cultured with analogous untreated cells. Analysis by flow cytometry over time shows the rate of exchange of the fluorescent membrane component to the non-fluorescent population as a shift in mean fluorescent intensity (MFI).*

3.2 Results and discussion

The initial aim was to develop a broadly deployable assay that would allow the facile quantification and mechanistic characterisation of the exchange of membrane components between cells by flow cytometry (Scheme 1). The recently reported bodipy-modified cholesterol

(1, Scheme 2), which readily inserts into eukaryotic cell membranes, was used to determine whether this exchange could be visualised (Figure 1).[19]

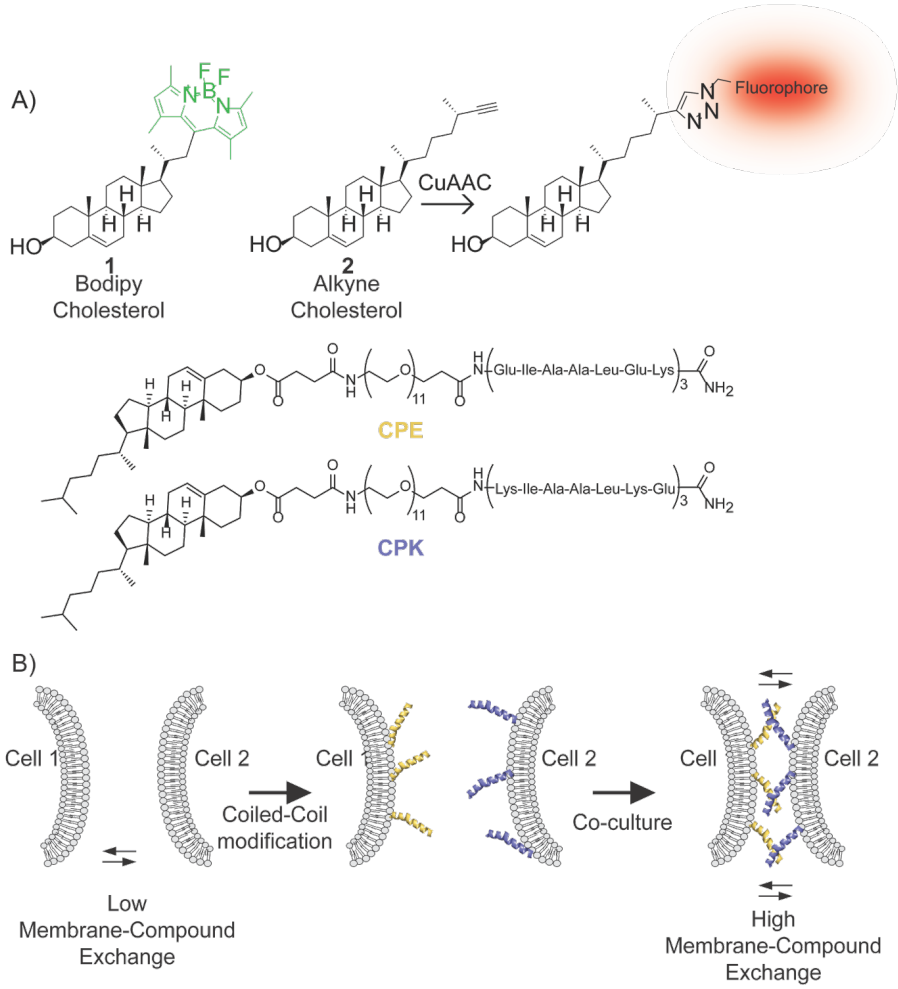

Scheme 2 *(A) Structures of bodipy-cholesterol (Bdp-Ch,* ***1****), alkyne-cholesterol (Alk-Ch,* ***2****), cholesterol modified* E_3 *(CPE) and* K_3 *(CPK) peptides. (B) Schematic representation of coiled-coil formation and its use to prolong cell-cell contact thus enhancing membrane compound exchange.*

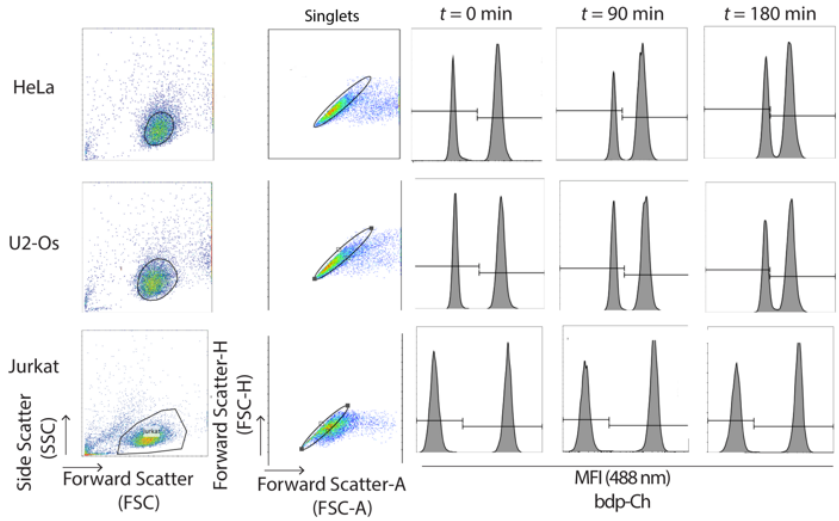

Figure 1 *The flow cytometry assay indicates cholesterol exchange between live HeLa and U2-Os cells, whereas no exchange occurs between Jurkat cells. Cells were treated with 5 μM bdp-Cholesterol (1, Scheme 1) for 18 h. Labelled and unlabelled live cells were co-cultured and flow cytometry was completed. The cell population was gated based on FSC-A vs. SSC-A (cell doublets were gated out using FSC-H vs. FSC-A) and histograms of mixed cells; t = 0, 90 and 180 mins are shown for each cell line with mean fluorescent intensity (MFI) gated accordingly.*

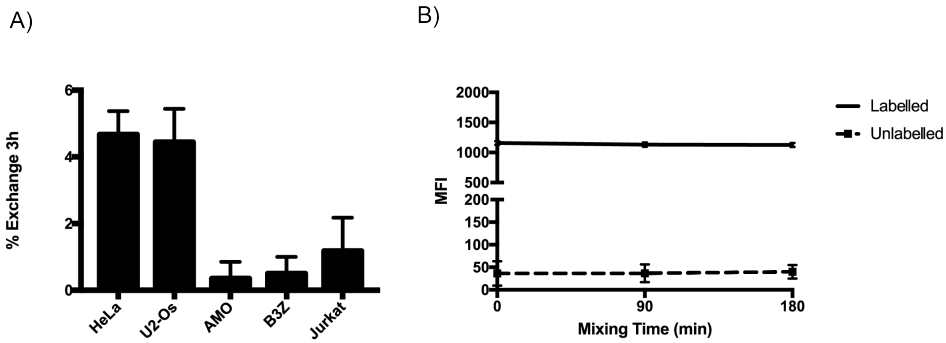

Figure 2 *Exchange rates of bodipy cholesterol (bdp-Ch 1) are cell-type and live-cell dependent. Cells were incubated overnight with bodipy cholesterol and then mixed with unlabelled cells for 3 h. Flow cytometry results were analysed and showed differences in the lipid exchange rates for the different cell lines. (A) Expression of fluorescent signal exchange after 3 h for different cell lines indicating that the lipid exchange depends on the cell line. (B) Fixation abolished lipid exchange of HeLa cells; HeLa cells fixed using 2% PFA for 15 mins prior to co-culture. Data are represented as mean ± SD. Error bars SD.*

To study whether exchange of this lipid could be observed, various cell lines (HeLa,[26] U2-Os,[27] Jurkat,[28] AMO,[29] and the B3Z T cell[30]) were incubated with **1** as described.[19] Unlabelled cells were then mixed with labelled cells and co-cultured at 37 °C for different times. The amount of exchange of the fluorescently labelled cholesterol over time between these two populations was then determined using flow cytometry (Figure 1 and Figure 2A). In this assay, the rate of exchange of bodipy cholesterol (bdp-Ch 1) was shown to vary significantly between the different cell lines: after three hours HeLa and U2-Os had exchanged 4.5 ± 0.17% and 4.4 ± 0.05% of 1 respectively. Jurkat, AMO and B3Z cells on the other hand had exchanged < 1% (0.9 ± 0.23%, 0.4 ± 0.03% and 0.6 ± 0.12% respectively) (Figure 3A and Figure 3B). It was hypothesized that cell-cell contact might be the driving force for membrane lipid exchange as no exchange between suspension cell lines – which have limited cell-cell contact – was observed. The rate of exchange (% exchange, ΔMFI, eq 1) was normalised to live cells based on scatter plots and cellular fluorescence. The ΔMFI was calculated as the amount of fluorescent intensity the unlabelled (negative) cells gained at time t = 180 mins of co-culture with labelled (positive) cells in correlation with the total fluorescent intensity (the initial fluorescently labelled cell population) (eq 1).

$$\Delta MFI = \frac{MFI_{\text{negative } (t = 180 \text{ mins})} - MFI_{\text{negative}(t=0 \text{ mins})}}{MFI_{\text{positive } (t=0 \text{ mins})}} \qquad \text{(eq 1)}$$

Here, flow cytometry was used to determine the differences in cholesterol exchange between live HeLa cells as a function of lipid concentrations. Cells were treated with bodipy-modified cholesterol (bdp-Ch, 1; 1 μM, 5 μM and 10 μM) for 18 hours before mixing with unlabelled live cells. Upon flow cytometry analysis, the cell

populations were gated based on forward scatter area (FSC-A) and side scatter area (SSC-A) characteristics (cell doublets were gated out using FSC-A vs. FSC-H). An increase in the percentage of a new-labelled cell population and a decrease in the number of unlabelled cells was observed, indicating that rate of exchange of cholesterol 1 is concentration dependent (Figure 3C).

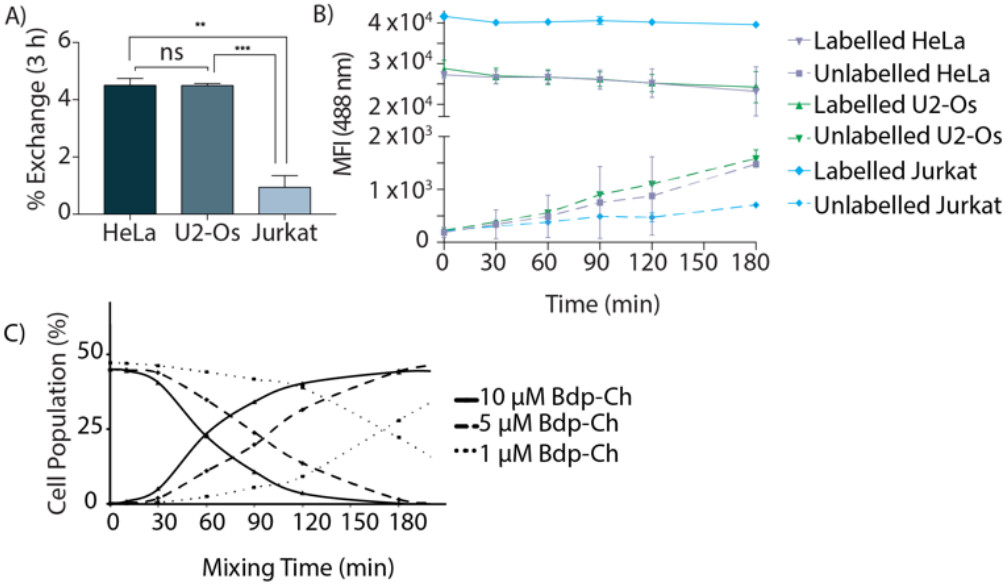

Figure 3 *(A) The percentage exchange or ΔMFI of the fluorescent signal exchange after 3 h co-culturing was calculated using ΔMFI = (MFInegative(t = 180 mins) − MFInegative(t = 0 mins))/MFIpositive(t = 0 mins). Data are represented as mean ± SD. Error bars SD; *p < 0.05; **p < 0.01; ***p < 0.001; ns = not significant; unpaired t-tests. (B) Mean fluorescent intensity (MFI) of labelled and unlabelled cells over varied co-culturing time periods. Data are represented as mean ± SD. Error bars SD. (C) Cholesterol exchange is concentration dependent. In live HeLa cells, the amount of co-culturing time for 25% of the unlabelled population to get labelled varies significantly under different lipid concentrations. Cells were treated with 1 µM, 5 µM or 10 µM bdp-Ch 1 for 18 h prior to co-culturing with unlabelled live cells.*

In order to study that the observed exchange rates were not due to the fluorescent label, unmodified bodipy-488 was used as a control and, as expected, did not exchange (Figure 4), showing that the sterol moiety is essential for the exchange reaction. Altering the ratio of labelled vs. unlabelled cells (1:1, 1:5, 1:10) and vice versa, or increasing the culture volume, also affected the rate of exchange (Figure 5), showing that close contact is necessary for the membrane compound exchange. It was found that the higher the fraction of labelled cells, the faster the exchange: 1:1 ratio exchanged 19 times faster than a 1:10 ratio of labelled vs. unlabelled cells (3.9 ± 0.5% vs. 0.2 ± 0.05%; Figure 5).

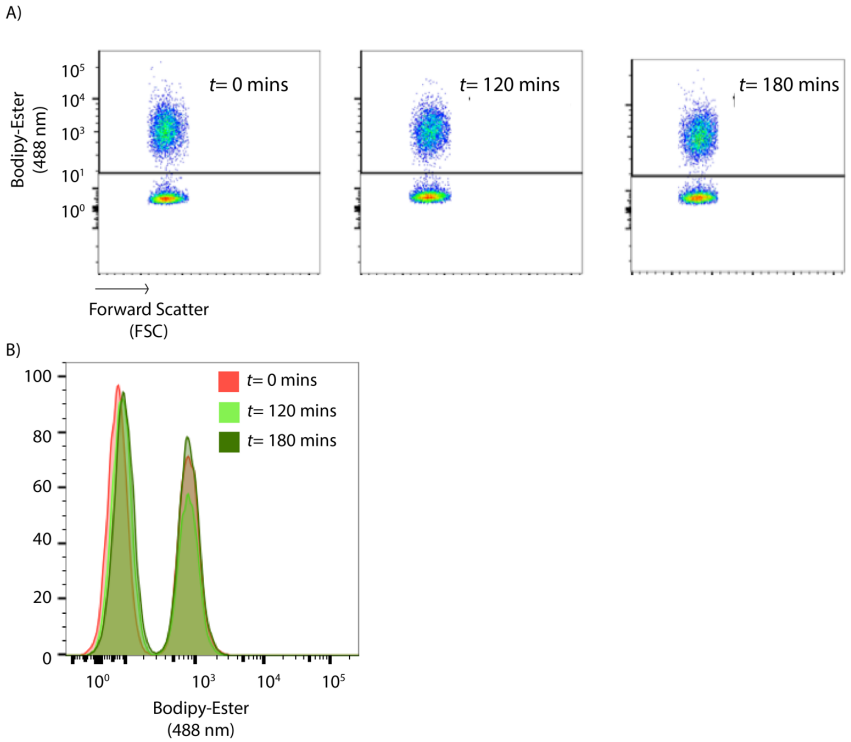

Figure 4 *Exchange of bodipy-488. Flow cytometry assay indicates no bodipy is exchanged between labelled and unlabelled HeLa-cells. Cells treated with bodipy-ester (5 µM for 24 h) were mixed with unlabelled HeLa cells. (A) Scatter plots and (B) overlay histograms of mixing experiments (t=0, 120 and 180 mins) showing any shift.*

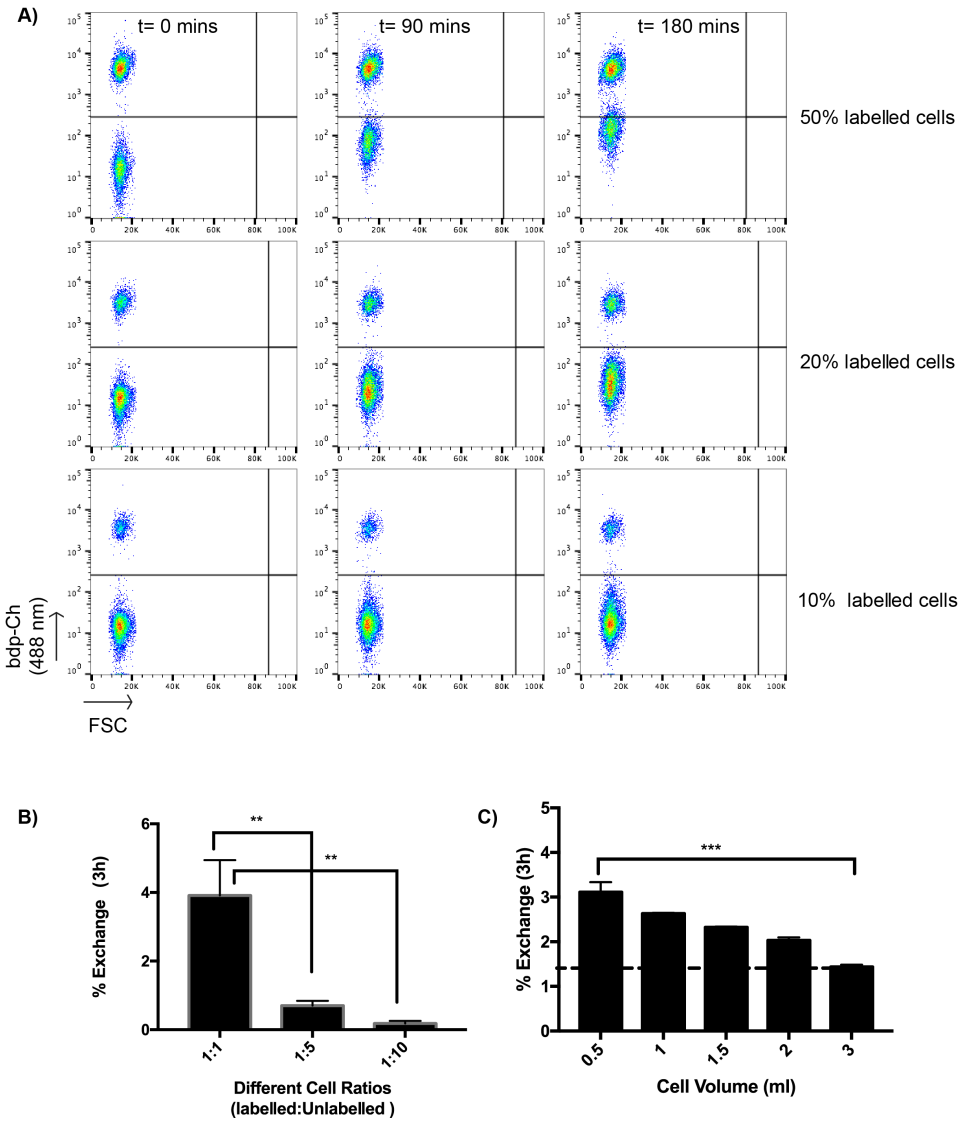

Figure 5 *Cell ratios affect cholesterol exchange: HeLa cells were mixed at either different ratio of labelled vs. unlabelled cells (1:1, 1:5, 1:10) or different culture volume. (A, B) Flow cytometry analysis (t=60, 90, 180 mins) shows exchange rates to be dependent on fluorescent cell fraction. I Flow cytometry analysis after 180 mins showed rated to be dependent on the culture media volume. Data are representing as mean ± SD. Error bars SD; *p<0.05; **p<0.01; ***p<0.001; unpaired t-tests.*

In order to exclude the possibility that the observed cholesterol exchange was due to endocytosis of cell debris, passive uptake from dead cells or exosomes, and rather due to a live-cell dependent process, a series of different control experiments was performed. Cell death was first quantified in the co-culture experiments, by adding membrane impermeable propidium iodide (PI) dye[31] to the cell co-cultures prior to flow cytometry assay showing that the number of dead cells was always <2% (Figure 6B and Figure 6C), even when low temperature or sodium azide were used. In case of fixed cells, a fixable viability dye for live/dead selection could be used instead. Then, in order to exclude the possibility that the observed cholesterol exchange was due to endocytosis of cell debris, unlabelled cells were co-cultured with the lysate from cells labelled with **1**. In this system, there was no lipid uptake or fluorescent labelling after three hours (Figure 6A) at a lysate concentration representing 5% dead cells. Hypothermia or metabolic inhibitors (such as sodium azide) have a major impact in energy-dependent metabolic or biological processes.[32–34] Moreover, when cells were co-cultured under these conditions, differences in the number of dead cells could not be observed (Figure 6B and Figure 6C). Upon ATP depletion with sodium azide or low temperature, membrane lipid exchange was minimised or abolished respectively, indicating that the cholesterol exchange is energy dependent (Figure 6D). Using a chemical fixation step, biological, biochemical and proteolytic processes could be inactivated and cellular components could be kept immobilised and as 'lifelike' as possible.[35,36] Consequently, paraformaldehyde-fixation prior to mixing abolished all exchange (Figure 2B) indicating that the lipid exchange is a live-cell dependent process.

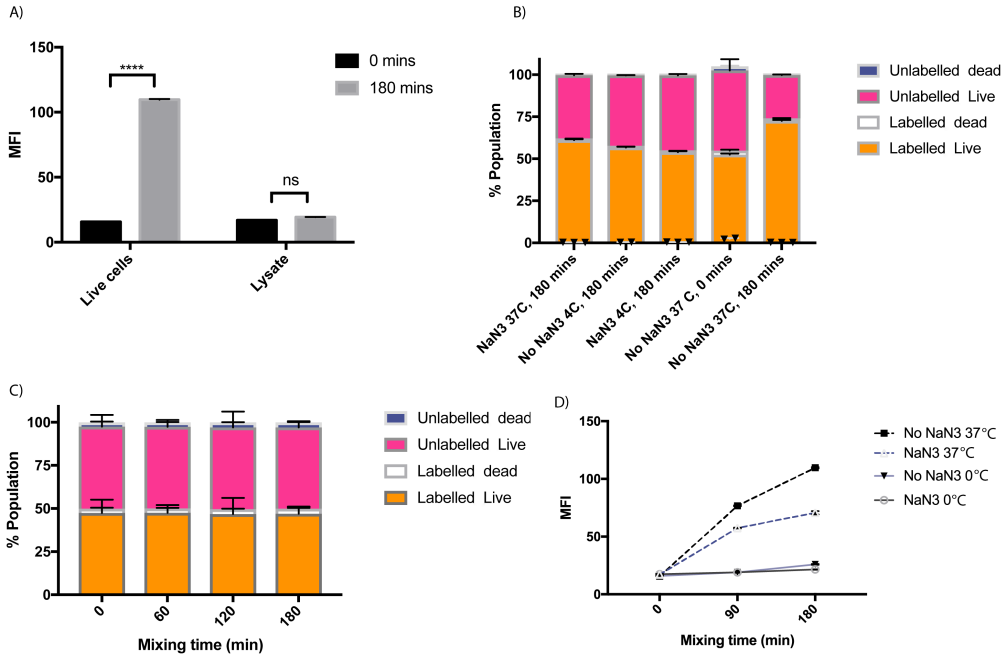

Figure 6 *Cell debris does not affect the lipid exchange in HeLa cells. (A) Labelled HeLa cells with bdp-Ch 1 were lysed by ultra-sonication and co-cultured with unlabelled cells at 37 °C for 3 h. MFI was calculated using flow cytometry and results showed any uptake of the fluorescent lipid difference. (B) Labelled HeLa-cells with bdp-Ch 1 were co-cultured for 3 h with unlabelled cells with or without 1 mM sodium azide at 37 °C or 4 °C. Propidium iodide (PI) used as live/dead dye. Flow cytometry analysis indicates <2% cell debris and lipid exchange independent of cell debris and only at 37 °C. (C) Labelled HeLa-cells with bdp-Ch 1 were co-cultured with unlabelled cells with 1 mM sodium azide at 4 °C for metabolic and energetic inhibition; flow cytometry analysis indicates <2% cell debris, the absence of toxicity during these conditions and the absence of lipid exchange due to cell debris. (D) Cellular energy is necessary for membrane lipid exchange. Labelled HeLa-cells with bdp-Ch 1 were co-cultured with unlabelled cells with 1 mM sodium azide for ATP depletion at 37 °C or 4 °C. Flow cytometry analysis indicates the absence of lipid exchange at 4 °C or the decrease of the exchange at 37 °C with sodium azide.*

To study whether the mechanism of exchange was based on the exchange of exosomes, the exchange of free **1** or cell-cell contact, unlabelled and labelled populations have been spatially separated in a trans-well assay (Figure 7A).[37] All sterol exchange was abolished,

even when large-pore (0.4 μm) membranes were used (through which exosomes can pass and cells cannot[38]), indicating that cell-cell contact is most likely responsible for the exchange of **1**. The absence of any incorporation of **1** in unlabelled cells after a supernatant transfer from a labelled population (Figure 7B) strongly supports the hypothesis that cell-cell contact is the main method of exchange of cholesterol in this system.

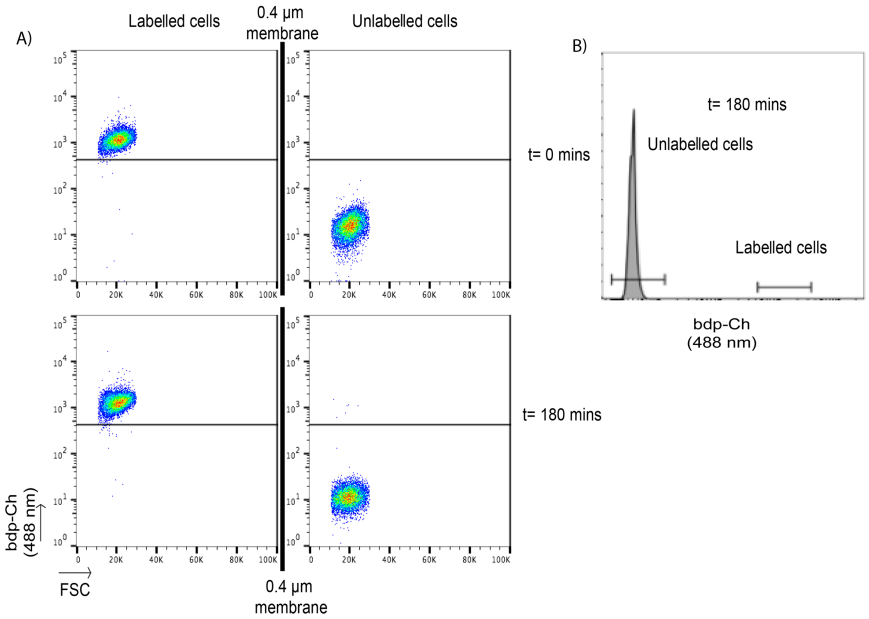

Figure 7 *HeLa cells show no lipid exchange when co-cultured in a trans-well plate. (A) Labelled HeLa-cells with bdp-Ch* ***1*** *were separated by a 0.4 µm membrane from unlabelled cells and incubated for 3 h. Flow cytometry analysis indicates the absence of lipid exchange. (B) Supernatant exchange. HeLa-cells were incubated with 1) and washed with PBS. After 1 h, the supernatant was collected and added to an unlabelled population of HeLa-cells for 3 h. No labelling was observed.*

To further investigate that close contact between cells is important for lipid transfer, testing was done as to whether forcing the cells into prolonged close proximity would enhance the exchange rate. A supramolecular approach was chosen, by which a pair of

complementary lipidated coiled-coil peptides was introduced[24,25] to force cells in close proximity in a non-covalent manner (Scheme 2, Figure 8). Coiled-coil-forming peptides E [$(EIAALEK)_3$] and K [$(KIAALKE)_3$] conjugated via a poly(ethylene glycol)$_{12}$ spacer with a cholesterol moiety (denoted CPE or CPK respectively) have been reported to insert spontaneously into cell membranes,[39–44] and were used here to study lipid exchange.

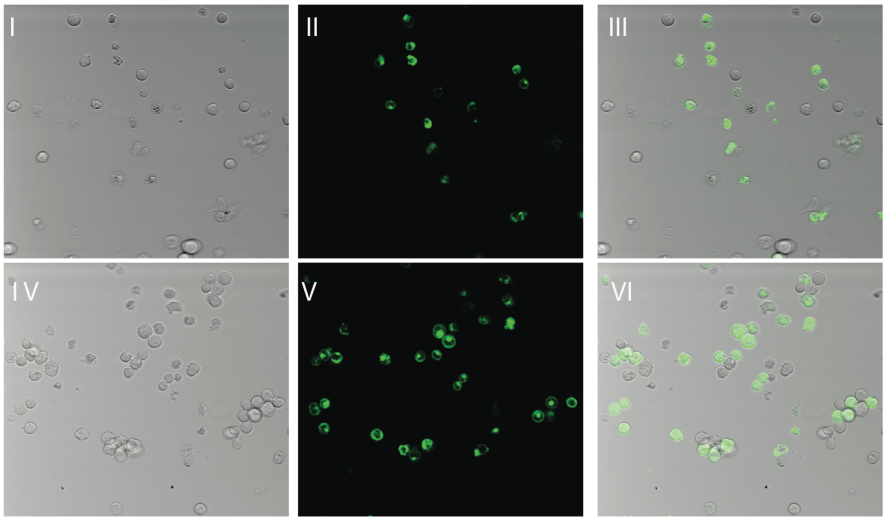

Figure 8 *Confocal microscopy of Jurkat cells with or without coiled coil. (I-III) Jurkat cells were labelled with 1 and co-cultured with unlabelled cells without the presence of lipidated coiled-coil peptides. (IV-VI) Jurkat cells were labelled with 1 and treated with 5 μM CPE and were co-cultured with unlabelled cells which had been pre-treated with 5 μM CPK.*

To study the effect of forced proximity on cholesterol exchange, lymphocytic Jurkat cells were used as these showed the lowest exchange rate (Figure 3A). The cells were labelled overnight with **1** and after washing were incubated with 5 μM cholesterol-CPE. In parallel, unlabelled cells were treated with 5 μM CPK. Next, the CPE- and CPK-modified Jurkat cells were mixed and the rate of exchange of 1 was determined. Flow cytometry results indicate that upon coiled-coil

formation between CPE- and CPK-modified cells, membrane-cholesterol exchange was enhanced 3-fold (from 1.0 ± 0.18% to 3.3 ± 0.35%) compared to coiled-coil peptide untreated cells (Figure 9A and 9B). The results are suggestive of the exchange rate of **1** being enhanced by forced membrane contact (Figure 9C). Moreover, confocal microscopy after three hours confirmed that upon coiled-coil formation, cells were in close proximity (Figure 8).

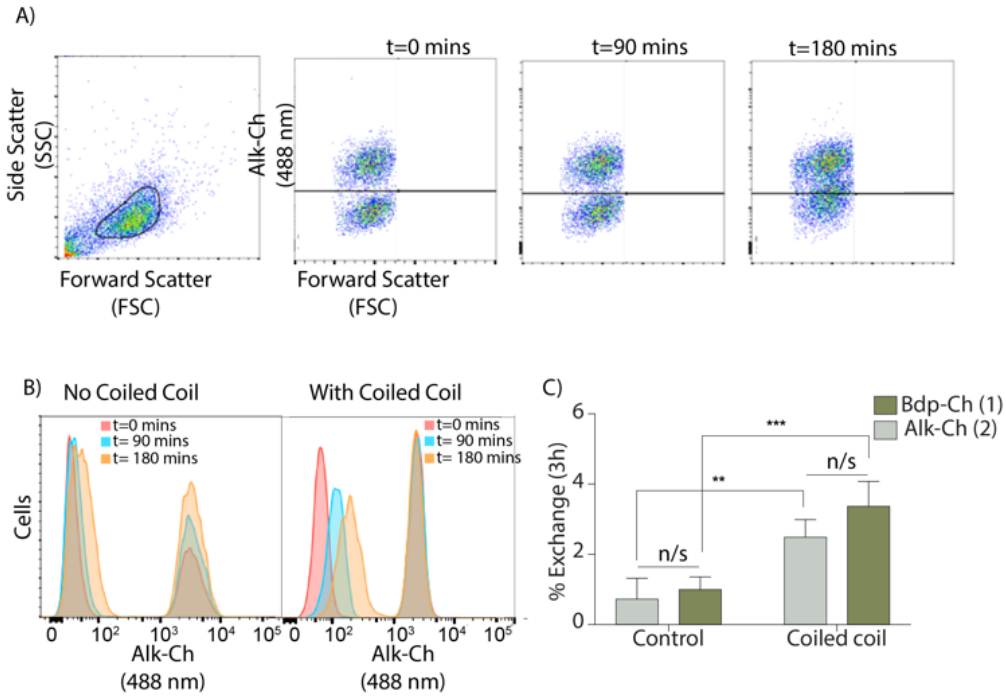

Figure 9 *(A) Forcing cells in close proximity using lipidated coiled-coil (CC) peptides enhances sterol exchange. The first dot-plot shows the gated cell population followed by three dot-plots showing the coalescence of the labelled and unlabelled cells using Alk-Ch (**2**) at t = 0, 90 and 180 mins. (B) Histograms of Jurkat cells over different co-culturing times using alk-Ch (**2,** Avanti) with and without coiled-coil peptides. (C) Exchange rates of **1** and **2** in Jurkat cells after 3 h co-culturing in the presence or absence of CC peptides. Both **1** and **2** show similar exchange rates between CC- and non-CC-labelled cell populations. Data are represented as mean ± SD. Error bars SD; *p < 0.05; **p < 0.01; ***p < 0.001; unpaired t-tests.*

Many membrane components are not amenable to selective fluorophore labelling and the bulky nature of such groups can affect the biological properties of the parent molecule. After establishing the exchange rate of fluorophore-modified cholesterol **1** between different cell types and manipulating these rates of exchange through forcing cell-cell contacts, the cytometry analysis was combined with the detection of bioorthogonal groups in a two-step approach to monitor the exchange of other membrane components.[45]

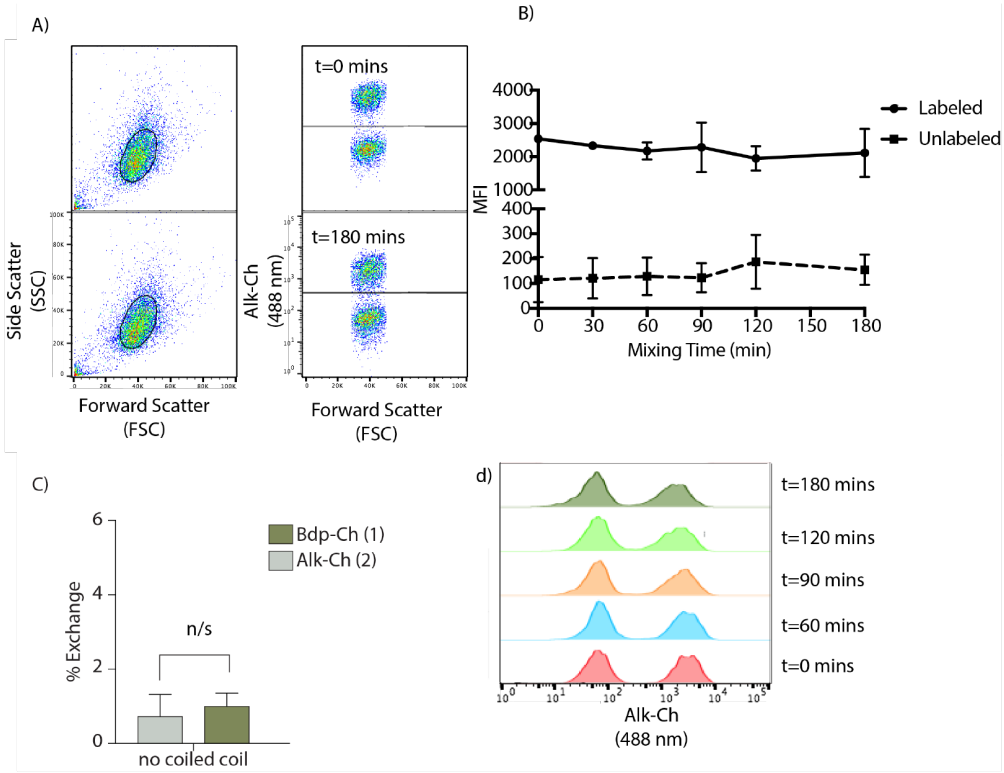

Figure 10 *Flow cytometry assay indicates no cholesterol exchange between live Jurkat cells. Cells were treated with cholesterol-alkyne (Alk-Ch 2, Avanti, 10 μM for 24 h). Labelled and unlabelled live cells mixed and labelled using copper-catalysed azide-alkyne cycloaddition (CuAAC) and flow cytometry assay showed any cholesterol exchange. (A) Dot plots and histograms of mixing cells at t=0 mins and t=180 mins. (B) MFI in different times. (C) Exchange rates of Alk-Ch (2) and bdp-Ch (1) in Jurkat cells in the absence of CC peptides. (D) Histograms in different times, showing no Alk-Ch (2) exchange. Data are represented as mean ± SD. Error bars SD.*

Bioorthogonal chemistry can be used to visualise non-genetically templated biomolecules in cells by means of incorporating a small biologically inert chemical group into a biomolecule class of choice and visualising these at the end of an experiment using tag-selective ligation chemistry.[22,23] The main advantage of this approach is that the small and stable bioorthogonal groups can be incorporated into non-templated molecules and can then hijack the biosynthetic pathways of these molecules. This approach has been used extensively to label many different cell biomolecules, such as glycans, lipids and nucleotides.[46,47] To determine whether a two-step bioorthogonal approach could be used to measure exchange kinetics, first the approach was validated using the recently reported alkyne-modified cholesterol **2**.[20] In a coiled-coil-enhanced exchange experiment in non-adherent Jurkat cells, a comparable 2.5-fold increase in the exchange rate with and without coiled-coil treatment was observed (from 0.7 ± 0.30% without CC to 2.5 ±0.25% with CC after three hours; Figure 9, Figure 10). For this experiment, live-cell compatible variants of the copper-catalysed azide-alkyne cycloaddition (CuAAC) were initially used.[48]

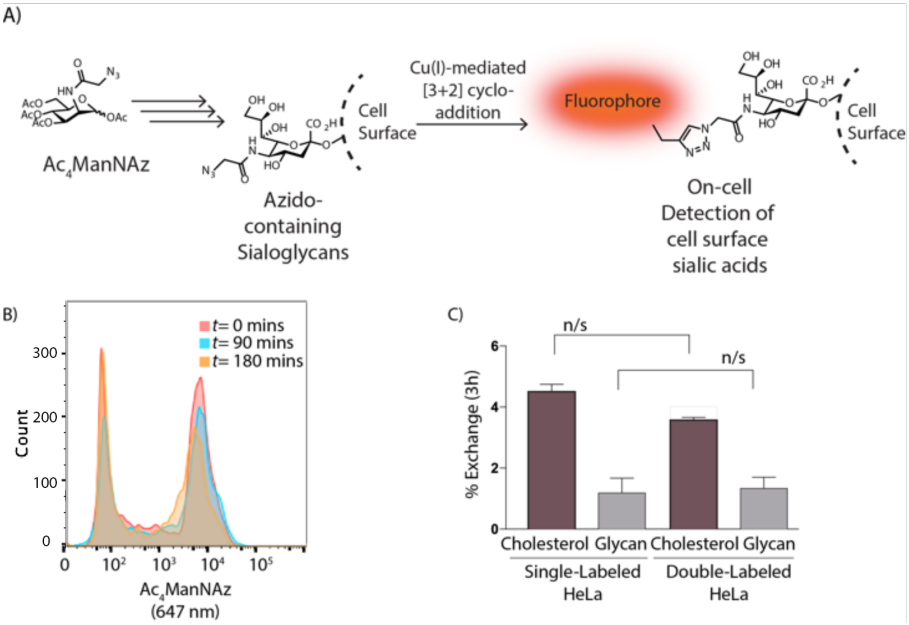

Figure 11 *(A) Schematic representation of cell surface glycan labelling. (B) Flow cytometry overlay histograms on different times show no enhancement of glycolipid exchange between Jurkat cells after coiled-coil formation; Jurkat cells were treated with Ac4ManNAz and CPE co-cultured with untreated cells with CPK and labelled with CuAAC. (C) ΔMFI [ΔMFI= ($MFI_{negative\ (180\ mins)}$-$MFI_{negative\ (0\ mins)}$ / $MFI_{positive\ (0mins)}$] expression of exchange after 3 h between sterol and glycan in single- and double-labelled co-culture experiments; data show lipid exchange independently of the glycan exchange. Data are represented as mean ± SD. Error bars SD; n/s p > 0.05; unpaired t-tests.*

Based on previously reported evidence that by using lower copper concentrations in combination with chelating ligands (TTMA, THPTA, BTTAA, etc.) toxicity could be minimised and be equally "non-toxic" with strain-promoted cycloadditions, [49–51] the conditions were optimised using the well-established WST-1 viability assay. However, despite the fact that these conditions did not significantly affect cell viability as measured by WST-1 viability assay and also 7-AAD (7-Aminoactinomycin D) viability dye (Figure 13), the cells displayed aberrant morphology as determined by flow cytometry (Figure 12). One explanation for this aberrant morphology could be that under

these conditions programmed cell death had commenced. Therefore, a fix-and-click protocol was used in which the cells were first paraformaldehyde-fixed (2%) prior to CuAAC labelling.[36,52] In flow cytometry, a cell traverses through a laser beam allowing the instrument to measure the amount of light which goes around the cell or cell size (FSC) and the amount of light which bounces off the internal particulates of a cell or cell granularity (SSC).[36,53] The ce'l's ability to scatter light is altered during cell death, reflecting morphological changes such as cell swelling or shrinkage.[53] Therefore changes in morphology of a dying cell can be detected using light scatter in flow cytometry.

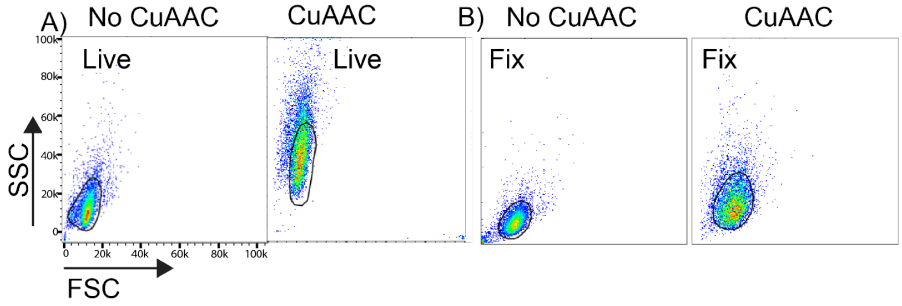

Figure 12 *Live-cell CuAAC affects cellular morphology. HeLa-cells treated with cholesterol-alkyne were subjected to CuAAC conditions with Alexa Fluor® 488 azide. (A) FSC/SSC before addition of CuAAC-reagent mix of unfixed and fixed cells. (B) FSC/SSC after addition of reagents to unfixed and fixed cells. Fixed cells retain their FSC/SSC profile, whereas live cells broaden their FSC/SSC value distribution.*

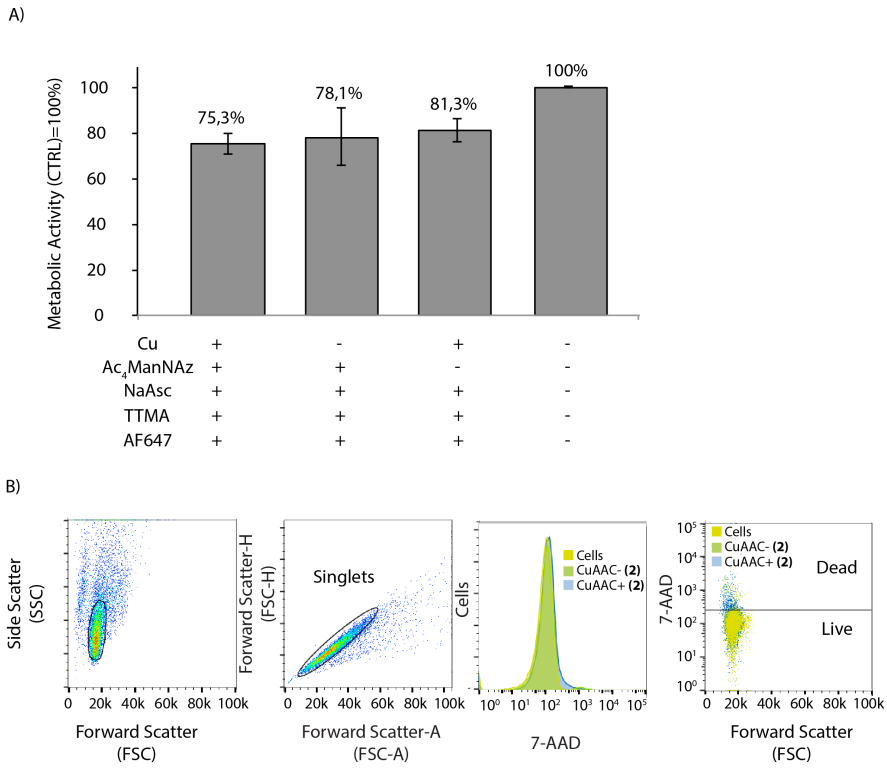

Figure 13 *CuAAC does not have a major impact in cell viability. (A) Cells were treated with/without Ac4ManNAz for 72 h or with Alk-Ch (2, Avanti) 10 uM, and then subjected to CuAAC (with or without catalyst) conditions for 5 mins (100 µM CuSO4, 250 µM TTMA [(Tris((1-((O-ethyl)carboxymethyl)-(1,2,3-triazol-4-yl))methyl)amine] ligand, 2.5 mM sodium ascorbate and 3 µM Alexa Fluor® 647 Alkyne or Alexa Fluor® 488 azide). Cells were washed 3 times. The cell WST-1 viability assay[84] shows no difference in cell viability under these CuAAC conditions, despite the observed morphological changes in S10. (B) Cells treated with Alk-Ch (2, Avanti) 10 uM and were subjected to CuAAC; 7-AAD viability dye was used and no major cell toxicity (<4 %) was defined.*

Having established the suitability (and limitations) of a bioorthogonal approach to detect cholesterol exchange, a similar approach was used to determine whether the exchange of another integral membrane component could be monitored: sialoglyoproteins and sialoglycolipids. These vital membrane components have been associated with cell-cell communication, metastatic behaviour, human disease and cell recognition.[55] HeLa cells were first labelled using a

bioorthogonal analogue of the metabolic precursor of sialic acid, per-O-acetylated N-2-azidoacetylmannosamine (Ac_4ManNAz),[21] which is converted to sialic acid inside the cell and transferred to nascent galactose-terminated glycans in the trans-Golgi network (Figure 11A). Previously well-established protocols indicate that a sufficient amount of corresponding sialic acids is biosynthesised and presented in cell surfaces after three-day treatment with the specific metabolic sialic acid precursors.[50,56–58] Here, HeLa cells were treated with 50 μM Ac_4ManNAz for 72 hours prior to mixing and co-culturing with untreated HeLa cells. Flow cytometry after paraformaldehyde fixation (2%) showed that the rate of exchange of the sialoglycome was significantly slower (0.98 ±0.40% after three hours) compared to cholesterol exchange (Figure 11B and Figure 11C).

This lack of exchange was not due to the Ac_4ManNAz labelling, as the exchange of **1** in cells labelled with both Ac_4ManNAz and **1** was unaffected (Figure 11C). A speculation about the biological significance of the absence of exchange could be made: the observed slower exchange of glycans between cells may reflect reduced freedom of movement of these larger sialoglycolipids in the cell membrane, or their specific function in cell adhesion.[59-61]

3.3 Conclusions

This study demonstrates that different mammalian cells exchange membrane components in a time- and cell-type dependent manner. This exchange appears to be due to cell-cell contacts and can be enhanced when cells are forced in close proximity. The exchange of sialylated membrane components appears to be significantly slower compared to sterols, indicating the presence of differential control mechanisms of exchange for these components. Radio-labelled

cholesterol in combination with mass spectroscopy and targeted metabolomics could be used in later stages for validation of the aforementioned technique. These experiments could be used to study the exchange of other lipids as well, such as inflammatory mediators[62,63] and mediators of neuronal signaling[64,65] as these have been shown to be amenable to bioorthogonal or fluorescent modification[66]. This will likely help to improve understanding of the role of these compounds in cell-cell communication, cell interactions and disease development.

3.4 Experimental methods

Reagents

Cholesterol and all other chemical reagents were purchased at the highest grade available from Sigma-Aldrich and used without further purification. All solvents were purchased from Biosolve. Phosphate buffered saline (PBS) consisted of 5 mM KH_2PO_4, 15 mM K_2HPO_4, 150 mM NaCl, pH 7.4. Silica gel column chromatography was performed using silica gel grade 40-63 μm (Merck). Thin-layer chromatography (TLC) analysis was performed using aluminium-backed silica gel TLC plates (60_F 254, Merck), visualisation by UV absorption at 254 nm and/or staining with $KMnO_4$ solution. NMR spectra (^1H and ^{13}C) were measured on a Bruker AV-400MHz spectrometer at ambient temperature at the Leiden Institute of Chemistry NMR facility. Chemical shifts are recorded in ppm. Tetramethylsilane (TMS) is used as an internal standard. Multiplicity was reported as follows: s = singlet, d = doublet, dd = doublet of doublets, t = triplet, q = quartet, m = multiplet, br = broad. Electrospray LC-MS analysis was performed on a PE SCIEX: API 3000 LC/MS/MS system using a Gemini 3u C18 110A analytical column (5μ particle size, flow: 1.0 ml/mins), on which the absorbance was measured at 214

and 254 nm. Solvent system for LC-MS: A: 100% water, B: 100% acetonitrile, C: 1% trifluoroacetic acid (TFA) (aq). MALDI-TOF mass spectra were acquired using an Applied Biosystems Voyager System 6069 MALDI-TOF mass spectrometer. α-Cyano-4-hydroxycinnamic acid (CHCA) was used as matrix in all cases. Sample concentrations were ~0.3 mg/ml. HPLC-ELSD analysis was performed using a Shimadzu HPLC set-up equipped with two LC-8A series pumps coupled to a Shimadzu ELSD-LT II detection system. Separation (Vydac 214 MS C4 column, 5u, 100 × 4.6 mm, flow rate: 15 mL/mins), in all instances, was carried out over a linear gradient of 10-90% B over 20 minutes with an initial five-minute hold at 10% B. HPLC buffers: A: H_2O (0.1% TFA); B: acetonitrile (0.1% TFA). The drift tube temperature for ELSD was set at 37 °C and the nitrogen flow-rate at 3.5 bar.

Flow cytometry[36,53]

Flow cytometry assays were performed using the Merck Guava® easyCyte 12HT Benchtop Flow Cytometer and all flow cytometry data was analysed using FlowJo™ v10.1 (FlowJo, LLC). Counting and characterization was performed by measuring 10,000 events in triplicate and concatenation of this data. For manual gating, the outermost ring of the dot plot was selected. Quadrants were manually selected to illustrate fluorescence plots. No compensation was required.

Flow cytometry is a technology that simultaneously measures and then analyses multiple physical characteristics of single particles, usually cells, as they flow in a fluid stream through a beam of light. Light scattering occurs when a particle deflects incident laser light. Correlated measurements of forward-scattered light (FSC) and side-

scattered light (SSC) can allow for differentiation of cell types in a heterogeneous cell population. FSC is proportional to cell-surface area or size, whereas SSC is proportional to cell granularity or internal complexity

Cholesterol exchange assay

For the study of cholesterol exchange, cells were incubated with Bdp-Cholesterol 1 (TopFluor®, Avanti) for 18 hours at 37 °C. Cells were washed six times, before co-culture with unlabelled cells. For the study of exchange of adherent cells, the cells were detached prior to exchange using EDTA/PBS for 15 minutes and seeded in a 96-V-plate for the mixing and exchange.

Coiled-coil enhancement of exchange reaction

For the coiled-coil formation labelled cells were treated with 5 μM CPE and the unlabelled cells with 5 μM CPK for 10 minutes at 37 °C. Cells were washed twice with PBS and resuspended in fresh media. Cells were mixed and co-cultured for different time periods (20,000 cell/100μl treated+ 20000 cell/100μl untreated) in media with or without serum. Fluorescence was then measured using Guava® easyCyte 12HT Benchtop Flow Cytometer and results analysed using FlowJo™ v10.1 (FlowJo, LLC).

Bioorthogonal sialylated glycan exchange assay

For the glycan studies, cells were incubated with 50 μM Ac_4ManNAz for 72 hours at 37 °C. Adherent cells were detached using 2 mM EDTA/PBS for 15 minutes and mixed in a 96-V-plate with unlabelled cells. For the coiled-coil mediated exchange enhancement, cells were treated with 5 μM CPE and 5 μM CPK for 10 minutes at 37 °C prior to mixing. Cells were washed twice with PBS and resuspended in fresh

media. Cells were mixed and co-cultured for different time periods (20,000 cell/100μl treated+20,000 cell/100μl untreated) in media with or without serum. Prior to labelling cells were fixed with paraformaldehyde (PFA) 2% for 15 minutes at room temperature. The PFA was removed (2 x washing) and the cells were resuspended in PBS. Then the CuAAC mix was added. Click solution comprised of 1 mM CuSO4, 100 μM TTMA [(Tris((1-((O-ethyl)carboxymethyl)-(1,2,3-triazol-4-yl))methyl)amine] ligand, and 2 mM sodium ascorbate and 2 μM Alexa Fluor® 647 alkyne (Invitrogen). After 20 minutes, the cells were washed three times with PBS, prior to incubation with 3% bovine serum albumin (BSA) for 30 minutes to remove unreacted fluorophore. The cells were then washed and flow-cytometry was performed. For the cholesterol-alkyne assay, the cells were incubated for 18 hours at 37 °C with 5 μM cholesterol-alkyne 2 (Avanti) in full media[20]. Cells were then co-cultured, fixed and labelled using the above biorthogonal labelling protocol but with 2 μM Alexa Fluor® 488 azide (Invitrogen).

Mammalian cell culture

Cells were cultured in 25 cm^2 flasks and split at 70-80% confluence (three times per week). The flasks were incubated at 37 °C at 7.0% CO_2. The medium was refreshed three times a week. Cells used in all biological experiments were cultured for a maximum of 8 weeks. Adherent cell cultures with a maximum confluence of 70-80% were trypsinised and centrifuged (1.5 mins, 2000/4000 rcf (live/fixed cells), and the cells were resuspended using fresh media. 10 μL of cell suspension and 10 μL of trypan blue were mixed and pipetted into a cell counting slide, and cells were counted using a BioRad TC10 automated cell counter. The cell suspension was diluted to the appropriate seeding density.

HeLa[25], U2Os[27] cells were cultivated in Dulbecco's Modified Eagle's Medium (DMEM), supplemented with 10% foetal calf serum, 2 mM L-glutamine, 1% penicillin and 1% streptomycin. Cells were cultured in an atmosphere of 7% CO_2 at 37 °C. Medium was refreshed every two days and cells passaged at 70% confluence by treatment with trypsin-EDTA (0.05% trypsin). Jurkat[28] 1 and AMO cells were grown in RPMI 1640 medium supplemented with 10% heat-inactivated foetal calf serum, 2 mM L-glutamine, penicillin 100 l.U./mL and streptomycin 50 μg/mL. CTL hybridoma, B3Z[30] was cultured in IMDM medium supplemented with 10% FCS, 2 mM glutamax, 0.25 mM 2-Mercaptoethanol, penicillin 100 l.U./mL and streptomycin 100μg/mL in the presence of hygromycin B (500 μg/ml).[67]

Live cell confocal microscopy

Cells were seeded on a 35 mm dish (3 x 10^5) in a complete media after the addition of 5 μM bdp-Ch 1 for 18 hours. The following day, prior to the confocal microscopy, lipidated coiled-coil peptides were added as follows: 5 μM final concentration of CPE was added to bdp-Ch treated cells and 5 μM of CPK was added to unlabelled cells; both were incubated at 37 °C for 10 minutes. After three washing steps, fresh media was added and cells were transferred into an 8-well μ-slide (Ibidi, cat. 80826) by mixing 1 x 10^4 bdp-Ch-CPE-modified cells with an equal amount of CPK-modified cells per well. Samples were imaged with a Leica TCS SP8 confocal microscope (63x oil lens, N.A.=1.4).

WST-1 cytotoxicity assay[54]

The cell proliferation reagent WST-1 (CAS 150849-52-8) was used to assess cell viability. This assay is based on the cleavage of a tetrazolium salt (WST-1) to soluble formazan dye by the mitochondrial dehydrogenase of living cells. At indicated time-points, 10 ul of a

freshly made mixture of WST-1 and PMS-OMe (90 uM WST-1 and 181 μM PMS-OMe) were added to each well, and the plates were incubated at 37 °C for four hours. Subsequently, the optical densities of the plates were detected at 450 nm (formazan formation) as measured using a 96-well plate reader. The cytotoxicity was expressed as percentage over control.

Transwell assay[68]

Labelled cells were prevented from directly contacting unlabelled cells using a transwell 0.4 μm-pore membrane (Costar). Cells were seeded in a 6-well plate with full DMEM media with or without the addition of 5 μM bdp-cholesterol (TopFLuor®, Avanti) and cells incubated 24h at 37 °C. Cells were detached with 2.5 mM PBS/EDTA, washed and then re-suspended in DMEM media and then counted. Labelled cells (in 0.3 mL of medium) were added in the upper compartment (done in 6-well plates) and unlabelled cells (in 0.5 mL of medium) placed in the lower chamber separated from targets. The inserts were then picked up using gloves and transferred onto the top of the unlabelled HeLa cell culture with the addition of 2 ml of fresh media into the inserts. The cells were incubated for three hours at 37 °C, and then collected and analysed with flow cytometry.

Synthesis of Ac_4ManNAz

Ac_4ManNAz (Tetra-O-Acetyl-N-azidoacetylmannosamine) was synthesised in full accordance with the reported procedure.[56]

^{1}H NMR (400 MHz, $CDCl_3$), δ= 6.04 (d, 1H), 5.91 (d, 1H), 5.49 (d, 1H), 5.33 (d, 1H), 5.18 (dd, 1H), 5.00-4.97 (m, 1H), 4.81 (d, 1H), 4.77 (d, 1H), 4.55 (d, 1H), 4.54 (dd, 1H), 4.52 (d, 1H), 4.4 (m, 2H), 4.32 (m, 7H), 4.1 (m, 1H), 2.14 (s, 3H), 2.11 (s, 3H), 2.04 (s, 6H), 1.99 (s, 6H), 1.5 (s, 3H),

1.34 (s, 3H). LC-MS (ESI): m/z [M+H]+, calc. for $C_{16}H_{22}N_4O_{10}$: 431.37; found 431.37.

Synthesis of peptides

CPE (cholesterol-PEG_{12}-peptideE) and CPK (cholesterol-PEG_{12}-peptideK) were synthesised and purified as previously reported.[39] Peptide sequences were $(EIAALEK)_3$ and $(KIAALKE)_3$ for E and K respectively.

3.5 References

1 C. M. Waters and B. L. Bassler, *Annu. Rev. Cell Dev. Biol.*, 2005, **21**, 319–346.

2 P. H. Raven, G. B. Johnson, J. B. Losos and S. R. Singer, *Biology*, McGraw-Hill Education, New York, 2004.

3 R. C. Lai, F. Arslan, M. M. Lee, N. S. K. Sze, A. Choo, T. S. Chen, M. Salto-Tellez, L. Timmers, C. N. Lee, R. M. El Oakley, G. Pasterkamp, D. P. V de Kleijn and S. K. Lim, *Stem Cell Res.*, 2010, **4**, 214–222.

4 G. Turturici, R. Tinnirello, G. Sconzo and F. Geraci, *Am. J. Physiol. Cell Physiol.*, 2014, **306**, 621–633.

5 X. Niu, K. Gupta, J. T. Yang, M. J. Shamblott and A. Levchenko, *J. Cell Sci.*, 2009, **122**, 600–610.

6 E. Ikonen, *Nat. Rev. Mol. Cell Biol.*, 2008, **9**, 125–138.

7 K. A. Solanko, M. Modzel, L. M. Solanko and D. Wüstner, *Lipid Insights*, 2015, **8**, 95–114.

8 Y. Lange, C. M. Cohen and M. J. Poznansky, *Proc. Natl. Acad. Sci. U. S. A.*, 1977, **74**, 1538–1542.

9 S. Lev, *Nat. Rev. Mol. Cell Biol.*, 2010, **11**, 739–750.

10 J.E. Ferrell Jr, K.J. Lee and W.H. Huestis, *Biochemistry*, 1985, **24**, 2857–2864.

11 L. R. McLean and M. C. Phillips, *Biochemistry*, 1984, **23**, 4624–4630.

12 M. C. Phillips, W. J. Johnson and G. H. Rothblat, *Biochemistry*, 1987, **906**, 223–276.

13 W. A. Prinz, *Prog. Lipid Res.*, 2007, **46**, 297–314.

14 J. T. Crowley, A. M. Toledo, T. J. LaRocca, J. L. Coleman, E. London and J. L. Benach, *PLoS Pathog.*, 2013, **9**, e1003109.

15 M. Mittelbrunn and F. Sánchez-Madrid, *Nat. Rev. Mol. Cell Biol.*, 2012, **13**, 328–335.

16 A. M. Skinner, S. L. O'Neil and P. Kurre, *PLoS One*, 2009, **4**, e6219.

17 M. A. Deverall, E. Gindl, E.-K. Sinner, H. Besir, J. Ruehe, M. J. Saxton and C. A. Naumann, *Biophys. J.*, 2005, **88**, 1875–86.

18 S. Ly, F. Bourguet, N. O. Fischer, E. Y. Lau, M. A. Coleman and T. A. Laurence, *Biophysj*, 2014, **106**, L05–L08.

19 M. Hölttä-Vuori, R. L. Uronen, J. Repakova, E. Salonen, I. Vattulainen, P. Panula, Z. Li, R. Bittman and E. Ikonen, *Traffic*, 2008, **9**, 1839–1849.

20 K. Hofmann, C. Thiele, H.-F. Schött, A. Gaebler, M. Schoene, Y. Kiver, S. Friedrichs, D. Lütjohann and L. Kuerschner, *J. Lipid Res.*, 2014, **55**, 583–591.

21 E. Saxon and C. R. Bertozzi, *Science*, 2000, **287**, 2007–2010.

22 E. M. Sletten and C. R. Bertozzi, *Angew. Chemie - Int. Ed.*, 2009, **48**, 6974–6998.

23 C. Besanceney-Webler, H. Jiang, T. Zheng, L. Feng, D. Soriano del Amo, W. Wang, L. M. Klivansky, F. L. Marlow, Y. Liu and P. Wu, *Angew. Chem. Int. Ed. Engl.*, 2011, **50**, 8051–8056.

24 H. Robson Marsden and A. Kros, *Angew. Chem. Int. Ed. Engl.*, 2010, **49**, 2988–3005.

25 B. D. N. Woolfson, *Advances*, 2005, **70**, 79–112.

26 M. T. Kubicek, G. O. Gey and W. D. Coffman, *Cancer Res.*, 1952, **12**, 264–265.

27 J. Ponten and E. Saksela, *Int. J. Cancer*, 1967, **2**, 434–447.

28 U. Schneider, H. U. Schwenk and G. Bornkamm, *Int. J. Cancer*, 1977, **19**, 621–626.

29 S. Shimizu, T. Takiguchi, M. Fukutoku, R. Yoshioka, Y. Hirose, S. Fukuhara, H. Ohno, Y. Isobe and S. Konda, *Leukemia*, 1993, **7**, 274–280.

30 J. Karttunen and N. Shastri, *Proc. Natl. Acad. Sci.*, 1991, **88**, 3972–3976.

31 B. S. Cummings and R. G. Schnellmann, *Curr. Protoc. Pharmacol.*, 2004, Chapter 12, Unit 12.8.

32 V. P. Torchilin, R. Rammohan, V. Weissig and T. S. Levchenko, *Proc. Natl. Acad. Sci. U. S. A.*, 2001, **98**, 8786–8791.

33 M. Tsubaki, *Biochemistry*, 1993, **32**, 174–182.

34 J. Harvey, S. C. Hardy and M. L. Ashford, *Br. J. Pharmacol.*, 1999, **126**, 51–60.

35 E. C. T. Yeung, C. Stasolla, M. J. Sumner and B. Q. Huang, in *Plant Microtechniques and Protocols*, Springer International Publishing, 2015, 22–43.

36 H. M. Shapiro, *Practical Flow Cytometry*, John Wiley & Sons, New Jersey, Fourth., 2003.

37 J. Iqbal, K. Anwar and M. M. Hussain, *J. Biol. Chem.*, 2003, **278**, 31610–31620.

38 M. K. Herroon, E. Rajagurubandara, D. L. Rudy, A. Chalasani, A. L. Hardaway and I. Podgorski, *Oncogene*, 2013, **32**, 1580–1593.

39 H. R. Zope, F. Versluis, A. Ordas, J. Voskuhl, H. P. Spaink and A. Kros, *Angew. Chem. Int. Ed. Engl.*, 2013, **52**, 14247–14251.

40 F. Versluis, J. Voskuhl, B. Van Kolck, H. Zope, M. Bremmer, T. Albregtse, A. Kros, B. van Kolck, H. Zope, M. Bremmer, T. Albregtse and A. Kros, *J. Am. Chem. Soc.*, 2013, **135**, 8057–8062.

41 L. Kong, S. H. C. Askes, S. Bonnet, A. Kros and F. Campbell, *Angew. Chemie - Int. Ed.*, 2015, **55**, 1396–1400.

42 N. Lopez Mora, A. Bahreman, H. Valkenier, H. Li, T. Sharp, D. N. Sheppard, A. Kros and A. Davis, *Chem. Sci.*, 2016, **7**, 1768–1772.

43 J. Yang, A. Bahreman, G. Daudey, J. Bussmann, R. C. L. Olsthoorn and A. Kros, *ACS Cent. Sci.*, 2016, **2**, 621–630.

44 J. Yang, Y. Shimada, R. C. L. Olsthoorn, B. E. Snaar-Jagalska, H. P. Spaink and A. Kros, *ACS Nano*, 2016, **10**, 7428–7435.

45 G. Charron, *Acc. Chem. Res.*, 2011, **44**, 699–708.

46 X. Zhang and Y. Zhang, *Molecules*, 2013, **18**, 7145–7159.

47 D. M. Patterson, L. A. Nazarova and J. A. Prescher, *ACS Chem. Biol.*, 2014, **9**, 592−605.

48 V. Hong, N. F. Steinmetz, M. Manchester and M. G. Finn, *Bioconjugate Chem.*, 2010, **21**, 1912–1916.

49 C. Uttamapinant, A. Tangpeerachaikul, S. Grecian, S. Clarke, U. Singh, P. Slade, K. R. Gee and A. Y. Ting, *Angew. Chemie - Int. Ed.*, 2012, **51**, 5852–5856.

50 D. Soriano Del Amo, W. Wang, H. Jiang, C. Besanceney, A. C. Yan, M. Levy, Y. Liu, F. L. Marlow and P. Wu, *J. Am. Chem. Soc.*, 2010, **132**, 16893–16899.

51 C. Uttamapinant, M. I. Sanchez, D. S. Liu, J. Z. Yao and A. Y. Ting, *Nat. Protoc.*, 2013, **8**, 1620–1634.

52 L. A. Herzenberg, *Nat. Immunol.*, 2006, **7**, 681–685.

53 G. C. Salzman, S. B. Singham, R. G. Johnston and C. F. Bohren, in *Flow Cytom. Sorting*, Wiley, New York, 1990, 81–107.

54 M. J. Stoddart, *Mamm. Cell Viability Methods Protoc.*, 2011, **740**, 21–25.

55 N. M. Varki and A. Varki, *Lab Invest*, 2007, **87**, 851–857.

56 S. T. Laughlin and C. R. Bertozzi, *Nat. Protoc.*, 2007, **2**, 2930–2944.

57 F. R. Maxfield and D. Wüstner, *Methods Cell Biol.*, 2012, **108**, 367–393.

58 L. Yang, J. O. Nyalwidhe, S. Guo, R. R. Drake and O. J. Semmes, *Mol. Cell. Proteomics*, 2011, **10**, 1–16.

59 D. H. Dube and C. R. Bertozzi, *Nat. Rev. Drug Discov.*, 2005, **4**, 477–488.

60 S. Iyer, R. M. Gaikwad, V. Subba-Rao, C. D. Woodworth and I. Sokolov, *Nat. Nanotechnol.*, 2009, **4**, 389–393.

61 H. Jiang, B. P. English, R. B. Hazan, P. Wu and B. Ovryn, *Angew. Chemie Int. Ed.*, 2015, **54**, 1765–1769.

62 B. D. Levy, C. B. Clish, B. Schmidt, K. Gronert and C. N. Serhan, *Nat. Immunol.*, 2001, **2**, 612–619.

63 M. Winkler, *BJOG An Int. J. Obstet. Gynaecol.*, 2003, **110**, 118–123.

64 M. van der Stelt and V. Di Marzo, *Neuromolecular Med.*, 2005, **7**, 37–50.

65 F. A. Iannotti, V. Di Marzo and S. Petrosino, *Prog. Lipid Res.*, 2016, **62**, 107–128.

66 M. P. Baggelaar, F. J. Janssen, A. C. M. Vanesbroeck, H. Dendulk, M. Allara, S. Hoogendoorn, R. McGuire, B. I. Florea, N. Meeuwenoord, H. Vandenelst, G. A. Vandermarel, J. Brouwer, V. Dimarzo, H. S. Overkleeft and M. Vanderstelt, *Angew. Chemie - Int. Ed.*, 2013, **52**, 12081–12085.

67 G. Cafri, A. Sharbi-Yunger, E. Tzehoval and L. Eisenbach, *PLoS One*, 2013, **8**, 1–7.

68 M. K. Herroon and I. Podgorski, *Bio-protocol*, 2015, **7**, 956–963.

4

Identifying membrane lipid exchange between immune cells

4.1 Introduction

The transfer of cell membrane components such as surface lipids and proteins between immune cells is an area of intense investigation.[1] Cells communicate with a wide variety of mechanisms including both exosome secretion and direct cell-cell contact.[2-4] Cellular membrane components can also be exchanged with the formation of gap junctions, nanotubes, and processes such as direct membrane component transfer and trogocytosis.[5-8] During antigen presentation, lymphocytes and antigen-presenting cells (APCs) form a rigidly structured contact; i.e. immune synapse (IS) as a mechanism of communication.[9,10] The exact mechanism for cellular membrane exchange or which components can be exchanged is still unknown. However, it has been

suggested that direct contact or close distance between the two cells plays an essential role.[11,12] Between immune cells, the membrane exchange of proteins via direct contact in CD8+ T cells was first described by Hudrisier *et al.* and later by others.[13–18] Recently, Daubeuf *et al.* have described the ability of T cells to "steal" components from the membranes of target cells.[1,19] However, the role of specific lipids in this exchange – as well as the rate at which non-proteins are exchanged – remains unknown, as does the directionality of the approach.

Chapter 3 described how forced cell-to-cell contacts between non-exchanging cells can result in the exchange of lipids and glycans.[20] It was hypothesized that the synaptic contact between a T cell is a natural variant of such a forced contact. The cells often remain in very close proximity for more than 3 hours with the contact surface between the two cells not being atypical.[21–23] As such, it was postulated that synapse formation could also enhance membrane exchange. This hypothesis was further fuelled by the observations that T cells are in serious need of nutrients and lipids to ensure their proper activation.

To date this exchange of membrane lipids along the immunological synapse has not been reported on. In the past lipophilic fluorescent chemical tracers have been used between cells, suggesting membrane compound exchanges. However, a possible complication with these dyes is the fact that they show a severe fluorescent loss due to modifications. Additionally, many different experimental steps, such as fixation, dye concertation or cell concentration, might affect the final fluorescent intensity of lipophilic dyes.

Bioorthogonal chemistry can be used instead to visualise non-genetically templated biomolecules in cells incorporating a small

biologically inert chemical group into a biomolecule class of choice and visualising these at the end of an experiment using tag-selective ligation chemistry.[24–26] The benefit of this approach is that the small and stable bioorthogonal groups can be incorporated into non-templated molecules, and they can hijack the biosynthetic pathways of these molecules. This approach has been used extensively to label many different cell biomolecules, such as glycans, lipids and nucleotides.

The exchange of plasma membrane components has been used as the fundamentals in assays for trogocytosis analysis protocols (TRAP) for detecting fluorescent components such as proteins, lipids or glycoconjugates.[27–30] In this chapter an adaptable strategy based on TRAP assays is presented, in which fluorescent and clickable lipids were used to determine the membrane component exchange between APC and T cells in co-culture. A range of sterols and aliphatic acids were screened in an attempt to learn more about the effect of their biochemical characteristics and structure on their behaviour in trogocytosis tests, and possibly to shed light on the still unanswered question of the cellular and molecular mechanisms of membrane component exchange between immune cells.

4.2 Results and discussion

This work aimed to develop a methodology that would allow the facile quantification of the exchange of membrane components between immune cells. Chapter 3 described the optimisation of the kinetic study of cholesterol exchange between mammalian cells using flow cytometry.[20] The occurrence of membrane compound exchange can be demonstrated by labelling the membrane of APCs using modified lipids or fluorescent sterols and observing the existence of these probes onto the target cells; i.e. lymphocytes after their co-culture. Membrane

component exchange was calculated based on the fluorescent intensity of the acceptor cell upon co-culture with donor cells.

The particular lipids were selected based on their ability to be incorporated in cell membranes, and for their structure or biochemical properties to not be affected by the presence or absence of a fluorophore. The studies outlined previously revealed a bodipy-cholesterol (TopFluor®[31]) and cholesterol-alkyne[32] analogue which lead to very efficient incorporation of the sterols into live cells. It was found that between mammalian cells, membrane sterol of the plasma membrane tend to exchange in different rates between cells upon direct contact.[20] Therefore, the tendency of sterols or palmitate lipid to efficiently incorporate into immune cells such as bone marrow derived dendritic cells (BMDCs) and T cells was examined. Indeed it was found that certain lipids have a much stronger tendency to exchange between cells than others.

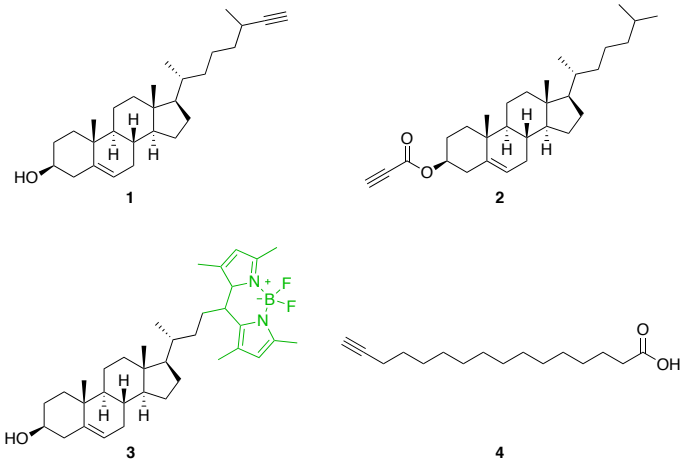

Figure 1 *Library of different lipids used: (1) Alkyne-cholesterol, cholesterol-click, Avanti Polar Lipids; (2) cholesterol propiolic acid, O-Click; (3) TopFluor® Cholesterol, bodipy-cholesterol, Avanti Polar Lipids; (4) palmitic acid (15-yne), palmitic-click, Avanti Polar Lipids. Cells were incubated for 24 h with 10 uM of each lipid.*

Initially a possible exchange of membrane lipids (Figure 1) between these cells as a result of their close direct contact was investigated. To study the lipid exchange between live cells, either naïve T cells (splenocytes) were labelled with clickable or fluorescent lipids and co-cultured with BMDC cultures or vice versa for 48 hours. Azides and alkynes are the archetypal bioorthogonal group due to their absence and small size respectively in biological systems.[33] The former can be modified using different bioorthogonal chemical reactions such as the copper-(I)-catalysed cycloaddition with terminal alkynes (CuAAC) with the smallest available modification highly suitable for lipid modification.[34–36] Flow cytometry of the population of T cells co-cultured for 48 hours with labelled-BMDC showed that T cells acquired membrane sterol from BMDC. Strikingly, this experiment showed a potent lipid-type dependence of exchange between them.

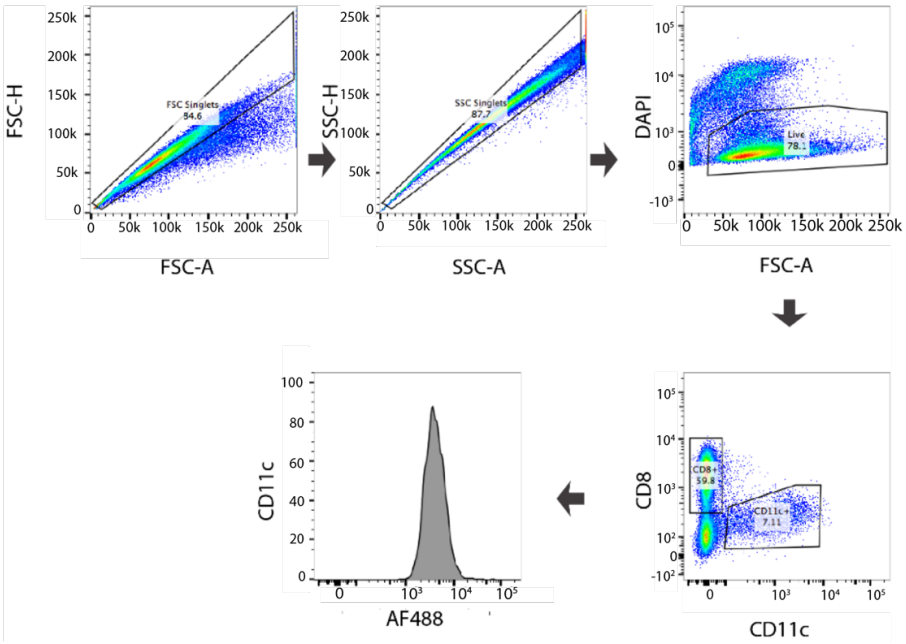

Figure 2 *The gating strategy used for the analysis of bone marrow derived dendritic cells (BMDCs) co-incubated with T-cells (splenocytes). Initially, cells were analysed for FSC-A versus FSC-H and SSC-A versus SSC-H to exclude doublet cells. The cells were then analysed with a live/dead (DAPI) staining versus FSC-A, and a gate was drawn to include all dye-negative cells. The combination of these gates served to analyse CD8 versus CD11c staining in the various samples. The mean fluorescent intensity (MFI) of the acceptor cell was measured, calculating the amount of the exchanged compounds.*

The aim of co-culturing BMDCs (acceptor) with naïve T cells (donor) was to gather evidence regarding the significance of their membrane component interactions *in vitro*. BMDCs co-cultured with T cells stimulate the generation of mature cells and influence certain stages of immune cell development (Figure 2). To determine whether cell-cell contact, soluble lipids or exosome exchange[37–39] was the predominant route of exchange, the unlabelled and labelled populations of cells were separated from one another in a trans-well assay.[20] In this system, the rates of exchange were found to be abolished when the cells were separated by a 0.4 μm membrane. The results showed that, in order for

the BMDCs to apply those interactions with T cells, direct cell-cell contact must exist between them. Fixation of the donor cell's membrane using paraformaldehyde (PFA) inhibits the transfer of membrane components between cells (Figure 3). Cells treated with unmodified bodipy-488 and co-cultured at 37 °C for 24 hours with unlabelled cells showed no exchange of fluorescence (Figure 3).

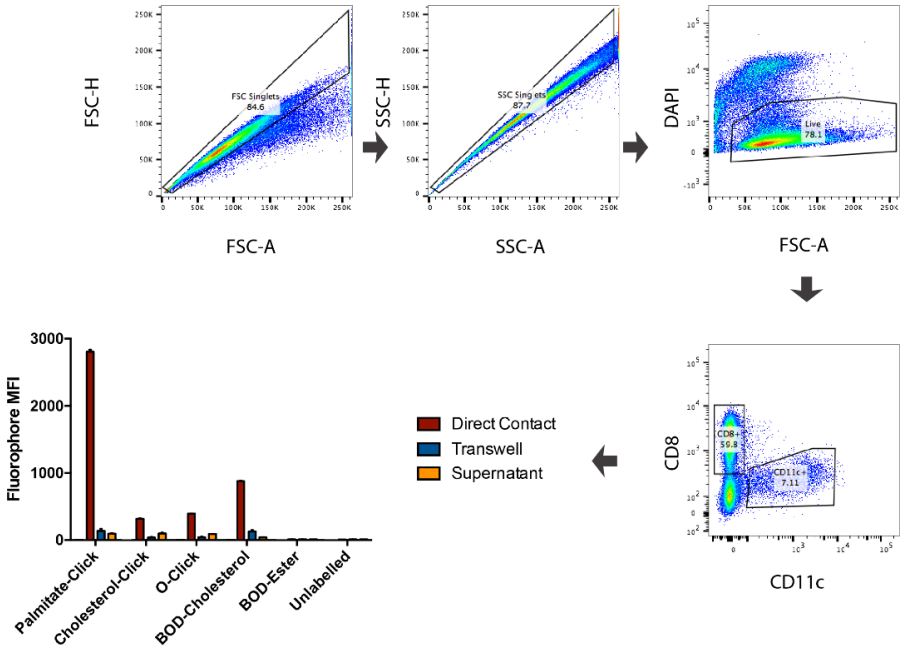

Figure 3 *Cells were analysed based on the protocol described in Figure 2. The MFI of the acceptor cell was measured, calculating the amount of the exchanged compounds. Red: direct contact between BMDC (acceptor) and CD8 (donor); Blue: transwell assay; labelled T cells were separated by a 0.4 µm membrane from unlabelled BMDC and incubated for 48 h. Flow cytometry analysis showed no lipid exchange; Yellow: supernatant exchange. T cells were incubated with different lipids: (1) Alkyne-Cholesterol, Cholesterol-Click; (2) Cholesterol propiolic acid, O-Click ;* (3) *TopFluor® Cholesterol, Avanti Polar Lipids, BOD-Cholesterol; (4) palmitic acid (15-yne), Avanti Polar Lipids, Palmitic-Click) all at final concertation 10 µM. After 1 h, cells were washed 3 times and the supernatant collected and added to an unlabelled population of splenocytes for 48 h. The absence of labelling was observed. Cells labelled with a live/dead dye, antibody surface staining (CD11c for BMDC and CD8 for T cells), and after PFA 1% fixation, with CuAAC. A control fluorophore bodipy ester at final concertation of 10 µM used. Data expressed as mean ± SEM (n=3) and is representative of 3 independent experiments. **p <0.01, unpaired t-test.*

Thereafter the previous protocol was applied in order to study whether the presence of an epitope and the subsequent activation of T cells was playing a role in the lipid exchange. Thus, OT-I transgenic T cells, which express a T-cell receptor (TCR) that recognises SIINFEKL, were co-cultured with BMDC. OT-I cells were treated with **1** (Alkyne-cholesterol, Ch-Alk) or **4** (palmitic acid (15-yne)) at final concertation of 10 μM with or without the addition of 10 nM SIINFEKL and co-cultured with BMDC for 24 hours. Fluorescence microscopy and flow cytometric analysis was used in order to confirm the importance of the epitope in the membrane exchange as well as to localise the uptaken lipids. At the end of the incubation, cells were gently removed, labelled with CuAAC and tested by flow cytometry for fluorescence increase of BMDC as a result of lipid exchange with OT-I. Lipid transfer occurred only upon the presence of the epitope SIINFEKL, indicating that the T-cell activation is vital for the membrane compound exchange. Cells were also co-cultured in a microscopy chamber plate in order to visualise the exchanged lipids. After the T cells were removed, the residual adherent BMDCs were directly examined by fluorescence microscopy to investigate the localisation of the transferred lipids from the OT-I to the BMDC (Figure 4).

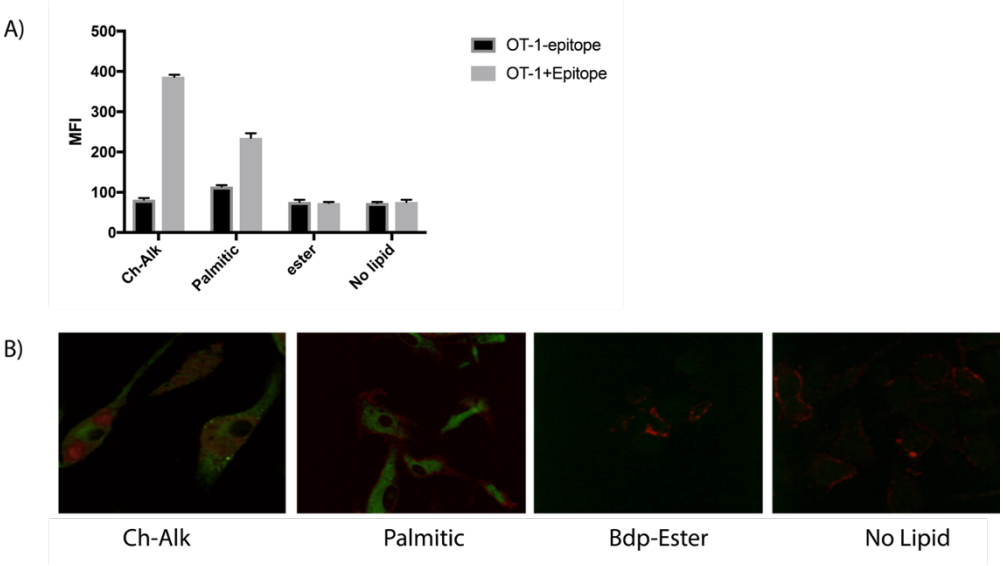

Figure 4 *Membrane transfer between OT-I and BMDC cells increased in the presence of SINFEEKL epitope. OT-I cells were labelled with different lipids (**1** Alkyne-cholesterol, Ch-Alk, Avanti Polar Lipids; **4** palmitic acid (15-yne), Avanti Polar Lipids) at final concentration of 10 μM, with or without the addition of 10nM SIINFEKL, and co-cultured with BMDC for 24 h. Cells labelled with CuAAC (click solution comprised of 1 mM CuSO4, 100 μM TTMA ligand, 2 mM sodium ascorbate and 2 μM Alexa Fluor® 488 azide). (A) MFI of unlabelled BMDC after co-culture. Increase of the fluorescence intensity indicated the lipid transfer from the OT-I cells. Data shows the MFI of BMDC cells expressing CD11C. (B) Confocal microscopy images indicate the localisation of the transferred lipids from the OT-I to the BMDC after SIINFEKL treatment. A control fluorophore bodipy ester at final concentration of 10 μM was used. Data expressed as mean ± SEM (n=3) and is representative of 3 independent experiments. **p <0.01, unpaired t-test.*

4.3 Conclusions

Previous results suggested that cell membrane lipids might not be equally transferred during cell-cell contact. However, there does appear to be a specific rate of selectivity in the classes of cell membrane components transferred from antigen-presenting cells to T cells. The precise mechanism of exchange between these cells requires further study, but likely requires the formation of a synapse after direct contact between donor and acceptor cells. It has been shown that abnormalities in T-cell development could be affected by the capture

of membrane fragments such as lipids. This study demonstrates that BMDCs can perform capture of membrane lipids. These findings could lead to alternative approaches to the exchange of membrane lipids in immune cells, focusing on manipulating the targeting lipids for restricting undesirable processes, in order to understand immunotherapies.

4.4 Experimental methods

Reagents

Cholesterol and all other chemical reagents were purchased at the highest grade available from Sigma-Aldrich and used without further purification. All solvents were purchased from Biosolve. Phosphate buffered saline (PBS): 5 mM KH_2PO_4, 15 mM K_2HPO_4, 150 mM NaCl, pH 7.4. Silica gel column chromatography was performed using silica gel grade 40-63 μm (Merck). TLC analysis was performed using aluminium-backed silica gel TLC plates (60_F 254, Merck), visualisation by UV absorption at 254 nm and/or staining with $KMnO_4$ solution. NMR spectra (^1H and ^{13}C) were measured on a Bruker AV-400MHz spectrometer at ambient temperature at the Leiden Institute of Chemistry NMR facility. Electrospray LC-MS analysis was performed on a PE SCIEX: API 3000 LC/MS/MS system using a Gemini 3u C18 110A analytical column (5μ particle size, flow: 1.0 ml/mins), on which the absorbance was measured at 214 and 254 nm. Solvent system for LC-MS: A: 100% water, B: 100% acetonitrile, C: 1% TFA (aq). TFA (aq). Fluorophore Alexa Fluor® 488 Azide was purchased from Thermo Fisher Scientific. Compounds 1 (Alkyne-Cholesterol, Cat No: 700146, CAS 1631985-09-5, Avanti Polar Lipids), 3 (TopFluor® Cholesterol, Cat No: 810255, CAS: 878557-19, Avanti Polar Lipids) and 4 (Palmitic acid (15-yne), Cat No: 900400, CAS: 99208-90-9, Avanti Polar Lipids) were

commercially available. Compound 2 was prepared in full accordance with the reported procedure.[40] Samples were imaged with a Leica TCS SP8 confocal microscope (63x oil lens, N.A.=1.4).

Flow cytometry[41]

Flow cytometry assays were performed using the Merck Guava® easyCyte 12HT Benchtop Flow Cytometer and all flow cytometry data was analysed using FlowJo™ v10.1 (FlowJo, LLC). Counting and characterization was performed by measuring 10,000 events in triplicate and concatenation of this data. For manual gating, the outermost ring of the dot plot was selected. Quadrants were manually selected to illustrate fluorescence plots.

Co-culturing BMDC with naïve T cells

All mice were bred and maintained under specific pathogen-free conditions under protocols approved by the Animal Welfare Committee of the Max Planck Institute of Immunobiology and Epigenetics, Freiburg, Germany. Mice used in all *in vitro* and *in vivo* experiments were 6–10 weeks of age and were age/sex matched.

Bone marrow derived dendritic cells (BMDC) were generated from 6 mice bone marrow. Bone marrow was flushed from femurs and tibia and cells were cultured in a complete RPMI supplemented with 8% heat-inactivated foetal calf serum, 20 μM 2 Mercaptoethanol, 2 mM glutamax, 50μg/mL streptomycin and 100 l.U./mL penicillin and in the presence of 20 ng/mL GM-CSF (Peprotech, cat #315-03-250). Medium was replaced on day 3 of culture and the cells were used between day 6 and 7.

Spleens were isolated from the same mice and single-cell suspensions prepared by filtering through a 70 μm filter, followed by red blood cell lysis (RBC Lysis Solution, Qiagen). For the T-cell stimulation, 5 ug/mL aCD3 (BioXCell, clone 17A2, BE0002) in PBS were used. Thereafter aCD28 was added, at 0.5 ug/mL(BioXCell, clone 37.51, product number BE0291). Human IL-2 was used at a final concentration of 100 U/mL (Peprotech, cat #200-02-1000).

Splenocytes were then incubated with lipids **1**, **2**, **3** and **4** (final concentration 10 μM) for 24 hours. The cells were washed and co-cultured with BMDC for 48 hours, before being collected and labelled with a live/dead dye, antibody surface staining (CD11c for BMDC and CD8 for T cells), and after PFA 1% fixation, with CuAAC (for the cells treated with lipids **1**, **2** and **4**). The click solution comprised of 1 mM CuSO4, 100 μM TTMA [(Tris((1-((O-ethyl)carboxymethyl)-(1,2,3-triazol-4-yl))methyl)amine] ligand, 2 mM sodium ascorbate and 2 μM Alexa Fluor® 488 azide (Invitrogen). After 20 minutes, the cells were washed three times with PBS, prior to incubation with 3% BSA (bovine serum albumin) for 30 minutes to remove unreacted fluorophore. The cells were then washed and flow-cytometry was performed.

Co-culturing BMDC with OT-I T cells (SINFEEKL)

Immature dendritic cells were obtained from the bone marrow of 12-week-old C57BL/6 mice under specific pathogen-free conditions. The mice were euthanized by cervical dislocation; bone marrow of tibiae and femurs was flushed out and washed with PBS. Cells were grown in dendritic cell selection medium (IMDM containing granulocyte-macrophage colony stimulating factor (GM-CSF) (2:1 v/v) containing 8% FCS, penicillin/streptomycin (100 units/mL), glutamax (2 mM) and β-mercaptoethanol (20 μM). The cells were incubated in non-

adhesive petri dishes at 37 °C, 5% CO_2, under humidified air. Cells were selected for 10 days (37 °C; 5% CO2) and subcultured every two to three days before use in the assays.

OT-I T cells were provided by M. Camps (Leiden University Medical Centre) from OT-I/CD45.1 mice spleen. OT-I cells were labelled with different lipids (**1** Alkyne-Cholesterol, Ch-Alk, Avanti Polar Lipids; **4** palmitic acid (15-yne), Avanti Polar Lipids at final concentration 10 μM) for 24 hours with or without the addition of 10 nM SIINFEKL (kindly provided by Dr. Joanna B. Pawlak). Cells were washed and then co-cultured with BMDC for 48 hours. Thereafter cells were collected and labelled with an antibody surface staining (CD11c for BMDC and CD8 for T cells), and after PFA 1% fixation, with CuAAC (for the cells treated with lipids **1**, **2** and **4**). The click solution comprised of 1 mM CuSO4, 100 μM TTMA [(Tris((1-((O-ethyl)carboxymethyl)-(1,2,3-triazol-4-yl))methyl)amine] ligand, 2 mM sodium ascorbate and 2 μM Alexa Fluor® 488 azide (Invitrogen). After 20 minutes, the cells were washed three times with PBS, prior to incubation with 3% BSA for 30 minutes to remove unreacted fluorophore. The cells were then washed and flow cytometry and confocal microscopy performed.

Transwell assay

Donor T cells were prevented from being in direct contact with BMDC cells using a transwell 0.4 μm-pore membrane (Costar®). Splenocytes were seeded in a 6-well plate with full RPMI media with the addition of lipids **1**, **2**, **3** and **4** and cells incubated for 24 hours at 37 °C. T cells were washed and then re-suspended in DMEM media. Treated T cells (in 0.3 mL of medium) were added in the upper compartment (done in 6-well plates) and unlabelled BMDC cells (in 0.5 mL of medium)

placed in the lower chamber separated from targets. The inserts were then picked up using gloves and transferred onto the top of the unlabelled BMDC cell culture with the addition of 2 ml of fresh media into the inserts. The cells were incubated for 48 hours at 37 °C. Cells were then collected and labelled with a live/dead dye, antibody surface staining (CD11c for BMDC and CD8 for T cells), and after PFA 1% fixation, with CuAAC (for the cells treated with lipids **1**, **2** and **4**). The click solution comprised of 1 mM CuSO4, 100 μM TTMA [(Tris((1-((O-ethyl)carboxymethyl)-(1,2,3-triazol-4-yl))methyl)amine] ligand, 2 mM sodium ascorbate and 2 μM Alexa Fluor® 488 azide (Invitrogen). After 20 minutes, the cells were washed three times with PBS, prior to incubation with 3% BSA for 30 minutes to remove unreacted fluorophore. The cells were then washed and flow-cytometry was performed.

Synthesis of cholesterol propiolic acid (O-Chol) (2)

Cholesterol propiolic acid (**2**) was synthesised in full accordance with the reported procedure.[40] A solution of DMAP (0.01 eq) and DCC (1 eq) in dichloromethane was added slowly over 30 minutes by syringe to a solution of propiolic acid (1 eq) and a cholesterol (1.1 eq) in dichloromethane at 0 °C to give a dark reddish suspension. The mixture was allowed to stir at room temperature until the acid was consumed (determined by TLC). Upon completion, the mixture was filtered through a layer of celite, the filtrate concentrated in vacuo. The crude product was purified by column chromatography (Rf=0.5, hexane/EtOAc 9:1) to afford **2** as a yellowish solid (40%). 1H NMR (300 MHz, $CDCl_3$): d=5.4 (d, 1H), 4.70 (dd, 1H), 2.80 (s, 1H), 2.40 (dd, 2H), 2.00–0.80 (m, 38H), 0.7 ppm (s, 3H); LC-MS (ESI): m/z calcd for $C_{30}H_{46}O_2$: 439.35 [M+H]+; found: 439.36.

4.5 References

1 S. Daubeuf, M. A. Lindorfer, R. P. Taylor, E. Joly and D. Hudrisier, *J. Immunol.*, 2010, **184**, 1897–1908.

2 A. Anel, A. Gallego-Lleyda, D. de Miguel, J. Naval, L. Martínez-Lostao, A. Anel, A. Gallego-Lleyda, D. de Miguel, J. Naval and L. Martínez-Lostao, *Cells*, 2019, **8**, 1–15.

3 M. Mittelbrunn and F. Sánchez-Madrid, *Nat. Rev. Mol. Cell Biol.*, 2012, **13**, 328–335.

4 J. West and P. K. Newton, *Proc. Natl. Acad. Sci. U. S. A.*, 2019, **116**, 1918–1923.

5 D. M. Davis, *Nat. Rev. Immunol.*, 2009, **9**, 543–555.

6 F. Zeng and A. E. Morelli, *Semin. Immunopathol.*, 2018, **40**, 477–490.

7 A. K. Horst, K. Neumann, L. Diehl and G. Tiegs, *Cell. Mol. Immunol.*, 2016, **13**, 277–292.

8 E. Jash, P. Prasad, N. Kumar, T. Sharma, A. Goldman and S. Sehrawat, *Cell Commun. Signal.*, 2018, **16**, 1–9.

9 M. L. Dustin, M. W. Olszowy, A. D. Holdorf, J. Li, S. Bromley, N. Desai, P. Widder, F. Rosenberger, P. A. van der Merwe, P. M. Allen and A. S. Shaw, *Cell*, 1998, **94**, 667–677.

10 A. Kupfer, C. R. F. Monks, B. A. Freiberg, H. Kupfer and N. Sciaky, *Nature*, 1998, **395**, 82–86.

11 R. E. Cone, J. Sprent and J. J. Marchalonis, *Proc. Natl. Acad. Sci. U. S. A.*, 1972, **69**, 2556–2560.

12 D. M. Davis, *Nat. Rev. Immunol.*, 2007, **7**, 238–243.

13 D. Hudrisier, J. Riond, H. Mazarguil, J. E. Gairin and E. Joly, *J. Immunol.*, 2001, **166**.

14 C. Théry, L. Zitvogel and S. Amigorena, *Nat. Rev. Immunol.*, 2002, **2**, 569–579.

15 J. Reed and S. A. Wetzel, *J. Immunol.*, 2019, **202**, 2873–2887.

16 C. Chiozzini, E. Olivetta, M. Sanchez, C. Arenaccio, F. Ferrantelli and P. Leone, *J. Mol. Med.*, 2019, **97**, 1139–1153.

17 D. Hudrisier, B. Kessler, S. Valitutti, C. Horvath, J. C. Cerottini and I. F. Luescher, *J. Immunol.*, 1998, **161**, 553–562.

18 J. Tabiasco, E. Espinosa, D. Hudrisier, E. Joly, J.-J. Fournié and A. Vercellone, *Eur. J. Immunol.*, 2002, **32**, 1502–1508.

19 S. Daubeuf, A. Aucher, C. Bordier, A. Salles, L. Serre, G. Gaibelet, J.-C. Faye, G. Favre, E. Joly and D. Hudrisier, *PLoS One*, 2010, **5**, e8716.

20 D. Poulcharidis, K. Belfor, A. Kros and S. I. van Kasteren, *Chem. Sci.*, 2017, **52**, 12081–12085.

21 C. Cassioli and C. T. Baldari, *Cells*, 2019, **8**, 2–25.

22 A. Ortega-Carrion and M. Vicente-Manzanares, *F1000Research*, 2016, **5**, 1–11.

23 F. Finetti, C. Cassioli and C. T. Baldari, *F1000Research*, 2017, **6**, 1–9.

24 E. M. Sletten and C. R. Bertozzi, *Angew. Chemie - Int. Ed.*, 2009, **48**, 6974–6998.

25 K. Lang and J. W. Chin, *Bioconjug. Chem.*, 2014, **9**, 16–20.

26 C. Besanceney-Webler, H. Jiang, T. Zheng, L. Feng, D. Soriano del Amo, W. Wang, L. M. Klivansky, F. L. Marlow, Y. Liu and P. Wu, *Angew. Chem. Int. Ed. Engl.*, 2011, **50**, 8051–8056.

27 A.-L. Puaux, J. Campanaud, A. Salles, X. Préville, B. Timmerman, E. Joly and D. Hudrisier, *Eur. J. Immunol.*, 2006, **36**, 779–788.

28 S. Daubeuf, A. Aucher, S.-G. Sampathkumar, X. Preville, K. J. Yarema and D. Hudrisier, *Immunol. Invest.*, 2007, **36**, 687–712.

29 A. Machlenkin, R. Uzana, S. Frankenburg, G. Eisenberg, L. Eisenbach, J. Pitcovski, R. Gorodetsky, A. Nissan, T. Peretz and M. Lotem, *Cancer Res.*, 2008, **68**, 2006–2013.

30 A. K. Späte, H. Bußkamp, A. Niederwieser, V. F. Schart, A. Marx and V. Wittmann, *Bioconjug. Chem.*, 2014, **25**, 147–154.

31 M. Hölttä-Vuori, R. L. Uronen, J. Repakova, E. Salonen, I. Vattulainen, P. Panula, Z. Li, R. Bittman and E. Ikonen, *Traffic*, 2008, **9**, 1839–1849.

32 K. Hofmann, C. Thiele, H.-F. Schött, A. Gaebler, M. Schoene, Y. Kiver, S. Friedrichs, D. Lütjohann and L. Kuerschner, *J. Lipid Res.*, 2014, **55**, 583–591.

33 V. Hong, N. F. Steinmetz, M. Manchester and M. G. Finn, *Bioconjugate Chem.*, 2010, **21**, 1912–1916.

34 M. Grammel and H. C. Hang, *Nat. Chem. Biol.*, 2013, **9**, 475–84.

35 E. Saxon, S. J. Luchansky, H. C. Hang, C. Yu, S. C. Lee and C. R. Bertozzi, *J. Am. Chem. Soc.*, 2002, **124**, 14893–902.

36 S. J. Luchansky, H. C. Hang, E. Saxon, J. R. Grunwell, C. Yu, D. H. Dube and C. R. Bertozzi, *Methods Enzymol.*, 2003, **362**, 249–72.

37 S. Beloribi, E. Ristorcelli, G. Breuzard, F. Silvy, J. Bertrand-Michel, E. Beraud, A. Verine and D. Lombardo, *PLoS One*, 2012, **7**, e47480.

38 K. A. Ahmed and J. Xiang, *J. Cell. Mol. Med.*, 2011, **15**, 1458–1473.

39 S. H. Jalalian, M. Ramezani, S. A. Jalalian, K. Abnous and S. M. Taghdisi, *Anal. Biochem.*, 2019, **571**, 1–13.

40 S. Kohrt, N. Santschi and J. Cvengroš, *Chem. - A Eur. J.*, 2016, **22**, 390–403.

41 H. M. Shapiro, *Practical Flow Cytometry*, John Wiley & Sons, New Jersey, Fourth., 2003.

5

In vitro supramolecular modification of L-form bacteria using lipidated coiled-coil peptides

5.1 Introduction

The biotechnology industry enjoys more success and influence than ever before.[1,2] Biotechnological innovations and discoveries help to improve the quality of life worldwide. Industrial biotechnology uses microorganisms to produce chemicals, materials and energy.[3,4] One of the most important producers are actinomycetes, which are best known for producing a plethora of useful compounds.[5,6] Among them are about two-thirds of all antibiotics that are used in the clinic, as well as various antifungals, anthelmintics and anti-tumour agents.[7,8] Despite this vast arsenal of useful metabolites, we are facing a massive challenge concerning the alarming increase in the number of bacteria that have become insensitive to virtually all antibiotics.[9–11] Therefore, there is a need to find new antimicrobials and new biotechnological production methods. For example, elimination of the cell wall could

increase the secretion of proteins and prevent the synthesis of cell-wall fragments which can have toxic immune-stimulatory effects.[9,12,13] This has also spurred interest in finding new compounds in numerous ways, for instance by isolating compounds from untapped sources,[8,14] or by cultivating different organisms together.[15] The latter could induce activation of biosynthetic gene clusters that are otherwise inactive.[16] Co-cultures could potentially also lead to novel chemical structures due to the combined biochemical activity of the organisms that grow together. However, finding suitable conditions for co-culturing can be problematic and time-consuming when more than two different organisms are involved. This severely limits its use on a large scale.

An attractive alternative to synthetic communities is to create synthetic hybrid cells, which contain chromosomes of different organisms equipped with a multitude of biosynthetic gene clusters. One factor that makes a fusion between cells complicated is the presence of the cell wall, which envelopes bacteria and protects them from harsh environmental conditions. In theory, protoplasts, which are generated by enzymatically degrading the cell wall, could be used. Indeed, protoplast fusion has been used in the past in classical strain crossing approaches but is limited to closely related species. Furthermore, protoplasts are intrinsically unstable and will immediately regenerate a cell wall, thereby effectively making them fusion-incompetent.[17–19] A better alternative would be to use cells that can indefinitely propagate without their cell wall. This alternative dramatically increases the time and thus likelihood for fusion to take place. These variants, called L-forms (or L-phase, L-phase bacteria, or cell-wall-deficient bacteria (CWD), have been generated from a broad range of bacteria, including the antibiotic-producing actinomycetes, by inhibiting crucial steps in the biosynthesis pathway of the cell wall (Figure 1).[13,18,20] L-forms

morphology is adaptable and allows cells to surpass environmental difficulties, for example, hyperosmotic stress conditions or treatment with antibiotics.[21] The complete absence of the cell wall has critical physiological consequences: like protoplasts, L-form cells are highly sensitive to osmotic changes and require high levels of sucrose for osmoprotection.[9] Additionally, the proliferation of such L-form cells no longer depends on the highly organised cell-division machinery, but is based on simple biophysical principles.[7,17,22] Claessen *et al.* have expanded on this research by providing proof that cell-wall-deficient strains can propagate solely under hyperosmotic stress conditions.[9] This evidence is a milestone for the environmental relevance of such bacteria.[9] As a result, these cells have been suggested to resemble primordial life forms that existed well before the cell wall evolved.

Cell-cell fusion can be achieved by a variety of approaches, including chemical, biological and physical methods.[23] Membrane fusion is a controlled process in nature and shows a broad variety, from viral and eukaryotic to extracellular fusion, and is regulated by a variety of functional proteins.[24] Previously, fusion of plant protoplasts was induced by polyethylene glycol (PEG)[19] and since then it has been applied in many different applications including mammalian-cells fusion for the development of hybridomas, albeit with very low efficiency.[25] During neuronal exocytosis, transport vesicles are being docked to the plasma membrane by the formation of coiled-coils within complementary SNARE protein subunits, located on the cell membrane.[24,26] Moreover, SNARE proteins have been associated with the formation of autophagosome and also have been identified between mammalian and fungus cells.[27] Additionally, SNARE proteins function in the processes of small shuttling vesicles like neuronal exocytosis, or bigger transport containers such as the proenzyme

granules of pancreatic cells. In this process, complementary SNARE protein subunits present on opposing membranes assemble into an interacting structure by coiled-coil formation.[28-34] As a result this assembly drives the facing cell membranes into close proximity, resulting eventually in lipid mixing and associated content transfer.

The application of supramolecular concepts *in vitro* and *in vivo* in order to study the impact in biological processes is relatively new. One approach includes chemically adjusted systems being inserted into cell membranes in order to modify or regulate cellular behaviours via external synthetic signals.[35] Lipidated peptides have been used extensively in biological systems because their behaviour can be carefully regulated by modifying the cargo's hydrophilicity and the anchor's hydrophobicity resulting in membrane incorporation.[36] However, typically, this procedure disrupts normal cell function of the resulting hybrid cells, and the number of surviving cells is very low.[37] To overcome this barrier, a simple and straightforward biomimetic model system inspired by the eukaryotic SNARE proteins was used. Many different synthetic systems have been designed in order to imitate membrane fusion. However, the essential characteristics of natural membrane fusion are not always achieved; for example coupled surface recognition, helical coiled-coil formation and disruption of the contact site which is followed by fusion; i.e. content and lipid mixing.[38-40] An entirely artificial membrane fusion system which retains the essential characteristics of SNARE-mediated fusion has been designed by the Kros laboratory and consists of a pair of lipidated coiled-coil peptides (Scheme 1).[28,41-44] In this system, the complementary lipid-peptide conjugates (CPK_3 and CPE_3) are comprised of the peptides K_3 [(Lys-Ile-Ala-Ala-Leu-Lys-Glu)$_3$] and E_3 [(Glu-Ile-Ala-Ala-Leu-Glu-Lys)$_3$], which are linked via a polyethylene

glycol (PEG) spacer to a cholesterol moiety (Scheme 2). As a result these lipidated peptides readily insert into the membrane bilayer due to the hydrophobic cholesterol anchor (Scheme 1).[45]

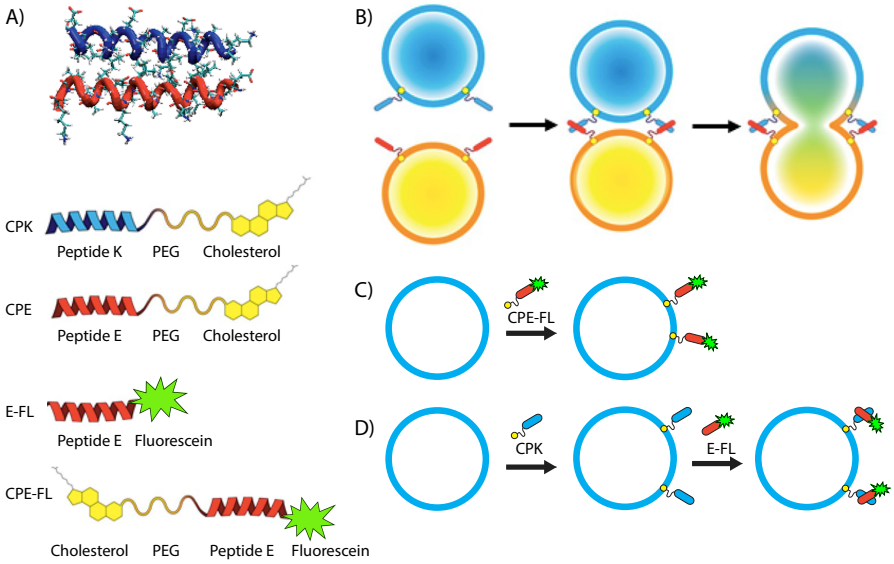

Scheme 1 A peptide-mediated model system for membrane fusion. (A*) The coiled-coil structure of peptides E and K (adapted from PDB 1UOI), the lipidated peptides CPE and CPK, fluorescently labelled peptide E-FL and the fluorescently labelled lipidated peptide CPE-FL. (B) Targeted L-form bacteria fusion mediated by coiled-coil formation between CPE modified L-forms and CPK modified L-forms. While the two populations are mixed (left), coiled-coils are formed between the two complementary peptides (middle), and cell fusion occurs (right). (C) Insertion of fluorescently labelled lipidated E peptide (CPE-FL) into plain alpha L-form bacteria membrane. (D) CPK inserts into plain alpha L-form bacteria membrane, and coiled-coil is formed with the fluorescently labelled peptide E. (Images are not to scale)*

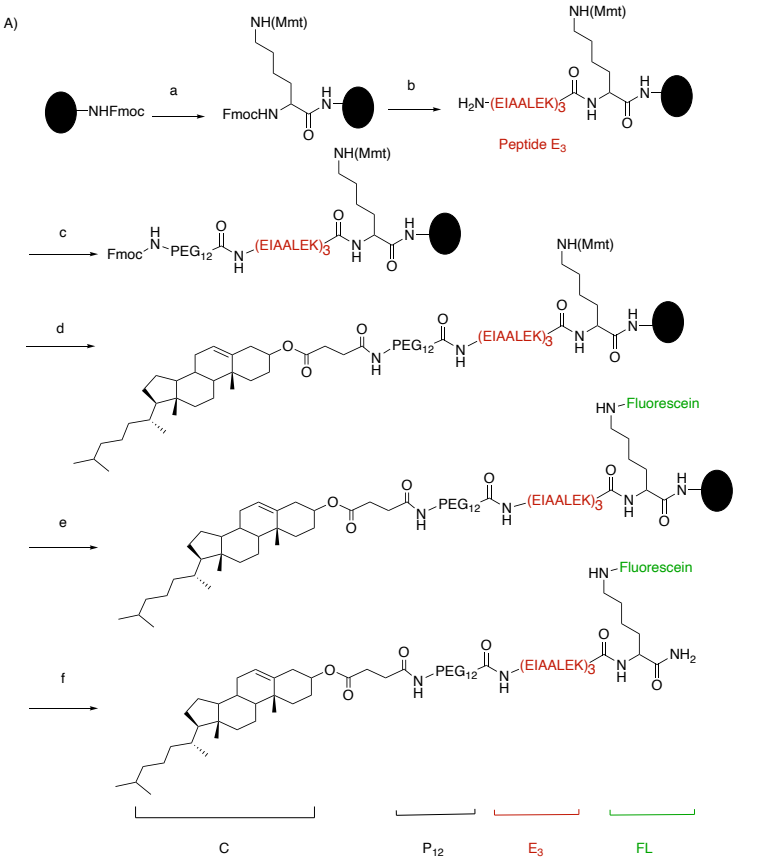
A)
NH(Mmt)
NHFmoc
a
FmocHN
b
H2N-(EIAALEK)3
Peptide E3
c
Fmoc
PEG12
(EIAALEK)3
d
e
HN-Fluorescein
f
NH2
C
P12
E3
FL
B)
g
H2N-(KIAALKE)3
Peptide K3
h
i
j
(KIAALKE)
K3

Scheme 2 *Synthetic procedure of lipopeptide CPE-FL (A) and CPK (B). (A) Reagents and conditions: a) (1) Resin deprotection using 20% piperidine in DMF, rt, 30 mins; (2) Fmoc-Lys(mmt)-OH, HOBt, DIC, DMF, overnight, rt; b) solid phase peptide synthesis; c) Fmoc-PEG$_{12}$-COOH, HOBt, DIC, DMF, overnight, rt; d) (1) 20% piperidine in DMF, rt, 30 mins; (2) cholesteryl hemisuccinate, HOBt, DIC, DMF, overnight, rt; e) (1) 1% TFA/DCM, rt, 10 mins (3 times); (2) 5(6) Carboxyfluorescein, HOBt, DIC, DMF, overnight, rt; f) TFA/TIS/H2O (95:2.5:2.5 v/v) for 1.5 h. (B) Reagents and conditions: g) solid phase peptide synthesis; h) Fmoc-PEG$_{12}$-COOH, HOBt, DIC, DMF, overnight, rt; i) (1) 20% piperidine in DMF, rt, 30 mins; (2) cholesteryl hemisuccinate, HOBt, DIC, DMF, overnight, rt; j) TFA/TIS/H2O (95:2.5:2.5 v/v) for 1.5 h.*

In this chapter a supramolecular approach was applied to induce coiled-coil formation at the surface of L-form bacterial membranes (Scheme 1). In turn this allows an extensive variety of molecules to be conjugated onto the L-form outer surface via noncovalent interactions. In the first step, the lipidated coiled-coil peptides CPE/CPK insert immediately into the cell membranes due to the cholesterol moiety via hydrophobic interactions while the PEG_{12} spacer provides the sufficient flexibility which is needed to facilitate potent molecular recognition between the two complementary coiled-coil peptides. For this, a solution of the cholesterol-modified peptide E or the cholesterol-modified peptide K was added to L-forms, resulting in the spontaneous integration of these peptides into the L-form membrane. In the second step, the complementary coiled-coil peptide was added resulting in coiled-coil formation.

This chapter presents evidence – for the first time – of surface modification of living L-form cells, as a first step towards to L-form fusion, using cell-compatible coiled-coil peptides. L-form modification resulting in fusion will enable the study of fundamental questions related to the origin of cellular complexity, regeneration of different actinomycetes, and strain improvements.

5.2 Results and discussion

Initially, testing was done to ascertain whether the L-form bacterial membrane incorporates cholesterol-modified coiled-coil peptides. In order to demonstrate coiled-coil formation at the surfaces of L-form bacteria, the ability of the cholesterol moiety to insert into the L-form membrane was investigated. Alpha L-forms (wild-type non-fluorescence L-forms (1000 cells/ μL) derived from actinomycetes) were incubated for 30 minutes with carboxyfluorescein-labelled CPE (CPE-FL) at a final concentration of 5 μM. Subsequently, confocal microscopy and flow cytometry were used to visualise and quantify CPE incorporation within the treated cells. As expected, L-forms became highly fluorescent, indicative of successful CPE-FL incorporation (Figures 1 and 2).

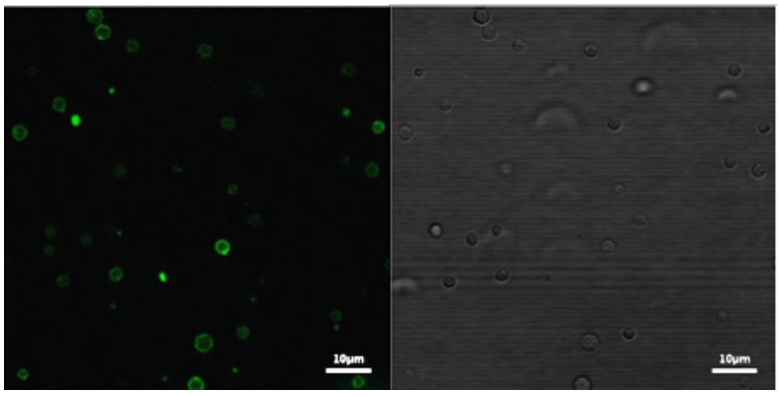

Figure 1 *Confocal microscopy images (fluorescence, bright field) of alpha L-forms cells. The L-forms were treated with 5 μm final concentration of fluorescently labelled CPE (CPE-FL) at 37 °C. After 30 mins confocal microscopy images were taken. Scale bar: 10 μm.*

An investigation was then undertaken into whether the peptides at the L-form surface were accessible for coiled-coil formation with complementary peptide K. For this, alpha L-forms were incubated with fluorescent coiled-coil peptides in the presence or absence of a cell membrane anchor. A 5 μM CPK solution was added to L-forms for 30 minutes and unbound CPK was removed by washing the L-forms. The L-forms were then incubated for 10 minutes with a 10 μM solution of carboxyfluorescein- labelled peptide E (FL-E). After three washing steps in order to remove any free FL-E, confocal microscopy and flow cytometry were used to visualise and quantify the efficiency of modification of the treated cells. As expected, the membrane of the L-forms was highly fluorescent, indicating that the CPK was successfully incorporated. When addition of CPK to L-forms was omitted, no fluorescence could be observed (Figure 2A). This confirmed successful coiled-coil formation between the CPK inserted into the L-form membrane and peptide FL-E. Furthermore, the reversed path also resulted in coiled-coil formation by first adding lipidated peptide CPE to the L-forms, followed by incubation with the fluorescently labelled peptide K (FL-K) (Figure 2A).

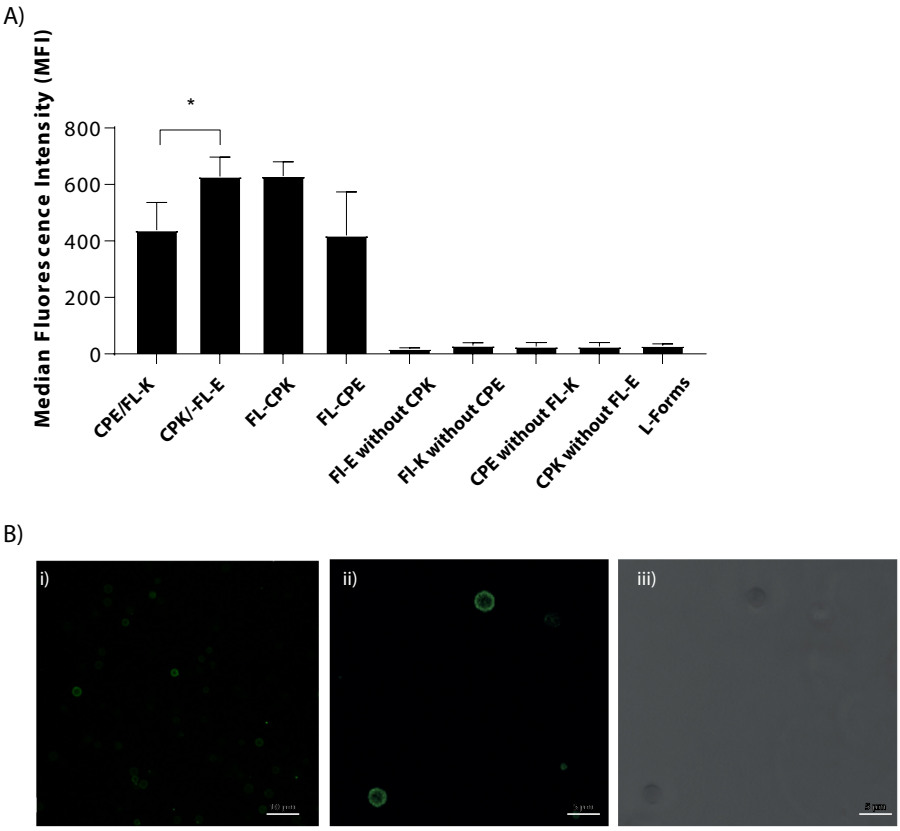

Figure 2 *Alpha L-form bacteria incubated with different types of fluorescent peptides. (A) Flow cytometry indicates coiled-coil labelling of L-form membrane. (B) Confocal microscopy images of CPK/FL-E modified L-forms (i scale bar: 15 µm; ii-iii scale bar: 5 µm). The assay was set up in triplicate. Data are represented as median ± SD. Error bars SD; *p < 0.05; **p < 0.01; ***p < 0.001.*

Thus, the membranes of cell-wall-deficient bacteria can be modified by this system without using complicated and time-consuming protocols such as protein engineering.[46–48] Not only can the required coiled-coil peptides be synthesised within a day but this overall supramolecular approach for cell membrane modification is also fast. To date, the exact membrane composition of L-form bacteria is not known, and membrane biophysics could influence the lipid insertion. However, L-forms treated with either CPK-FL or CPK/FL-E showed around

1.5-fold higher fluorescence intensity than the respective L-forms which were treated with CPE-FL or CPE/FL-K (Figure 2A). This flow cytometry analysis seems to indicate that the membrane composition favours the positively charged peptide K over the negatively charged peptide E. Nevertheless, more studies are needed in order to clarify the individual behaviour of these coiled-coil peptides at the L-form surface.

These initial studies demonstrated the formation of coiled-coils at the surface of L-form bacteria by directly adding a cholesterol peptide-conjugate in the L-Form bacteria medium, followed by the incubation with the complementary peptide. This enables the docking of different molecules and nanoparticles on the surface of bacteria using this method. Kros *et al.* have shown that by the formation of coiled-coils between peptides E and K, 100 nm liposomes can be bound at surfaces of various materials.[49] Also, coiled-coils mediate docking of liposomes on mammalian cells *in vitro* as well as *in vivo* on the surface of one-day-old zebrafish embryos.[29,41,45] For this reason, it was interesting to study whether liposome docking is also possible at a cell-wall-deficient bacterial membrane. For this, the membrane of L-form bacteria was functionalised with CPK, and next fluorescent liposomes containing 1 mol% SR-B (sulforhodamine B) and 1 mol% CPE were added for 5–10 minutes. Moreover, in the same set-up, in order to accelarate the liposome-fusion events polyethylene glycol 1000 (PEG1000) was used as an additional fusogenic agent. It has been reported that during PEG-induced cell fusion (in concentrations between 30-50% w/w PEG) polyethylene glycol brings cell membranes into closer distance via dehydration and redistribution of intramembrane particles (IMPs).[50] Viability and fluorescent assays performed showed that concentration higher than 10% w/w of PEG could influence membrane integrity

(Figures 4 and 5). Thus, L-form bacteria were either incubated in the presence or absence of 5% w/w PEG1000 for one hour at 37 °C before liposome addition. Excess PEG1000 was removed and the cells were washed three times before the flow cytometry assay (Figure 3).

In this chapter flow cytometry was used to characterize L-form fusion events and this technique is briefly introduced here. In flow cytometry, forward scattered light (FSC) is related to the size of the particles, side scattered light (SSC) to their complexity and granularity.[51–53] The small size of the L-forms could pose a limitation for flow cytometry examination, mainly because of the difficulty to distinguish between cellular debris and small cells. Both fluorescence and forward scatter were used as dual trigger signals in order to successfully deal with this problem.[51,53] The properties measured include a particle's relative size (SSC-A vs. FSC-A), relative granularity (SSC-A vs. FSC-A) and relative fluorescence intensity. FSC presents an appropriate method of recognising particles greater than a given size without taking into consideration their fluorescence. [51–53]

Flow cytometry data from the L-form/liposome-docking assay revealed that the L-form bacterial membranes became fluorescent (Figure 3). In a control experiment, CPE liposomes were added to non-treated L-forms (i.e. no CPK pre-incubation) and, as expected, no fluorescence was observed (Figure 3). This confirms that using a complementary coiled-coil pattern, liposomes can be docked efficiently at the membranes of L-form bacteria. However, it was difficult to distinguish docking from fusion.

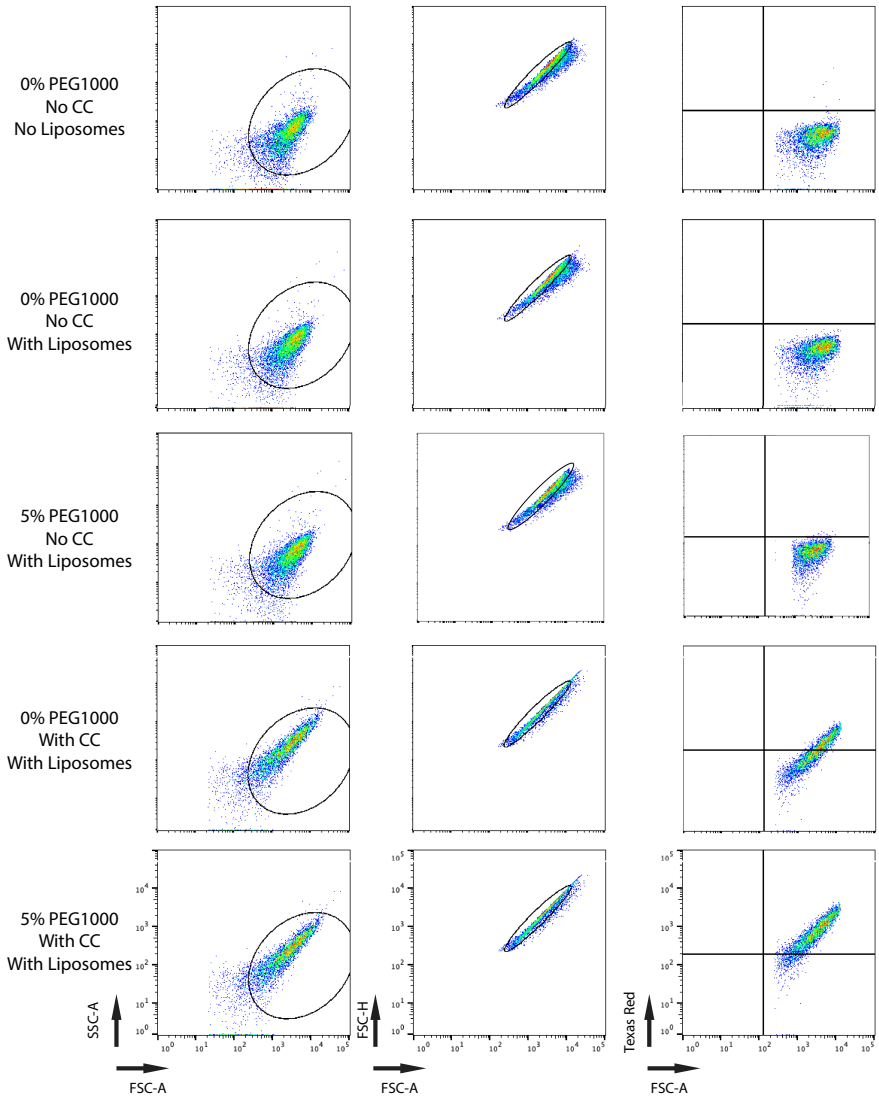

Figure 3 *Flow cytometry shows liposomes docking at the surface of L-form bacteria. CPE-decorated liposomes (total lipid concentration 0.25 mM with 1 mol% lipidated peptide CPE) loaded with 20 mM sulphorhodamine (SR-B) were added to the L-forms, without prior addition of CPK peptides. L-forms were treated with 5 μM final concentration of lipidated peptide CPK and were incubated for 5 mins. Subsequently, lipidated CPE-decorated liposomes (total lipid concentration 0.25 mM with 1 mol% lipidated peptide CPE) loaded with 20 mM sulphorhodamine (SR-B) were added to the L-forms. The L-form bacteria were incubated with or without 5% w/w PEG1000 for 1 h at 37 °C, before the excess PEG1000 was removed. All the experiments were performed at 37 °C.*

Next, the viability of modified L-forms as well as the effect of polyethylene glycol 1000 (PEG1000) on L-form/L-form fusion was examined. For this, fluorescent derivative L-form strains constitutively expressing green fluorescent protein (eGFP) were created. The L-forms were incubated together with different concentrations of PEG1000 (0, 5, 10 % w/w) for one hour at 37 °C (Figure 4). Excess PEG1000 was removed and the L-forms were studied with confocal microscopy and flow cytometry measurements. This showed that 10% w/w PEG1000 disintegrates the L-form membrane resulting in loss of fluorescence (Figures 4 and 5A). In a separate experiment, L-form bacteria were treated with coiled-coil peptides and incubated together in the presence of different concentrations of PEG1000 (0, 5, 10 % w/w).L-forms were then plated on solid l-phase medium (LPMA) and it was observed that some of the cells generated colonies, implying that these L-forms can proliferate (Figure 5). In addition, a live/dead viability assay was applied in order to visualise the viability of treated L-forms as an outcome of their membrane integrity. L-forms with an intact membrane will stain green (Cyto9, Figure 6), whereas dead or dying L-forms with a damaged membrane will stain red (PI). 10% w/w of PEG1000 dissociated the L-form membrane resulting in PI staining, whereas only Cyto9-labelled L-forms were observed when 5% w/w PEG1000 was used instead. In summary, this study showed that L-forms can proliferate after membrane modification.

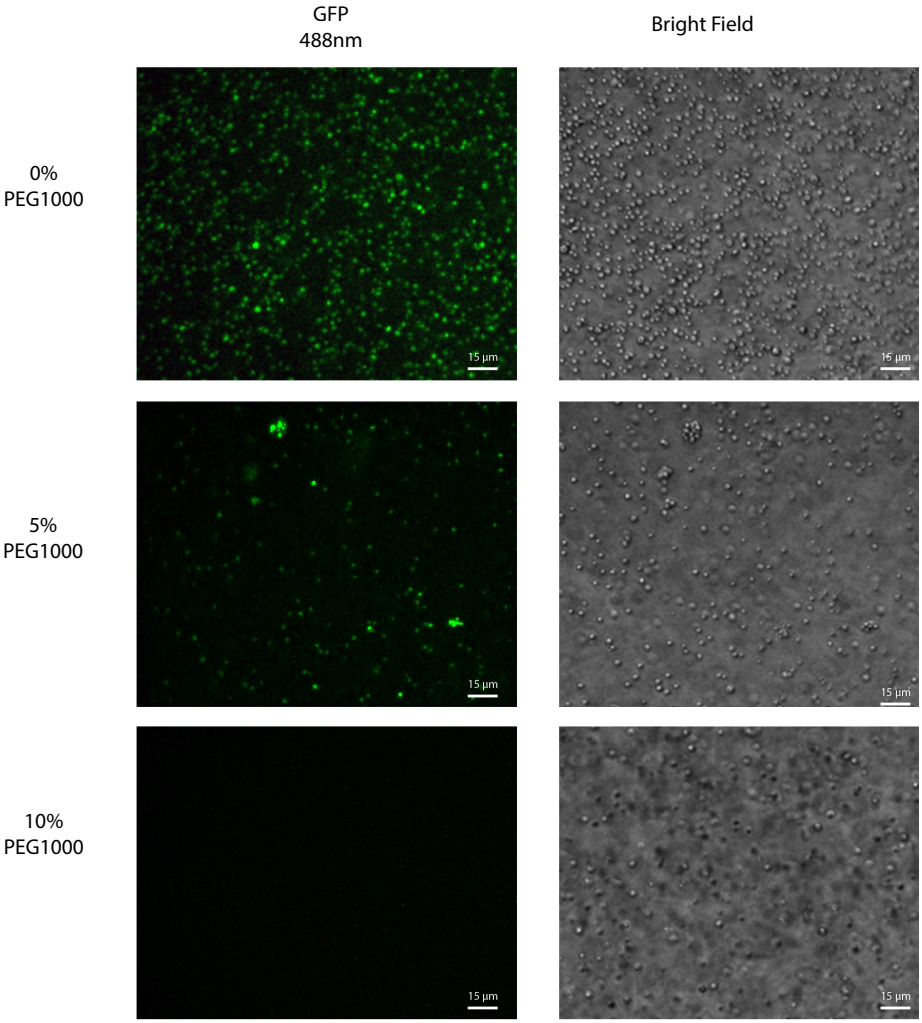

Figure 4 *Confocal microscopy images indicate that a high concentration of PEG1000 is dissociating the L-form membrane. GFP expressing L-form bacteria were treated with different concentrations of PEG1000 (0, 5, 10 % w/w) for 1 h at 37 °C. The excess PEG1000 was removed before confocal microscopy. Scale bar: 15 µm.*

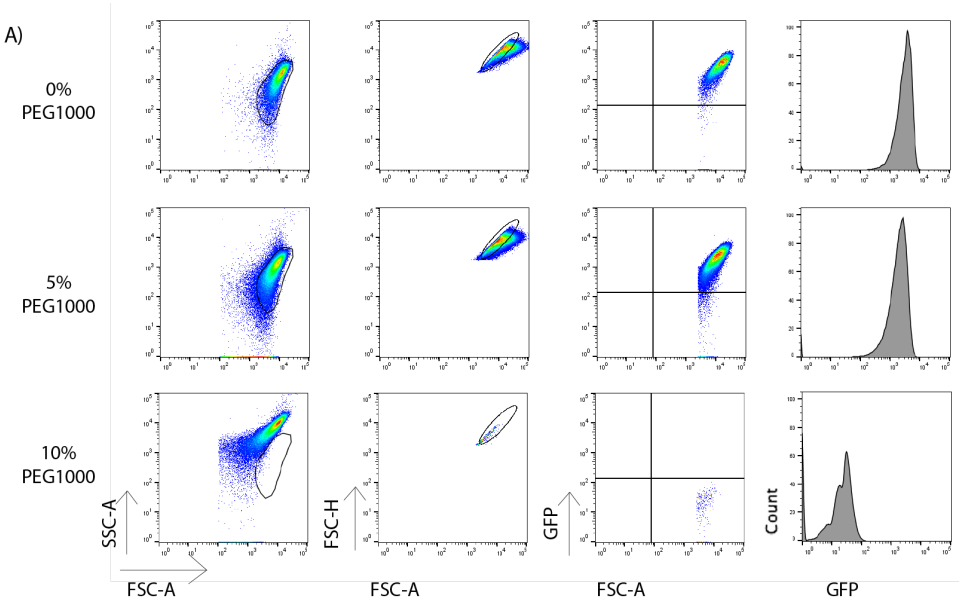

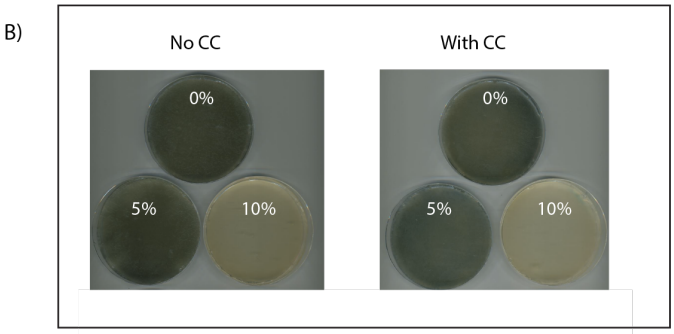

Figure 5 *Flow cytometry and agar plates assay indicate that a high concentration of PEG1000 is dissociating the L-form membrane. (A) GFP expressing L-form bacteria treated with different concentrations of PEG1000 before confocal microscopy. (B) Agar plates with treated L-form bacteria showed the effect of PEG1000 on their viability. L-form bacteria were treated with coiled-coil peptides and were then incubated together with different concentrations of PEG1000 (0, 5, 10 % w/w) for 1 h at 37 °C. The excess PEG1000 was removed. L-form bacteria were plated on agar plates in order to observe colony formation.*

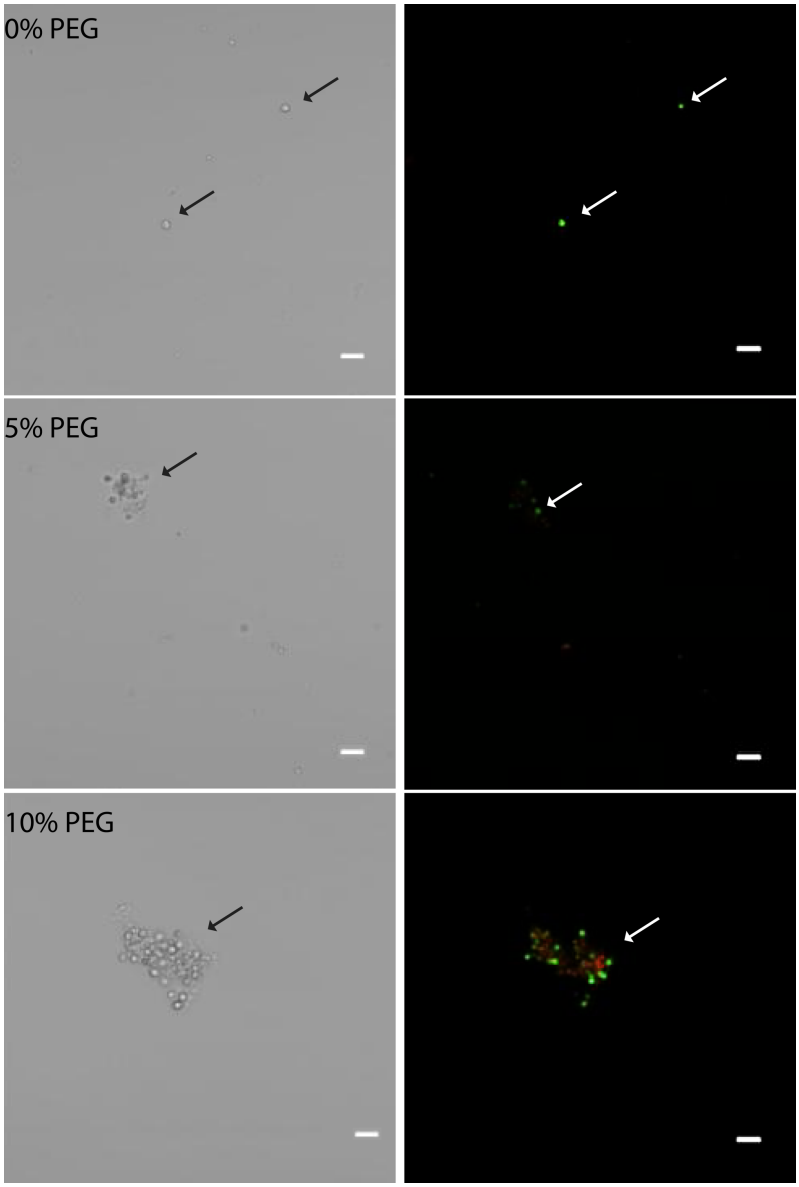

Figure 6 *Confocal microscopy images indicate that a high concentration of PEG1000 is dissociating the L-form membrane. Viability labelling analysed with confocal microscopy using SYTO9/PI. Fluorescence images of the same samples at 528 nm for SYTO9 signal (green) and 645 nm for PI signal (red) are shown. L-form bacteria were labelled with PI and SYTO9. L-form bacteria were treated with coiled-coil peptides and were then incubated together with different concentrations of PEG1000 (0, 5, 10 % w/w) for 1 h at 37 °C. The excess of PEG1000 was removed. Dead L-form bacteria exhibit yellow or red fluorescence. Arrows point L-form bacteria. Scale bar: 10 μm.*

Next, a study was undertaken to ascertain whether the lipopeptides CPE/CPK could induce L-form fusion using flow cytometry in combination with confocal microscopy, as PEG-induced L-form fusion is inefficient. Genetically modified L-form strains constitutively expressing either mCherry or eGFP were created for this experiment. Next, mCherry- and GFP-expressing L-forms were incubated with 10 μM of the lipidated coiled-coil peptides CPK and CPE respectively for 30 minutes, and any unbound lipopeptide was removed by washing the L-forms with media. In order to minimise L-form disruption during the washing steps, the cultures were collected and centrifuged at 2000 g for five minutes. Afterwards, the supernatant was carefully removed by decantation to avoid disturbance of the cells, and the cells resuspended in fresh LPB.[9] These mCherry and GFP L-forms were mixed and incubated with concentrations of PEG1000 (0 or 5 % w/w) for one hour at 37 °C. Excess of PEG1000 was removed by centrifugation twice and replaced with fresh LPB media. Wojcieszyn *et al.* observed that fusion event occurs at PEG concentrations around 50% w/w.[50] Therefore, as a positive control, L-forms were incubated with 50% w/w PEG1000 (Figure 7). In this experiment, L-form aggregation was observed by confocal microscopy and flow cytometry. Unfortunately, fused L-forms were not observed.

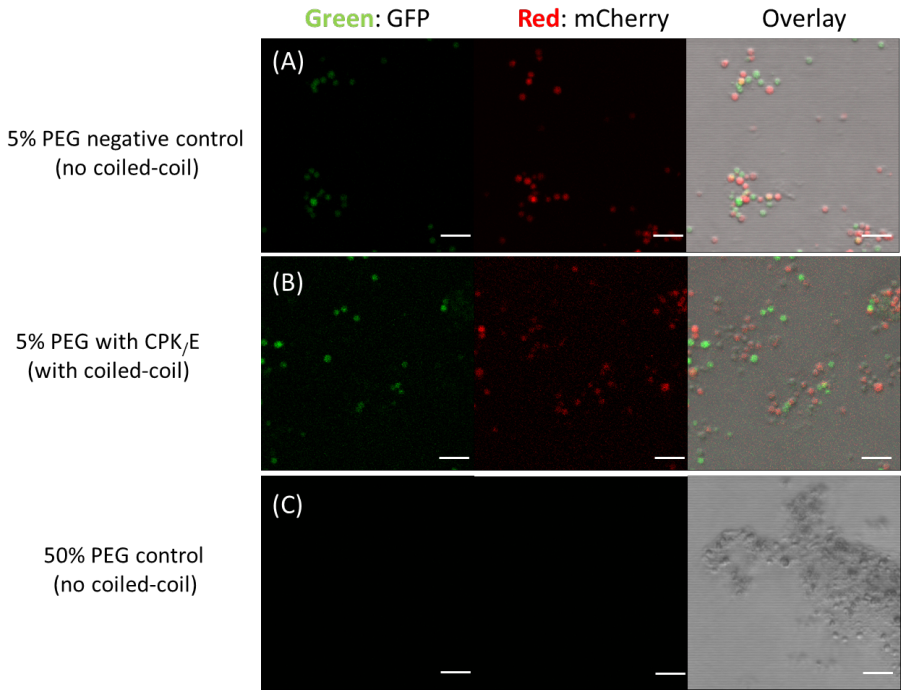

Figure 7 *Cell-cell fusion using CPE/CPK-mediated coil-coil formation combined with 5% PEG1000. L-forms were incubated in the presence of 5% PEG1000 without lipopeptides (A) or with 10 μM lipopeptides (B). GFP expressed L-forms were decorated with CPE and, upon mixing, mCherry expressed L-forms were decorated with CPK. Scale bar: 10 μm.*

Based on the light scattering characteristics, different populations of L-form bacteria were detected in the flow cytometry experiment: unfused/singlets, doublets/aggregates or fused cells. Singlets or aggregates of L-forms can be distinguished by their intrinsic characteristics. Flow cytometry results showed that there is a distinction between the effects of PEG1000 and coiled-coil modification (Figure 8). However, it was challenging to distinguish between fused with aggregated L-forms. It was assumed that PEG1000 induces aggregation and/or fusion of L-form bacteria, while the addition of lipidated coiled-coil peptides enhance the fusion (or aggregation) efficiency 3-fold. However, more control experiments are

required to confirm that L-form fusion occurred. For example, the effect of different salt concentrations or higher concentrations of coiled-coil peptides, with different PEG spacers and/or lipid moieties could have a more significant effect on L-form fusion. Moreover, as the molecular weight of polyethylene glycol (PEG) has a different effect on membranes[56], PEG with different molecular weights; (i.e. 400 Da, 6000 Da and/or 20000 Da) could be used as polymeric additives. Alternatively, antibiotic-resistant L-forms could be created and a dual-antibiotic selection applied to screen for fused L-forms.

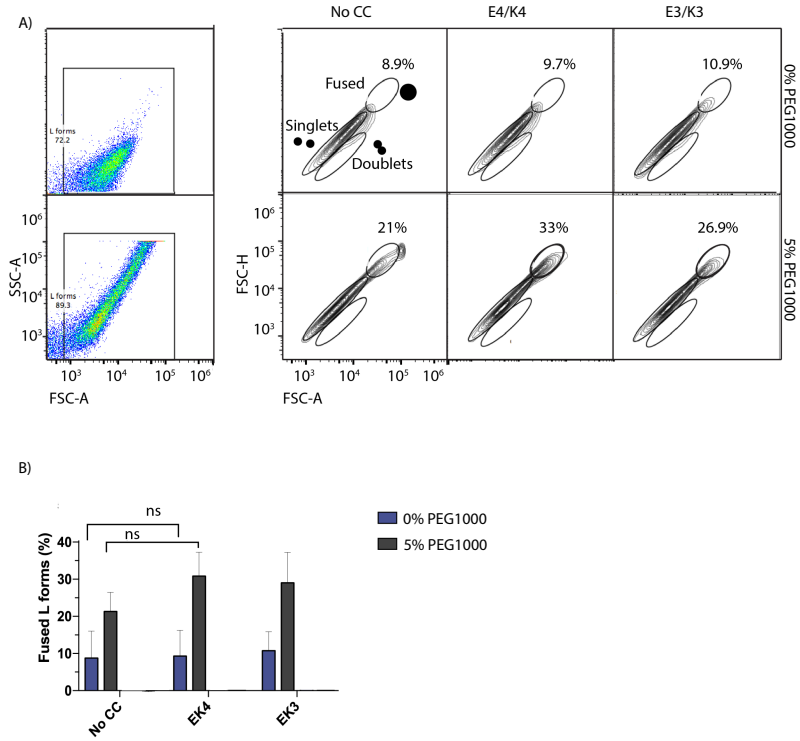

Figure 8 *Quantification of L-form fusion using flow cytometry. (A) Dot and contour plots of windows and gating strategy used for the identification of unfused singlets or doublets of L-forms present in the L-form population. The percentages indicate the relative amount of gated L-forms (Singlets, Doublets, Fused). (B) Plots of flow cytometry analyses showing the number of L-forms from the tail-end of FSC(H)-FSC(A) plots (potentially fused) depending on the concentration of PEG1000 and different coiled-coil peptides. The assay was set up in triplicate. Data are representing as percentage ± SD. *p < 0.05; **p < 0.01; ***p < 0.001*

5.3 Conclusions

A tool to modify the surface of L-form bacteria quickly and effectively was developed. A supramolecular method was used, with a complementary coiled-coil-forming peptide pair, in order to functionalise the membranes of L-form bacteria. Liposome docking tests proved that this approach can also be used to bind a wide variety of materials/molecules on the L-form membrane. This generic method demonstrates that living L-form bacteria can efficiently be aggregated using a combination of SNARE protein mimics and PEG1000. It is expected that PEG1000 may promote the initiation of the fusion event by membrane dehydration, after which the coiled-coil peptides could facilitate the actual membrane fusion event. Because of the small size of the bacteria as well as light scattering limitations, it was difficult to distinguish aggregated from fused cells. To overcome these limitations in this experimental set-up, a double antibiotic selection assay could be designed to select for fused L-forms. Additionally, coiled-coil peptides with different PEG-spacers, different peptide length or lipid moieties might have a positive effect in L-form bacterial fusion. It is expected that this method will be able to induce fusion between L-form cells of distinct species, whereby the chemistry of two living cells is merged into a new cell. Successful fusion and regeneration of different actinomycetes strains at high frequency would facilitate the discovery of new antibiotics and microbial strain improvement.

5.4 Experimental methods

Method and materials

Rink amide resin, Fmoc-protected amino acids, and 2-(6-Chloro-1-H-benzotriazole-1-yl)-1,1,3,3-tetramethylammonium hexafluorophosphate (HCTU) were purchased from Novabiochem. Trifluoroacetic acid (TFA), piperidine, diisopropylethylamine (DIPEA), N-methyl pyrrolidine (NMP), acetic anhydride, acetonitrile and dimethylformamide (DMF) were obtained from Biosolve. Triisopropylsilane (TIS), dichloromethane (DCM), diethyl ether, trimethylamine (TEA), cholesterol, succinic anhydride and sulforhodamine B were obtained from Sigma-Aldrich. 1,2-dioleoyl-sn-glycero-3-phosphocholine (DOPC) and 1,2-dioleoyl-glycerol-3-phosphatidylethanolamine (DOPE) were purchased from Avanti Polar Lipids. Cholesteryl hemisuccinate and 5,6-Carboxyfluorescein were obtained from Sigma-Aldrich. The Fmoc–Lys(MMT)–OH was purchased from VWR. The Fmoc–NH–$(PEG)_{12}$–COOH spacers were purchased from Iris Biotech. PBS buffer contains 15 mM K_2HPO_4, 150 mM NaCl, 5 mM KH_2PO_4 and has pH 7.4. The polyethylene glycol 1000 (PEG1000) was purchased from Merck Millipore.

Preparation of L-forms[9]

Bacterial strains (actinomycete *Kitasatospora viridifaciens*) used in this study were obtained from the Claessen Lab.[9] To support growth of cell-wall-deficient (CWD) cells, strains were grown on solid medium L-phase medium (LPMA), containing 20% sucrose, 0.5% glucose, 0.5% peptone, 0.01% MgSO4·7H2O, 0.5% yeast extract, 0.75% Iberian agar (all w/v). After autoclaving, the medium was supplemented with $MgCl_2$ (final concentration of 25 mM) and 5% (v/v) horse serum. L-phase broth (LPB) was used as a liquid medium to support the growth

of wall-deficient cells. LPB contains 0.25% bacto-peptone, 0.15% yeast extract, 0.15% oxoid malt extract, 0.64 M sucrose, 0.5% glucose, 1.5% oxoid tryptic soy broth powder (all w/v) and 25 mM $MgCl_2$. Cultures were incubated at 30 °C while shaking at 100 rpm.[9]

1*10[8] L-forms/ml with mCherry (red-fluorescent protein) expressed were incubated with 10 μM CPK, and 1*10[8] L-forms/ml with GFP (green-fluorescent protein) expressed were incubated with 10 μM CPE for 30 minutes, then modified L-forms were washed with medium twice for, followed by the addition of 50% w/w PEG1000 stock medium, and medium results in L-forms incubated with different concentrations of PEG1000 (0%, 5%, 10% w/w).

Confocal microscopy imaging

L-forms were seeded in an 8-well slide (μ-Slide 8 well; Ibidi, Munich, Germany) at a density of 1*105 L-forms per well in LBP. The fluorescent images were obtained using a Leica TCS SPE confocal laser scanning microscope (Leica Microsystems, Wetzlar, Germany) and analysed using the ImageJ software (National Institutes of Health, Bethesda, MD, USA). The wavelength settings for GFP and mCherry were Ex/Em: 488/510 nm (Ex laser: 488 nm) and 585/610 nm (Ex laser: 532 nm), respectively.

Flow cytometry[51–53]

L-forms were treated with 10 μM CPE/CPK peptides for 30 minutes, followed by two washing steps. In each washing step L-form cultures were collected and centrifuged at 2000 g for 5 minutes, before the supernatant was carefully removed by decantation and cells resuspended in fresh LPB. Then lipid-modified L-forms were incubated with different concentrations of PEG1000 (0%, 5%, 10% w/w). CPE-modified L-forms and CPK-modified L-forms were mixed and co-cultured for one hour at 37 °C. Flow cytometry assays were

performed using the Merck Guava® easyCyte 12HT Benchtop Flow Cytometer and all flow cytometry data were analysed using FlowJo™ v10.1 (FlowJo, LLC). Counting and characterization were performed by measuring 30,000 events in triplicate and concatenation of this data. For manual gating, the furthest ring of the dot plot was selected. Quadrants were selected manually to depict fluorescence plots. Compensation was not required.[51–53]

Any granular material inside the cell, cell shape and surface, as well as the nucleus are the main factors that can affect light scattering.[51–53] A heterogeneous cell population was differentiated using correlated measurements of side-scattered light (SSC) and forward-scattered light (FSC). The former is comparable to cell internal complexity or granularity, whereas the latter is comparable to the cell-surface area or size.[51–53]

Peptide synthesis

The cholesterol-modified peptides were synthesised as described elsewhere.[41] An automatic CEM peptide synthesiser on a scale of 250 μM was used for the synthesis of peptides K_3 $(KIAALKE)_3$ and E_3 $(EIAALEK)_3$. For the synthesis, Fmoc chemistry was applied, and rink amide resin with a loading of 0.69 mmol/g was used. Amino acid couplings were performed with 4 eq of the appropriate amino acid, 4 eq of the activator HCTU and 8 eq of the base DIPEA. Fmoc deprotection was performed with piperidine: DMF (4:6 v/v). Synthesis of fluorescently labelled peptides was performed on rink amide resin. After initial Fmoc deprotection using 20% piperidine in DMF, Fmoc-Lys (MMT)-COOH was coupled, using 4 eq of DIC and 4 eq of HOBt, for one hour. The resin was used to synthesise acetylated peptide E and K along with CPE using standard Fmoc chemistry

procedures described earlier.[28,41,44,55] Next, the side chain Lys(MMT) group was deprotected using TFA/ DCM (1%) for 10 minutes (3x). The resin was then neutralised using DIPEA/NMP (10:90 v/v) for 10 minutes (3x). 5(6)-Carboxyfluorescein (Sigma-Aldrich) was coupled using 4 eq of DIC, and 4 eq of HOBt dissolved in DMF and coupling was performed overnight. Fluorescently labelled lipopeptide was cleaved from the resin by shaking the resin with a mixture of TFA/TIS/H2O (95:2.5:2.5 v/v) for 1.5 hours. The cleavage mixture was precipitated in cold diethyl ether. The resulting fluorescently labelled crude products were purified by RP-HPLC using a Vydac C4 reversed phase column (214TP1022, 22 mm diameter, 250 mm length, 10 µm particle size). With a linear gradient from 20% to 80% of acetonitrile in water with 0.1% TFA (v/v) over 36 minutes with the flow of 20 mL/mins, the crude lipopeptides were eluted. Sample elution was detected by UV detection at 214 nm and 256 nm. By using LC-MS (Gemini 3 µ C18 column coupled with Finningan LCQ advantage max (Thermo) ESI-MS analyse), the purity of the collected fractions was verified.

$CP_{12}K_3$: LC-MS m/z Calcd. [1673.6, $M+2H]^{2+}$, found 1674.0. [1116.1, $(M+3H)^{3+}$], found 1116.5. $CP_{12}E_3$: LC-MS m/z Calcd. [1675.0, $M+2H]^{2+}$, found 1675.4. [1117.0, $(M+3H)^{3+}$], found 1117.4. Ac-$(EIAALEK)_3$K-Carboxyfluorescein (FL-E): LC-MS m/z Calcd. [1405.2, $M+2H]^{2+}$, Found 1405.6. [937.2, $(M+3H)^{3+}$], found 937.6. Ac-$(KIAALKE)_3$K-Carboxyfluorescein (FL-K): LC-MS m/z Calcd. [1403.8, $M+2H]^{2+}$, Found 1404.2. [936.2, $(M+3H)^{3+}$], found 936.6. Cholesterol-PEG12-$(EIAALEK)_3$K-carboxyfluorescein (CPE-FL): LC-MS m/z Calcd. [1918.1, $M+2H]^{2+}$, Found 1918.5. [1279.1, $(M+3H)^{3+}$], found 1279.5. Cholesterol-PEG_{12}-$(KIAALKE)_3$K-carboxyfluorescein (CPK-FL): LC-MS m/z Calcd. [1916.7, $M+2H]^{2+}$, Found 1917.1. [1278.1, $(M+3H)^{3+}$], found 1278.5.

Liposome sample preparation

Stock solutions of lipids with total concentration of 1 mM in $CHCl_3$ (DOPE/DOPC/CH, molar ratios 2:1:1) and 50 μM peptide (molar ratio 1:1 MeOH/ $CHCl_3$) were prepared. The peptide solutions were prepared by taking the appropriate amount of peptide stock, evaporating the solvent over a stream of air, adding Hanks' Balanced Salt solution (HBSS) followed by sonication for one minute at 55 °C. The liposomes were prepared by using appropriate amounts of lipid and peptide stock solutions, evaporating the solvent over a stream of air, adding HBSS and sonication for one minute at 55 °C.

5.5 References

1 D. E. Cameron, C. J. Bashor and J. J. Collins, *Nat. Rev. Microbiol.*, 2014, **12**, 381–390.

2 J. Li and W. E. Halal, *Nat. Biotechnol.*, 2002, **20**, 61–63.

3 S. W. Kim and H. Punnapayak, *Biotechnol. J.*, 2017, **12**, 1–2.

4 C. Chen and G. Reniers, *Adv. Biochem. Eng. Biotechnol.*, 2018, 1–25.

5 R. H. Baltz, *Antonie Van Leeuwenhoek*, 2001, **79**, 251–259.

6 K. Saparmyradov, S. Z. Validov, R. I. Tukhbatova, F. K. Alimova and M. N. Filimonova, *J. Comput. Theor. Nanosci.*, 2019, **16**, 216–222.

7 M. Leaver, P. Domínguez-Cuevas, J. M. Coxhead, R. A. Daniel and J. Errington, *Nature*, 2009, **457**, 849–53.

8 J. Bérdy, *J. Antibiot. (Tokyo).*, 2005, **58**, 1–26.

9 K. Ramijan, E. Ultee, J. Willemse, Z. Zhang, J. A. J. Wondergem, A. van der Meij, D. Heinrich, A. Briegel, G. P. van Wezel, D. Claessen, G. van Wezel and D. Claessen, *Nat. Commun.*, 2018, **9**, 5164–5177.

10 E. Banin, D. Hughes and O. P. Kuipers, *FEMS Microbiol. Rev.*, 2017, **41**, 450–452.

11 B. Aslam, W. Wang, M. I. Arshad, M. Khurshid, S. Muzammil, M. H. Rasool, M. A. Nisar, R. F. Alvi, M. A. Aslam, M. U. Qamar, M. K. F. Salamat and Z. Baloch, *Infect. Drug Resist.*, 2018, **11**, 1645–1658.

12 J. Errington, *Biochem. Soc. Trans.*, 2017, **45**, 287–295.

13 D. Claessen and J. Errington, *Trends Microbiol.*, 2019, (in press).

14 U. Aftab, D. L. Zechel and I. Sajid, *Biol. Res.*, 2015, **48**, 1–10.

15 S. T. Khan, H. Komaki, K. Motohashi, I. Kozone, A. Mukai, M. Takagi and K. Shin-ya, *Environ. Microbiol.*, 2011, **13**, 391–403.

16 R. H. Baltz, *J. Antibiot. (Tokyo).*, 2010, **63**, 506–511.

17 R. Mercier, Y. Kawai and J. Errington, *Cell*, 2013, **152**, 997–1007.
18 E. J. Allan, C. Hoischen and J. Gumpert, *Adv. Appl. Microbiol.*, 2009, **68**, 1–39.
19 K. N. Kao and M. R. Michayluk, *Planta*, 1974, **115**, 355–367.
20 R. Gleckman, A. Esposito and S. Madoff, *J. Clin. Microbiol.*, 1977, **5**, 225–226.
21 J. Errington, *Open Biol.*, 2013, **3**, 1–7.
22 P. Domínguez-Cuevas, R. Mercier, M. Leaver, Y. Kawai and J. Errington, *Mol. Microbiol.*, 2012, **83**, 52–66.
23 D. V. Gokhale, U. S. Puntambekar and D. N. Deobagkar, *Biotechnol. Adv.*, 1993, **11**, 199–217.
24 R. Jahn, T. Lang and T. C. Su, *Cell*, 2003, **112**, 519–533.
25 J. Yang and M. H. Shen, in *Nuclear Reprogramming*, Humana Press, New Jersey, 2006, 59–66.
26 R. Jahn and R. H. Scheller, *Nat. Rev. Mol. Cell Biol.*, 2006, **7**, 631–643.
27 K. Søreng, T. P. Neufeld and A. Simonsen, *Int. Rev. Cell Mol. Biol.*, 2018, **336**, 1–92.
28 H. Robson Marsden and A. Kros, *Angew. Chem. Int. Ed. Engl.*, 2010, **49**, 2988–3005.
29 J. Yang, A. Bahreman, G. Daudey, J. Bussmann, R. C. L. Olsthoorn and A. Kros, *ACS Cent. Sci.*, 2016, **2**, 621–630.
30 J. Yang, Y. Shimada, R. C. L. Olsthoorn, B. E. Snaar-Jagalska, H. P. Spaink and A. Kros, *ACS Nano*, 2016, **10**, 7428–7435.
31 D. Ungar and F. M. Hughson, *Annu. Rev. Cell Dev. Biol.*, 2003, **19**, 493–517.
32 H. M. Strauss and S. Keller, *Handb. Exp. Pharmacol.*, 2008, 461–482.
33 N. Lopez Mora, A. Bahreman, H. Valkenier, H. Li, T. Sharp, D. N. Sheppard, A. Kros and A. Davis, *Chem. Sci.*, 2016, **7**,

1768–1772.

34 W. Hong, *Biochim. Biophys. Acta - Mol. Cell Res.*, 2005, **1744**, 120–144.

35 B. R. Peterson, *Org. Biomol. Chem.*, 2005, **3**, 3607–3612.

36 F. Versluis, H. R. Marsden and A. Kros, *Chem. Soc. Rev.*, 2010, **39**, 3434–3444.

37 S. W. Hui, T. L. Kuhl, Y. Q. Guo and J. Israelachvili, *Colloids Surfaces B Biointerfaces*, 1999, **14**, 213–222.

38 A. Csiszar, N. Hersch, S. Dieluweit, R. Biehl, R. Merkel and B. Hoffmann, *Bioconjug Chem*, 2010, **21**, 537–543.

39 D. Dutta, A. Pulsipher, W. Luo, H. Mak and M. N. Yousaf, *Bioconjug. Chem.*, 2011, **22**, 2423–2433.

40 M. Ma and D. Bong, *Acc. Chem. Res.*, 2013, **46**, 2988–2997.

41 H. R. Zope, F. Versluis, A. Ordas, J. Voskuhl, H. P. Spaink and A. Kros, *Angew. Chem. Int. Ed. Engl.*, 2013, **52**, 14247–14251.

42 T. Zheng, J. Voskuhl, F. Versluis, H. R. Zope, I. Tomatsu, H. R. Marsden and A. Kros, *Chem. Commun.*, 2013, **49**, 3649–3651.

43 F. Versluis, J. Dominguez, J. Voskuhl and A. Kros, *Faraday Discuss.*, 2013, **166**, 349–359.

44 F. Versluis, J. Voskuhl, B. Van Kolck, H. Zope, M. Bremmer, T. Albregtse, A. Kros, B. van Kolck, H. Zope, M. Bremmer, T. Albregtse and A. Kros, *J. Am. Chem. Soc.*, 2013, **135**, 8057–8062.

45 L. Kong, S. H. C. Askes, S. Bonnet, A. Kros and F. Campbell, *Angew. Chemie - Int. Ed.*, 2015, **55**, 1396–1400.

46 M. K. Kang and D. Tullman-Ercek, *Methods*, 2018, 147, 66–72.

47 C. Saeui, M. Mathew, L. Liu, E. Urias and K. Yarema, *J. Funct. Biomater.*, 2015, **6**, 454–485.

48 C. A. Custódio and J. F. Mano, *ChemNanoMat*, 2016, **2**, 376–384.

49 J. Voskuhl, C. Wendeln, F. Versluis, E.-C. Fritz, O. Roling, H. Zope, C. Schulz, S. Rinnen, H. F. Arlinghaus, B. J. Ravoo and

A. Kros, *Angew. Chemie Int. Ed.*, 2012, **51**, 12616–12620.

50 J. W. Wojcieszyn, R. A. Schlegel, K. Lumley-Sapanski and K. A. Jacobson, *J. Cell Biol.*, 1983, **96**, 151–159.

51 H. M. Shapiro, *Practical Flow Cytometry*, John Wiley & Sons, New Jersey, Fourth., 2003.

52 G. C. Salzman, S. B. Singham, R. G. Johnston and C. F. Bohren, *Flow Cytom. Sorting*, 1990, 81–107.

53 H. M. Davey and D. B. Kell, *Microbiol. Rev.*, 1996, **60**, 641–96.

54 B. Chakrabarty, A. K. Ghoshal and M. K. Purkait, *J. Memb. Sci.*, 2008, **309**, 209–221.

55 E. Oude Blenke, J. Van Den Dikkenberg, B. Van Kolck, A. Kros and E. Mastrobattista, *Nanoscale*, 2016, **8**, 8955–8965.

6

In vivo and *in vitro* evaluation of a phospholipid ether analogue for the detection of tumours

6.1 Introduction

A primary goal in cancer research is the specific targeting and delivery of therapeutic agents or diagnostic imaging tools to tumours overpassing healthy tissues. Methods to achieve this goal are focusing on agents and tools already in development or approved, which target cell membrane. A wide variety of tumour-targeting methods has been developed based on nanoparticles, peptides, antibodies and viruses to deliver different cargos to cancer cells, for example imaging agents, radioactive isotopes and drugs.[1-6] To date, the available tools for cancer therapy can be placed in two categories: on the one hand are aspecific tools available for a wide variety of cancer types; i.e. radiation, surgery or chemotherapeutic drugs. On the other hand are cancer-specific tools based on the expression of genetic drug-targets in cancer cells

compared to healthy cells. Examples of the latter approach are targeting the epidermal growth factor receptor (EGFR) or the Philadelphia chromosome (BCR-ABL fusion).[7,8] In the clinic, many cancers reappear despite the advancement of novel treatments. Recent studies have shown that the cancer reappearance most likely occurs due to the cancer-cell resistance to the known therapies.[9–14] In addition, an ideal therapeutic model should eliminate the side effects on the healthy cells and incorporate cancer selectivity with an extensive anticancer mechanism.

In the late 1960s Snyder *et al.* performed an evaluation of the lipid composition of normal and neoplastic tissues.[15,16] These studies revealed that large quantities of ether lipids were found to be present in both animal and human tumour tissues. In the early 1980s, follow-up studies showed that cancer tissues expressed lower amounts of the O-alkyl glycerol monooxygenase enzyme AGMO (EC 1.14.16.5),[17] which could result in the accumulation of ether lipids in the membrane of hepatomas cells.[18] Subsequent studies in the early 2000s have shown that specific phospholipid ether (PLE) analogues which are not substrates for AGMO, also accumulate in breast, colon and pancreas tumours.[19–21]

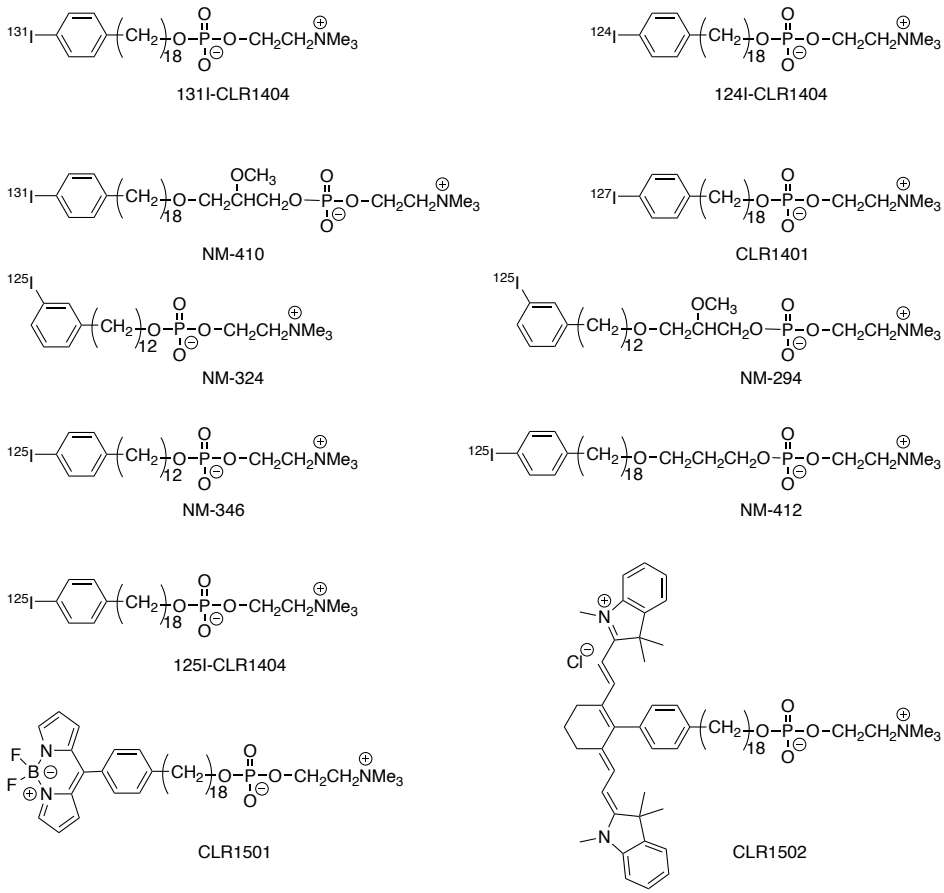

Figure 1 *Structures of phospholipid ether analogues (alkylphosphocholines; APC). A novel therapeutic platform is based on phospholipid ether analogues. Cellectar Biosciences has developed a phospholipid ether analogue-based platform that is currently being investigated for diagnostic and therapeutic oncologic applications. CLR1404 as a radioactive compound (^{125}I, ^{124}I, or ^{131}I), as a fluorescent analog (CLR1501), or as a near-infrared analog (CLR1502). ^{124}I-CLR1404 is currently under clinical investigation as a positron emission tomography (PET) tracer. CLR1502 is a near-infrared fluorescent labelled phospholipid ether analogue being investigated for regional imaging applications. [Structures reproduced from references: D. A. Deming, M. E. Maher, A. A. Leystra, J. P. Grudzinski, L. Clipson, D. M. Albrecht, M. K. Washington, K. A. Matkowskyj, L. T. Hall, S. J. Lubner, J. P. Weichert and R. B. Halberg,* PLoS One, *2014,* ***9****, e109668; and A. N. Pinchuk, M. A. Rampy, M. A. Longino, R. W. S. Skinner, M. D. Gross, J. P. Weichert and R. E. Counsell,* J. Med. Chem., *2006,* ***49****, 2155–2165.*]

Due to the avidity of these phospholipid ether analogues to accumulate in different tumours, they are being studied as therapeutic and diagnostic tools (Figure 1).[17,18,22–25] Recent studies have shown that the length of the phospholipid ethers plays an essential role in tumour docking in rat models. It has been reported by Pinchuk *et al.* that the alkyl chain of the PLE should have more than 11 methylene groups, and analogues with alkyl chain length between C15-C18 have the optimum tumour uptake in rat prostate cancer models.[26–28] Additionally, previous studies showed have shown that although the meta-iodinated alkylphosphocholine NM-324 (Figure 1) was more stable and giving high tumour uptake, it accumulated in nontarget tissues including bladder, kidneys and liver.[29] Therefore, the para-isomer NM-346 was used instead, which also displayed significant tumour uptake *in vivo*. Moreover, the PLE chain can be labelled with different therapeutic moieties or imaging markers.[29–31] The remarkable ability of specific radioiodinated PLE analogues to be visualised in different mammalian tumour cells using gamma camera (γ -camera) scintigraphy has been extensively described. For example, the radioisotope-labelled PLE analogue ^{124}I-18-(*p*-iodophenyl)octadecyl phosphocholine (CLR1404) is being used as a positron emission tomography (PET) tracer in patients with metastatic colon cancer.[27,29,32] Moreover, the PLE analogue CLR1502 has the same structure as CLR1404 but is labelled with a near-infrared fluorescent marker and is under investigation for oncologic imaging application, whereas the PLE analogue CLR1501 is labelled with a bodipy fluorescent marker (Figure 1). To date, the reason for the retention of PLE and analogues in cancer cells remains unknown, and the strategy for designing agents with such properties has been mostly empirical.[32,33] The hypothesis is that these PLE analogues have an affinity for tumour cell membranes because of their inability to be metabolised from cancer cells whereas

they are metabolised in healthy tissues.[34,35] These PLE analogues take advantage of the lipid composition of cell membrane as ports of entry into tumours.[36] This chapter reports on the synthesis of a modified fluorescent alkyl phospholipid ether analogue and its avidity to localise in different tumour cell lines *in vitro*. Moreover, the chapter describes – for the first time – the *in vivo* imaging testing of the modified fluorescent alkyl phospholipid in a zebrafish prostate cancer model.

6.2 Results and discussion

The synthetic approach taken here for the synthesis of the bodipy-labelled phospholipid ether analogue was based on the published procedure of Pinchuk *et al.*[29] and the copper(I)-catalysed alkyne-azide cycloaddition (CuAAC). To improve solubility and due to synthetic accessibility, the route was modified to include an alkoxy-group in C17 (Scheme 1). The building blocks were chosen based on their commercial availability of starting materials. Initially, the synthesis was started by the THP protection of 16-bromohexadecanol **1** to the 2-((16-bromohexadecyl)oxy)tetrahydropyran **2** as shown in Scheme 1. Next, the THP-protected halide **2** was further coupled with (4-azidophenyl) methanol in a Williamson ether reaction. The 16-((4-azidobenzyl)oxy) alcohol **4** obtained after THP-deprotection. This alcohol was converted into the corresponding azido-benzyloxy-alkylphosphocholine **5** according to published procedures.[26,29,37] Fluorescent coupling with bodipy-488 was accomplished by a copper-catalysed cycloaddition method routinely employed in our laboratory resulting in the bodipy-488-labelled alkylphosphocholine **6**.[38]

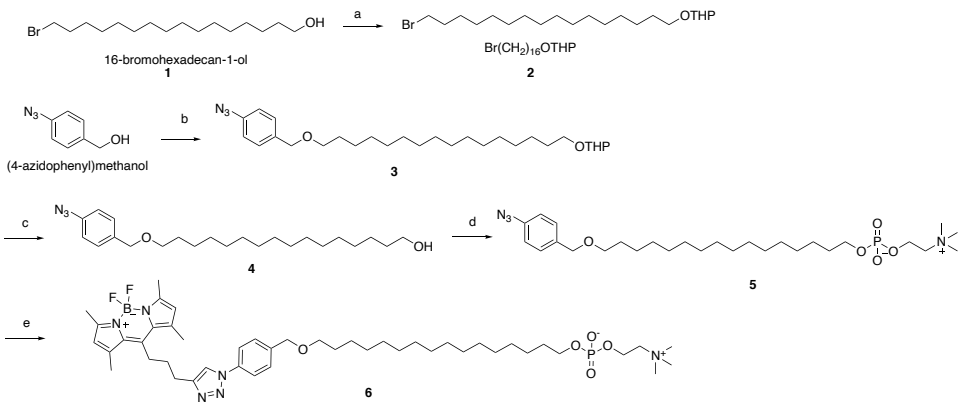

Scheme 1 *Reagents and conditions: (a) 3,4-dihydro-2H-pyran, PPTS, CH_2Cl_2, rt, 5h; (b) i) NaH, Dry THF, 0 °C, 30 mins; ii) Br(CH2)$_{16}$OTHP (**2**), TBAI, 0 °C, 5 h ; (c) PPTS, EtOH, 40 °C; (d) i) 2-chloro-1,3,2-dioxaphospholane 2-oxide, Et_3N, Benzene, rt, 24 h; ii) Me_3N, sealed bottle, 80 °C, 24 h (e) bodipy-alkyne, $CuSO_4$, NaASc, tBuOH: ACN: Water (1/1/1), 60 °C, 24 h.*

Following synthesis and purification, the accumulation of the fluorescently labelled phospholipid 6 was tested *in vitro*. Weichert *et.al* have reported the optimum localisation of CLR1501, a fluorescently labelled CLR1404 analog in different cancer cell lines (renal, colorectal, glioma, prostate), obtained after 24 h.[27] Therefore, three different cancer cell lines including cervical cancer (HeLa), prostate cancer (PC-3) and lung cancer (A459) as well as healthy primary dendritic cells (BMDC) were treated with bodipy-PLE **6** (5 or 10 μm final concentration). After 24 hours, confocal microscopy and flow cytometry results showed specific targeting of cancer cell lines and exceptionally high accumulation at PC-3 prostate cancer cells in plasma and organelle membranes (Figure 2).

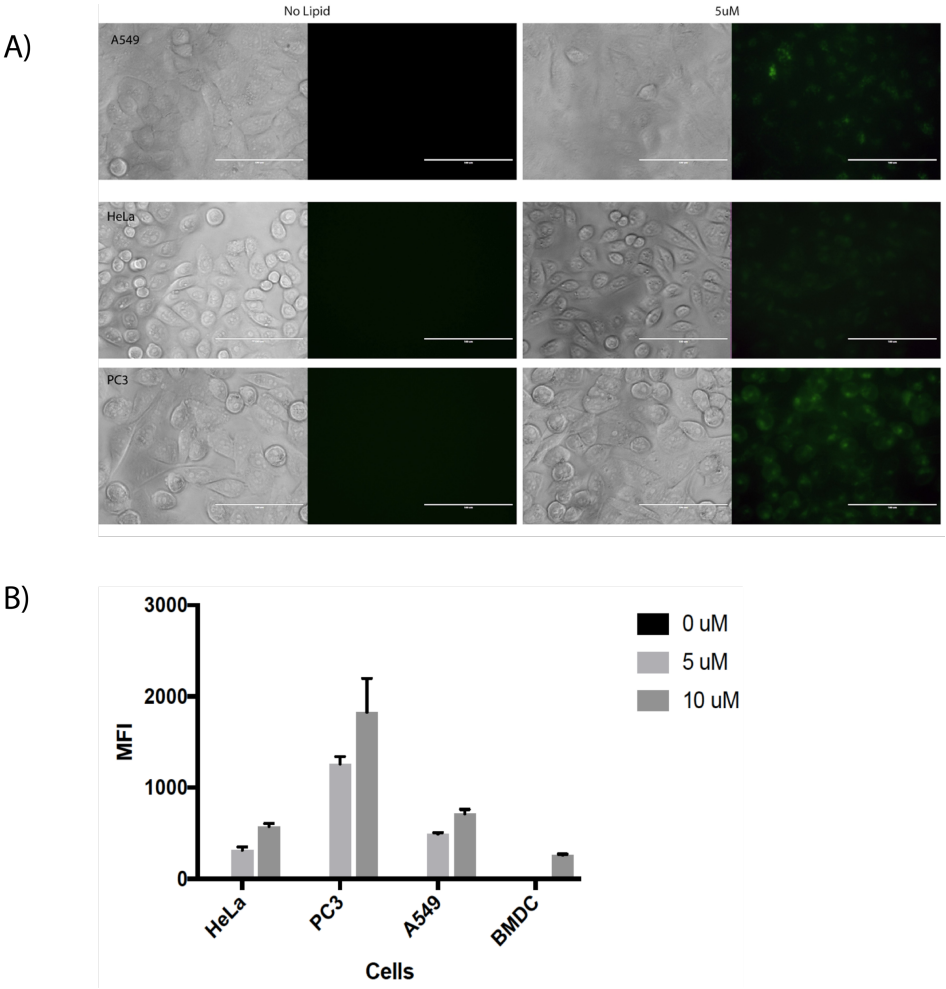

Figure 2 *Bodipy-labelled alkylphosphocholine 6 accumulates in specific cell line deposits. Lung (A549), cervix (HeLa), prostate (PC-3) human cell lines and bone marrow DC were treated with 5 or 10 µm final concentration of bodipy-PLE (**6**) at 37 °C. (A) Confocal microscopy images (fluorescence, bright field) of different cell lines. Scale bar: 10 µm. (B) Flow cytometry indicates a cell-line dependent docking. The assay was set up in triplicate. Data represented as median ± SD. Error bars SD.*

This cell-type dependent accumulation could be explained either due to different metabolism rates or the specific membrane affinity of the PLEs in cancer cells. Additionally, the accumulation of the similar structured ^{124}I-18-(p-iodophenyl)octadecyl phosphocholine (CLR1404) in mice bearing PC-3 prostate cancer xenografts was recently reported.[29] Next, the phospholipid ether analogue **6** was tested *in vivo* – for the first time – in a zebrafish model (*Danio rerio*). The zebrafish model has been studied as a powerful method for research in cancer biology.[39–43] A wide variety of cancers, for example, breast, colon and prostate cancer, has been studied using zebrafish embryo xenograft models.[39–43] An important advantage of zebrafish is their optical transparency. In this study a prostate cancer PC-3 model provided by L. Chen *et al*. was used.[39,42] This embryonic zebrafish cancer model represents a human tumour cell line that was used to determine the target (tumour cells) to nontarget ratio of PLE analogue **6**. These xenografts zebrafish were selected randomly. Based on prior studies, most of the zebrafish were expected to possess prostate tumour. The median age was two days old. All zebrafish were injected with **6** (1 nl) based on injected methods routinely employed at our laboratory.[41] Zebrafish tolerated this agent well without acute changes in activity or baseline weight. After one hour, zebrafish were prepared and imaged using confocal microscopy.

All zebrafish used contained a prostate cancer tumour. The bodipy-labelled alkylphosphocholine **6** is fluorescent in the FITC range (excitation 488 nm and emission 525 nm) and accumulation was quantified. At first, the circulation of the bodipy-lipid was tested in a wild-type zebrafish (Figure 3). The distribution of phospholipid ether analogue **6** in the wild-type fish (Figure 3) was examined and one hour post injection lipid **6** was cleared from circulation, most likely by

scavenger receptor stabilin-2. Besides, accumulation was observed in the sinusoidal endothelial cells (SECs) of zebrafish, which are homologous to mammalian liver endothelial cells.[41] Therefore, whether the phospholipid ether analogue **6** targets tumours was tested in the cancer model.[41]

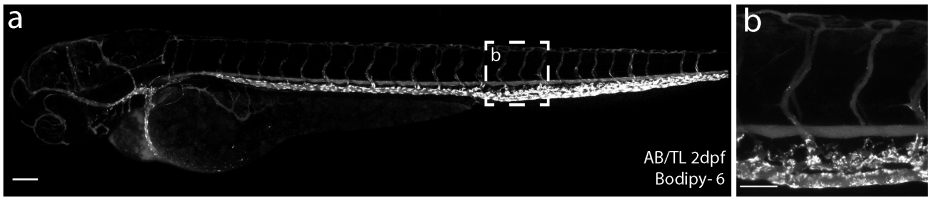

Figure 3 In vivo *distribution of bodipy-labelled alkylphosphocholine 6. (a) AB/TL (wild-type) zebrafish 2 days post fertilization (dpf) 1 h post-injection of the bodipy-labelled alkylphosphocholine* ***6****. Scale bar 100 um. (b) Caudal vein region showing uptake of bodipy-labelled alkylphosphocholine* ***6*** *by sinusoidal endothelial cells (SECs).* *Scale bar 50um.*

In a following experiment, alkylphosphocholine **6** was injected with prior administration of dextran sulphate (20 mg/ml) to competitively inhibit the uptake/clearance of stabilin-2-receptor(s).[41] As a result, the circulation lifetime of the alkylphosphocholine **6** was increased (Figure 4). In this study circulation of **6** was observed without significant accumulation in surrounding malignant or healthy tissues, therefore no co-localization between the prostate cancer cells PC-3 (magenta) and the lipid (green) was observed (Figure 4).

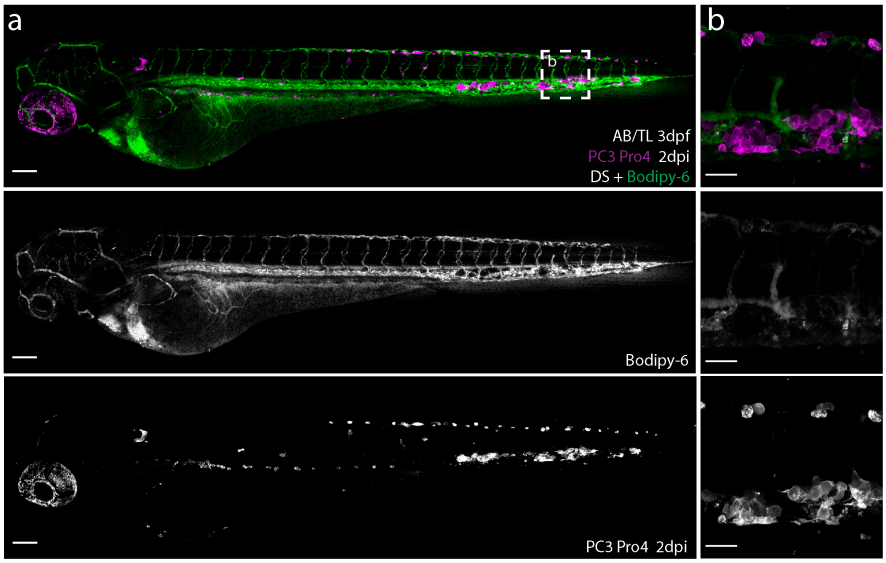

Figure 4 In vivo *distribution of bodipy-labelled alkylphosphocholine* ***6*** *in a xenograft zebrafish model after inhibition of SECs. (a) AB/TL zebrafish (3 dpf) 2 days post injected (dpi) with PC-3 Pro4 prostate malignant cells, 1 h after injection of dextran sulphate (DS 20mg/ml) followed by bodipy-labelled-****6****. Scale bar 100 um. (b) Caudal vein region showing the tumour cells (magenta) and the circulating bodipy-labelled* ***6*** *in green. Autofluorescence present in the eye region. Scale bar 50um.*

6.3 Conclusions

An initial study was performed to study whether a modified phospholipid ether analogue (**6**) is a potential tool for targeting prostate cancer membranes *in vitro* and in a zebrafish xenograft model *in vivo*. This phospholipid can be used with current fluorescence imaging devices to visualise prostate cancer *in vitro*. For *in vivo* studies, a zebrafish xenografts model was used. Moreover, zebrafish xenografts models are suitable for live cell imaging allowing the examination of circulation and distribution of labelled compounds in real time.[41–46] Nonetheless, zebrafish xenografts are considered complementary to murine models and have physiological and genetic similarities with humans.[41–46] A statistically significant accumulation of **6** was not noted in the invasive carcinomas as compared with the

healthy tissues of the zebrafish model. However, further studies should be made in different cancer models. Moreover, kinetic experiments and the use of agents that disrupt membranes could potentially shed some light on the docking mechanism of this ether phospholipid.

6.4 Experimental methods

Method and materials

All commercially available reagents and solvents were used without further purification. For "dry" solvents, solvents were dried accordingly before use over 4Å or 3Å molecular sieves. Column chromatography was performed using Merck silica gel 60 (0.040-0.063 mm). 1H and 13C NMR spectra were recorded using a Brüker AV-300 (300/75 MHz), AV- 400 (400/101 MHz), AV-500 (500/126 MHz) or AV-850 (850/214). Recorded data were interpreted and analysed using MestReNova 14 software. Chemical shifts are reported in ppm (δ). Synthesis of compounds was performed according to literature.[29]

2-((16-bromohexadecyl)oxy)tetrahydro-2Hpyran (**2**) was synthesised in full accordance with the reported procedure.[29] A solution of 16-bromohexadecan-1-ol (500 mg, 1,556 mmol) and 3,4-dihydro-2H-pyran (1,420 ml, 15,56 mmol) in dry dichloromethane (5 ml) containing pyridin-1-ium 4-methylbenzenesulfonate (39,1 mg, 0,156 mmol) was stirred at room temperature for five hours. Then, hexane was added and the solution washed with water, and dried over Na_2SO4. Flash chromatography in hexanes-ether (30:1) afforded the product 2-((16 bromohexadecyl) oxy) tetrahydro-2H-pyran (555 mg, 1,369 mmol, 88 % yield) as a white wax. 1H NMR (400 MHz,

Chloroform-d) δ 4.57 (t, J = 3.5 Hz, 1H), 3.87 (s, 1H), 3.73 (d, J = 9.4 Hz, 1H), 3.50 (dt, J = 10.6, 5.0 Hz, 1H), 3.40 (td, J = 6.9, 1.7 Hz, 3H), 1.85 (dd, J = 10.8, 4.4 Hz, 3H), 1.71 (d, J = 3.0 Hz, 1H), 1.56 (ddd, J = 22.0, 10.7, 6.7 Hz, 5H), 1.42 (t, J = 7.5 Hz, 2H), 1.34 – 1.24 (m, 23H).

2-((16-((4-azidobenzyl)oxy)hexadecyl)oxy)tetrahydro-2H-pyran (**3**) was synthesised in full accordance with the reported procedure.[29]. Sodium hydride (57,3 mg, 1,433 mmol) under argon at 0 °C was added to a solution of (4-azidophenyl) methanol (285 mg, 1,911 mmol) in dry THF (5 ml). Following stirring for 30 minutes, a solution of 2-((16-bromohexadecyl) oxy) tetrahydro-2H-pyran (387 mg, 0,955 mmol) in dry THF (5,00 ml) was cannulated, followed by the addition of tetrabutylammonium iodide (176 mg, 0,478 mmol). The reaction mixture was stirred for five hours, before saturated aqueous NH_4Cl solution was added. The mixture was then extracted with EtOAc and the combined layer was washed with water and brine, dried over Na_2SO4, filtered, and concentrated in vacuo. The residue was purified by flash chromatography (PS: Et2O 150:0, 150:1, 150:3) to afford 440 mg of yellow oil (a mixture of product and unreacted THP-alcohol).

16-((4-azidobenzyl)oxy)hexadecan-1-ol (**4**) was synthesised in full accordance with the reported procedure.[29] In a 25 mL round-bottomed flask was added 2-((16-((4azidobenzyl)oxy)hexadecyl)oxy) tetrahydro-2H-pyran (100 mg, 0,211 mmol) and pyridin-1-ium 4 methylbenzenesulfonate (5,31 mg, 0,021 mmol) in ethanol (5 ml) and the reaction mixture refluxed for 24 hours until TLC showed no starting material. The reaction was diluted with water (10,00 ml). The aq layer was extracted with ethyl acetate (10,00 ml) (3 x 10 mL). The organic layers were combined and washed with brine (10,00 ml) (2 x 10 mL). The organic layer was dried, filtrated and concentrated. Flash

chromatography in hexane-ethyl acetate (90:10-80:20) afforded the product (16-((4-azidobenzyl)oxy)hexadecan-1-ol (44 mg, 0,113 mmol, 53,5 % yield) as a white wax. 1H NMR (400 MHz, Chloroform-d) δ 7.26 (d, J = 8.4 Hz, 2H), 6.93 (d, J = 8.5 Hz, 2H), 4.39 (s, 2H), 3.57 (s, 2H), 3.38 (s, 2H), 1.98 (s, 1H), 1.52 (s, 4H), 1.25 – 1.13 (m, 24H).

16-((4-azidobenzyl)oxy)hexadecyl (2-(trimethylammonium)ethyl) phosphate) (**5**) was synthesised in full accordance with the reported procedure.[29] 2-chloro-1,3,2-dioxaphospholane 2-oxide (53,0 μl, 0,577 mmol) was added to the stirred solution of 16-((4-azidobenzyl)oxy)hexadecan-1-ol (125 mg, 0,321 mmol) in benzene (10 ml) containing triethylamine (67,0 μl, 0,480 mmol). This was followed by stirring overnight. The triethylamine hydrochloride salt was then filtrated, and the solvent evaporated in vacuo. The residue was transferred into a pressure bottle. A solution of 5 ml trimethylamine (3813 μl, 16,02 mmol)l in ethanol was added. The bottle was sealed and heated at 80 °C for 24 hours. The ethanol was then removed, and flash chromatography in DCM-methanol (gradient from 10:0 to 5:5) afforded the product (127 mg, 0,229 mmol, 71,5 % yield) as white solid. 1H NMR (300 MHz, Chloroform-d) δ 7.32 (d, J = 8.1 Hz, 2H), 7.04 – 6.94 (m, 2H), 4.45 (s, 2H), 4.35 (d, J = 10.1 Hz, 2H), 3.89 (s, 2H), 3.78 (d, J = 7.0 Hz, 2H), 3.19 – 3.01 (m, 2H), 2.85 (s, 2H), 2.05 (s, 9H), 1.37 – 1.23 (m, 26H).

16-((4-(4-(3-(5,5-difluoro-1,3,7,9-tetramethyl-5H-4l4,5l4-dipyrrolo[1,2-c:2',1'-f][1,3,2]diazaborinin-10-yl)propyl)-1H-1,2,3-triazol-1yl)benzyl)oxy)hexadecyl (2-(trimethylammonium)ethyl) phosphate (**6**). Fluorescent analogue bodipy-alkyne and 16-((4-azidobenzyl)oxy)hexadecyl (2-(trimethylammonium)ethyl)phosphate (40 mg, 0,072 mmol) were dissolved in a mixture of tBuOH: ACN:

water (1/1/1, 2mL), before an aqueous solution of sodium ascorbate (200 uL, 0.10 mM, 0.15 eq) and an aqueous solution of CuSO4 (200uL l 0.1 mM, 0.10 eq) were added. The reaction was mixture stirred at 60 °C for 12 hours, before being concentrated in vacuo. Flash chromatography in 5% MeOH in DCM afforded the compound as an orange solid (51 mg, 0,059 mmol, 82%). 1H NMR (850 MHz, Methanol-d4) δ 7.70 (d, J = 7.8 Hz, 1H), 7.44 (d, J = 7.9 Hz, 1H), 7.26 (d, J = 7.9 Hz, 1H), 6.94 (d, J = 7.9 Hz, 1H), 4.47 (s, 1H), 4.37 (s, 1H), 3.81 (dt, J = 37.0, 5.7 Hz, 4H), 3.60 (d, J = 5.4 Hz, 2H), 3.48 – 3.32 (m, 2H), 3.21 (t, J = 2.7 Hz, 19H), 3.03 – 2.97 (m, 1H), 2.78 (s, 1H), 2.33 (d, J = 11.5 Hz, 5H), 1.88 (p, J = 7.6 Hz, 1H), 1.66 (hept, J = 8.6, 8.2 Hz, 1H), 1.51 (dt, J = 19.9, 6.7 Hz, 5H), 1.24 – 1.13 (m, 27H).). 13C NMR (151 MHz, Methanol-d4) δ 183.54, 176.44, 170.78, 169.71, 166.27, 165.50, 161.19, 159.12, 156.57, 155.27, 154.10, 151.94, 151.20, 149.89, 148.50, 101.74, 101.49, 100.26, 100.00, 96.78, 95.55, 91.45, 78.47, 78.01, 77.87, 77.73, 77.59, 77.44, 77.30, 77.16, 60.95, 60.39, 60.35, 59.39, 59.38, 59.35, 59.31, 59.09, 59.06, 57.65, 55.85, 55.83, 55.50, 54.56, 45.10, 43.01.

Zebrafish intravenous injections

An embryonic zebrafish xenograft model containing prostate human cancer was developed and provided by L. Chen (Leiden University).[39] PC-3M-Pro4-mCherry prostate cancer cells (ATCC; RRID, CVCL_D579) were incubated at 33 °C for 24 hours prior to injection into zebrafish embryos. Zebrafish embryos at two days post-fertilisation (dpf) were immobilised using 1.2 mM tricaine methanesulfonate. 250 DiI-labelled prostate cancer cells in a volume of 5 nl were injected into the vein of Cuvier. Following injection, fish were carefully removed from the agarose/tricaine solution and transferred individually into 96-well plate imaging chambers created from 1% agarose using 3D-printed pins.[47]

The bodipy-labelled alkylphosphocholine **6** was injected into two- to three-day-old zebrafish embryos using a modified micrography protocol.[48] Embryos were anaesthetised in 0.01% tricaine and embedded in 0.4% agarose containing tricaine before injection. 1 nl of the lipid was injected in the common cardinal vein or duct of Cuvier.

Zebrafish imaging

Confocal z-stacks were captured on a Leica TCS SPE confocal microscope, using a 10× air objective (HCX PL FLUOTAR) or a 40× water-immersion objective (HCX APO L). Images were processed using the ImageJ.[49,50]

Confocal microscopy imaging

Cells were seeded in an 8-well slide (μ-Slide 8 well; Ibidi, Munich, Germany) at a density of $1*10^4$ cells per well in complete media without phenol red. Cells were treated with different concentrations (0, 5 and 10 μM) of bodipy-labelled alkylphosphocholine **6** overnight. Before confocal microscopy, cells were washed three times with PBS and fresh media. The fluorescent images were achieved using a Leica TCS SPE confocal laser scanning microscope (Leica Microsystems, Wetzlar, Germany) and analysed using the ImageJ software (National Institutes of Health, Bethesda, MD, USA). The wavelength settings for bodipy-488 Ex/Em: 488/510nm (Ex laser: 488 nm).

Mammalian cell culture

HeLa (cervix)[51], A549 (lung)[52,53] and PC-3 (prostate)[54] cells were cultivated in Dulbecco's Modified Eagle's Medium (DMEM), supplemented with 10% foetal calf serum, 2 mM L-glutamine, 1% penicillin and 1% streptomycin. Cells were cultured in an atmosphere of 7% CO_2 at 37 °C. The medium was refreshed every two days and cells passaged at 70%

confluence by treatment with trypsin-EDTA (0.05% trypsin). Cells were cultured in 25 cm^2 flasks and split at 70-80% confluence (three times per week). The flasks were incubated at 37 °C at 7.0% CO_2. The medium was refreshed three times a week. Cells used in all biological experiments were cultured for a maximum of 8 weeks. Adherent cell cultures with a maximum confluence of 70-80% were trypsinised and centrifuged [1.5 mins, 2000/4000rcf (live/fixed cells)], and the cells were re-suspended using fresh media. 10 μL of cell suspension and 10 μL of trypan blue were mixed and pipetted into a cell counting slide, and cells were counted using a BioRad TC10 automated cell counter. The cell suspension was diluted to the appropriate seeding density. BMDC cells were cultured in IMDM in non-adhesive petri dishes at 37 °C, 5% CO_2, under humidified air supplemented with 8% heat-inactivated foetal calf serum, 2 mM Glutamax, 20 µM β-Mercaptoethanol, 50 IU/mL penicillin and 50 μg/mL streptomycin, and recombinant GM-CSF (20 ng/mL, Peprotech, ref# 315-03) to a concentration of 0.5 x 106 cells/mL.

Flow cytometry

Cells were seeded in a 35 mm dish at a density of $5*10^5$ cells per well in complete media without phenol red. Cells were treated with different concentrations (0, 5 and 10 µM) of bodipy-labelled alkylphosphocholine **6** overnight. Before flow cytometry, cells were washed three times with PBS and fresh media. Flow cytometry assays were performed using the Merck Guava® easyCyte 12HT Benchtop Flow Cytometer, and all data were analysed using FlowJo™ v10.1 (FlowJo, LLC). Counting and characterization were performed by measuring 30,000 events in triplicate and concatenation of this data. For manual gating, the outermost ring of the dot plot was selected. Quadrants were manually selected to illustrate fluorescence plots. No compensation was required.

6.5 References

1 G. Ting, C.-H. Chang, H.-E. Wang and T.-W. Lee, *J. Biomed. Biotechnol.*, 2010, **2010**, 1–17.

2 A. Tedcastle, R. Cawood, Y. Di, K. D. Fisher and L. W. Seymour, *Drug Discov. Today*, 2012, **17**, 215–220.

3 M. Steiner and D. Neri, *Clin. Cancer Res.*, 2011, **17**, 6406–6416.

4 L. A. L. Fliervoet and E. Mastrobattista, *Adv. Drug Deliv. Rev.*, 2016, **106**, 63–72.

5 A. Fernandez-Fernandez, R. Manchanda and A. J. McGoron, *Appl. Biochem. Biotechnol.*, 2011, **165**, 1628–1651.

6 A. H. van der Luit, S. R. Vink, J. B. Klarenbeek, D. Perrissoud, E. Solary, M. Verheij and W. J. van Blitterswijk, *Mol. Cancer Ther.*, 2007, **6**, 2337–2345.

7 J. Wykosky, T. Fenton, F. Furnari and W. K. Cavenee, *Chin. J. Cancer*, 2011, **30**, 5–12.

8 H. Ayatollahi, M. R. Keramati, A. Shirdel, M. M. Kooshyar, M. Raiszadeh, S. Shakeri and M. H. Sadeghian, *Casp. J. Intern. Med.*, 2018, **9**, 65–70.

9 S. Bao, Q. Wu, R. E. McLendon, Y. Hao, Q. Shi, A. B. Hjelmeland, M. W. Dewhirst, D. D. Bigner and J. N. Rich, *Nature*, 2006, **444**, 756–760.

10 A. Singh and J. Settleman, *Oncogene*, 2010, **29**, 4741–4751.

11 J. H. Becker, Y. Gao, M. Soucheray, I. Pulido, E. Kikuchi, M. L. Rodríguez, R. Gandhi, A. Lafuente-Sanchis, M. Aupí, J. Alcácer Fernández-Coronado, P. Martín-Martorell, A. Cremades, J. M. Galbis-Caravajal, J. Alcácer, C. L. Christensen, P. Simms, A. Hess, H. Asahina, M. P. Kahle, F. Al-Shahrour, J. A. Borgia, A. Lahoz, A. Insa, O. Juan, P. A. Janne, K.-K. Wong, J. Carretero and T. Shimamura, *Cancer Res.*, 2019, **79**, 4439–4445.

12 H. Saleem, U. Kulsoom Abdul, A. Küçükosmanoglu, M. Houweling, F. M. G. Cornelissen, D. H. Heiland, M. E. Hegi, M. C. M. Kouwenhoven, D. Bailey, T. Würdinger and B. A. Westerman, *Drug Resist. Updat.*, 2019, **43**, 29–37.

13 P. A. Clark, M. Iida, D. M. Treisman, H. Kalluri, S. Ezhilan, M. Zorniak, D. L. Wheeler and J. S. Kuo, *Neoplasia*, 2012, **14**, 420–428.

14 C. Bellio, C. DiGloria, R. Foster, K. James, P. A. Konstantinopoulos, W. B. Growdon and B. R. Rueda, *Mol. Cancer Res.*, 2019, **17**, 431–445.

15 F. Snyder, M. L. Blank and H. P. Morris, *Biochim. Biophys. Acta*, 1969, **176**, 502–510.

16 F. Snyder and R. Wood, *Cancer Res.*, 1969, **29**, 251–257.

17 J. F. Soodsma, C. Piantadosi and F. Snyder, *Cancer Res.*, 1970, **30**, 309–311.

18 K. L. Meyer, S. W. Schwendner and R. E. Counsell, *J. Med. Chem.*, 1989, **32**, 2142–2147.

19 T. C. Lee, M. L. Blank, V. Fitzgerald and F. Snyder, *Arch. Biochem. Biophys.*, 1981, **208**, 353–357.

20 C. Gajate and F. Mollinedo, *Curr. Drug Metab.*, 2002, **3**, 491–525.

21 D. A. Deming, M. E. Maher, A. A. Leystra, J. P. Grudzinski, L. Clipson, D. M. Albrecht, M. K. Washington, K. A. Matkowskyj, L. T. Hall, S. J. Lubner, J. P. Weichert and R. B. Halberg, *PLoS One*, 2014, **9**, e109668.

22 R. Hernandez, K. L. Walker, J. J. Grudzinski, E. Aluicio-Sarduy, R. Patel, C. D. Zahm, A. N. Pinchuk, C. F. Massey, A. N. Bitton, R. J. Brown, P. M. Sondel, Z. S. Morris, J. W. Engle, C. M. Capitini and J. P. Weichert, *Commun. Biol.*, 2019, **2**, 1–10.

23 L. Kuerschner, D. Richter, H. K. Hannibal-Bach, A. Gaebler, A. Shevchenko, C. S. Ejsing and C. Thiele, *PLoS One*, 2012, **7**, e31342.

24 M. A. Rampy, R. S. Brown, A. N. Pinchuk, J. P. Weichert, R. W. Skinner, S. J. Fisher, R. L. Wahl, M. D. Gross, S. P. Ethier and R. E. Counsell, *J. Nucl. Med.*, 1996, **37**, 1540–1545.

25 M. Garland, J. J. Yim and M. Bogyo, *Cell Chem. Biol.*, 2016, **23**, 122–136.

26 M. A. Rampy, A. N. Pinchuk, J. P. Weichert, R. W. S. Skinner, S. J. Fisher, R. L. Wahl, M. D. Gross and R. E. Counsell, *J. Med. Chem.*, 1995, **38**, 3156–3162.

27 J. P. Weichert, P. A. Clark, I. K. Kandela, A. M. Vaccaro, W. Clarke, M. A. Longino, A. N. Pinchuk, M. Farhoud, K. I. Swanson, J. M. Floberg, J. Grudzinski, B. Titz, A. M. Traynor, H.-E. H.-E. Chen, L. T. Hall, C. J. Pazoles, P. J. Pickhardt and J. S. Kuo, *Sci. Transl. Med.*, 2014, **6**, 1–11.

28 J. M. Dean and I. J. Lodhi, *Protein Cell*, 2018, **9**, 196–206.

29 A. N. Pinchuk, M. A. Rampy, M. A. Longino, R. W. S. Skinner, M. D. Gross, J. P. Weichert and R. E. Counsell, *J. Med. Chem.*, 2006, **49**, 2155–2165.

30 J. Kruczek, M. Saunders, M. Khosla, Y. Tu and S. A. Pandit, *Biochim. Biophys. Acta - Biomembr.*, 2017, **1859**, 2297–2307.

31 S. P. Arlauckas, E. A. Browning, H. Poptani and E. J. Delikatny, *NMR Biomed.*, 2019, **32**, 1–24.

32 M. A. Rampy, A. N. Pinchuk, J. P. Weichert, R. W. S. Skinner, S. J. Fisher, R. L. Wahl, M. D. Gross and R. E. Counsell, *J. Med. Chem.*, 1995, **38**, 3156–3162.

33 K. P. Plotzke, M. A. Rampy, K. Meyer, M. Ruyan, S. J. Fisher, R. L. Wahl, R. W. Skinner, M. D. Gross and R. E. Counsell, *J. Nucl. Biol. Med.*, 1993, **37**, 264–272.

34 K. P. Plotzke, S. J. Fisher, R. L. Wahl, N. M. Olken, S. Skinner, M. D. Gross and R. E. Counsell, *J. Nucl. Med.*, 1993, **34**, 787–92.

35 P. A. Clark, A. J. Al-Ahmad, T. Qian, R. R. Zhang, H. K. Wilson, J. P. Weichert, S. P. Palecek, J. S. Kuo and E. V. Shusta, *Mol. Pharm.*, 2016, **13**, 3341–3349.

36 Y. C. Li, M. J. Park, S.-K. Ye, C.-W. Kim and Y.-N. Kim, *Am. J. Pathol.*, 2006, **168**, 1107–1118.

37 M. A. Rampy, T. S. Chou, A. N. Pinchuk, R. W. Skinner, M. D. Gross, S. Fisher, R. Wahl and R. E. Counsell, *Nucl. Med. Biol.*, 1995, **22**, 505–12.

38 R. Petracca, E. Romeo, M. P. Baggelaar, M. Artola, S. Pontis, S. Ponzano, H. S. Overkleeft, M. van der Stelt and D. Piomelli, *Chem. Commun.*, 2017, **53**, 11810–11813.

39 D. Hill, L. Chen, E. Snaar-Jagalska and B. Chaudhry, *F1000Research*, 2018, **7**, 1–16.

40 M. Hölttä-Vuori, R. L. Uronen, J. Repakova, E. Salonen, I. Vattulainen, P. Panula, Z. Li, R. Bittman and E. Ikonen, *Traffic*, 2008, **9**, 1839–1849.

41 F. Campbell, F. L. Bos, S. Sieber, G. Arias-Alpizar, B. E. Koch, J. Huwyler, A. Kros and J. Bussmann, *ACS Nano*, 2018, **12**, 2138–2150.

42 L. Chen, A. Groenewoud, C. Tulotta, E. Zoni, M. Kruithof-de Julio, G. van der Horst, G. van der Pluijm and B. Ewa Snaar-Jagalska, *Methods Cell Biol.*, 2017, **138**, 471–496.

43 S. A. Brittijn, S. J. Duivesteijn, M. Belmamoune, L. F. M. Bertens, W. Bitter, J. D. De Bruijn, D. L. Champagne, E. Cuppen, G. Flik, C. M. Vandenbroucke-Grauls, R. A. J. Janssen, I. M. L. De Jong, E. R. De Kloet, A. Kros, A. H. Meijer, J. R. Metz, A. M. Van Der Sar, M. J. M. Schaaf, S. Schulte-Merker, H. P. Spaink, P. P. Tak, F. J. Verbeek, M. J. Vervoordeldonk,

F. J. Vonk, F. Witte, H. Yuan and M. K. Richardson, *Int. J. Dev. Biol.*, 2009, **53**, 835–850.

44 F. Bootorabi, H. Manouchehri, R. Changizi, H. Barker, E. Palazzo, A. Saltari, M. Parikka, C. Pincelli and A. Aspatwar, *Int. J. Mol. Sci.*, 2017, 18, 1–15.

45 Y. M. Bradford, S. Toro, S. Ramachandran, L. Ruzicka, D. G. Howe, A. Eagle, P. Kalita, R. Martin, S. A. Taylor Moxon, K. Schaper and M. Westerfield, *ILAR J.*, 2017, **58**, 4–16.

46 C. Gutiérrez-Lovera, A. J. Vázquez-Ríos, J. Guerra-Varela, L. Sánchez and M. de la Fuente, *Genes (Basel).*, 2017, 8, 1–20.

47 J. N. Wittbrodt, U. Liebel and J. Gehrig, *BMC Biotechnol.*, 2014, **14**, 1–6.

48 B. M. Weinstein, D. L. Stemple, W. Driever and M. C. Fishman, *Nat. Med.*, 1995, **1**, 1143–1147.

49 J. Schindelin, I. Arganda-Carreras, E. Frise, V. Kaynig, M. Longair, T. Pietzsch, S. Preibisch, C. Rueden, S. Saalfeld, B Schmid, J.-Y. Tinevez, D. J. White, V. Hartenstein, K. Eliceiri, P. Tomancak and A. Cardona, *Nat. Methods*, 2012, **9**, 676–682.

50 C. A. Schneider, W. S. Rasband and K. W. Eliceiri, *Nat. Methods*, 2012, **9**, 671–675.

51 K. M. T. Gey G. O., Coffman W. D., *Cancer Res.*, 1952, **12**, 264–265.

52 M. Ferrari, *Nat. Rev. Cancer*, 2005, 5, 161–171.

53 Y. Matsumura and H. Maeda, *Cancer Res.*, 1986, **46**, 6387–6392.

54 M. E. Kaighn, K. S. Narayan, Y. Ohnuki, J. F. Lechner and L. W. Jones, *Invest. Urol.*, 1979, **17**, 16–23.

Summary

This thesis describes approaches to study cell-cell interactions, and explores the exchange of membrane components. In the first part, the rate of lipid exchange was studied, both during natural cell-cell contacts and during prolonged enforced contacts. In the second part, lipidated coiled-coil peptides were used to study the behaviour and potential fusogenic behaviour of these compounds on cell-wall-deficient L-forms of bacteria.

Chapter 2 provides a thorough review of membrane component exchange in cells as well as chemical approaches to enhance cell-cell contacts. Examples of mechanisms of intercellular transfer, biological effects of intercellular membrane component transfer and chemical strategies to enhance cell-cell contacts are described and their strengths and limitations discussed.

Components from the cell membrane can relocate between cells both *in vitro* and *in vivo*. This exchange of molecules plays an essential role in the regulation of cellular interactions and responses to the cell's environment. However, the exact mechanism and functional outcome of these exchanges remain to be elucidated in many cases.

The dynamics and kinetics of membrane compound exchange critically impacts many different biological activities in cells including cell-cell recognition, energy production, signal transduction and conversion, cell adhesion and foreign molecule identification. In **Chapter 3** an adaptable strategy utilising flow cytometry is presented, in which labelled membrane components are used to quantify their exchange rates between mammalian cells in co-culture, investigate the interactions between glycans and membrane lipids, and understand the exchange mechanism.

Using this approach, the rate of sterol exchange was shown to be highly cell-line dependent and the rate of sialic acid containing component exchange significantly slower than that of the sterolic lipids. Moreover, in a different experiment, a non-exchanging cell line was forced to exchange both sterols and carbohydrates when brought into prolonged close proximity using complementary coiled-coils.

Chapter 4 provides future implications for and directions towards quantification and identification of membrane lipid exchange between immune cells. It presents an adaptable strategy based on trogocytosis assays in which fluorescent and clickable lipids are used to determine the membrane component exchange between antigen-presenting and T cells in co-culture. A range of sterols and aliphatic acids were screened and their effect on trogocytosis was determined. It is generally accepted that cell membrane lipids might not be equally transferred during cell-cell contact. However, there does appear to be a specific rate of selectivity in the classes of cell membrane components transferred from antigen-presenting cells to T cells.

The precise mechanism of exchange between immune cells has yet to be discovered, but likely requires the formation of a synapse after direct contact between donor and acceptor cells. These findings might lead to alternative approaches of the exchange of membrane lipids in immune cells, focusing on manipulating either the targeting lipids for restricting undesirable processes, in order to understand immunotherapies

Chapter 5 deals – for the first time – with the surface modification of living cell-wall-deficient bacteria (i.e. L-form), as a first step towards bacterial fusion, using cell-compatible coiled-coil peptides. The L-forms used in this study have been generated from actinomycetes, by inhibiting crucial steps in the biosynthesis pathway of the cell wall. A supramolecular method was developed, based on a complementary

coiled-coil-forming peptide pair, to functionalise the membranes of L-form bacteria in an efficient manner. Besides L-form surface modification, this chapter also concerns the viability and liposome docking as well as potential membrane fusion.

Due to the small size of the bacteria as well as light scattering limitations, it was difficult to distinguish aggregated from fused cells. To overcome these limitations in the current experimental set-up, a double antibiotic selection assay could be designed to select for fused L-forms. Additionally, coiled-coil peptides with different PEG-spacers, peptide length or lipid moieties might have a positive effect in L-form bacterial fusion. It is expected that this method will be able to induce fusion between L-form cells of distinct species, whereby the chemistry of two living cells is merged into a new cell. Successful fusion and regeneration of different actinomycetes strains at high frequency would facilitate the future discovery of new antibiotics and microbial strain improvement.

Chapter 6 presents the synthesis of a fluorescent alkyl phospholipid ether analogue and an initial study into whether this modified phospholipid is a potential tool for targeting prostate cancer membranes.

This phospholipid is used with current fluorescence imaging devices to visualise prostate cancer *in vitro*. For *in vivo* studies, a zebrafish xenograft model was used. Zebrafish xenograft models are suitable for live-cell imaging, allowing the examination of circulation and distribution of labelled compounds in real time. However, further studies should be undertaken including different cancer models as well as kinetic experiments to shed light on the docking mechanism of this ether phospholipid analogue.

Summary in Greek

Περίληψη

Εξέχουσες προσεγγίσεις για τη μελέτη μεταξύ κυτταρικών αλληλεπιδράσεων

Η παρούσα διατριβή περιγράφει προσεγγίσεις πάνω στη μελέτη των αλληλεπιδράσεων κυττάρου-κυττάρου και διερευνά την ανταλλαγή των συστατικών της μεμβράνης.

Στο **πρώτο μέρος** μελετήθηκε ο ρυθμός της ανταλλαγής λιπιδίων, τόσο κατά τις φυσικές επαφές κυττάρου-κυττάρου όσο και κατά τη διάρκεια εκτεταμένων επιβαλλόμενων επαφών.

Στο **δεύτερο μέρος** χρησιμοποιήθηκαν λιπιδιωμένα σπειροειδή πεπτίδια για τη μελέτη της συμπεριφοράς και της πιθανής συντηκτικής συμπεριφοράς αυτών των ενώσεων σε βακτήρια με έλλειψη κυτταρικού τοιχώματος. Οι έρευνες χρησιμοποίησαν μεθόδους κυτταρομετρίας ροής και ομοεστιακής μικροσκοπίας για να μελετηθούν οι τροποποιήσεις της επιφάνειας των βακτηριδίων μορφής L και η πιθανή τήξη μεμβράνης.

Στο **Κεφάλαιο 2** περιγράφονται η λεπτομερής επισκόπηση της ανταλλαγής συστατικών της μεμβράνης στα κύτταρα, καθώς και οι χημικές προσεγγίσεις για την ενίσχυση των επαφών κυττάρου-κυττάρου. Περιγράφονται παραδείγματα μηχανισμών διακυτταρικής μεταφοράς, βιολογικών επιδράσεων μεταφοράς των διακυτταρικών συστατικών της μεμβράνης και χημικές στρατηγικές για την ενίσχυση επαφών κυττάρου-κυττάρου καθώς επίσης εξετάζονται οι αντοχές και οι περιορισμοί των.

Τα συστατικά από την κυτταρική μεμβράνη μπορούν να μεταφερθούν μεταξύ των κυττάρων τόσο *in vitro* όσο και *in vivo*. Αυτή η μοριακή ανταλλαγή παίζει σημαντικό ρόλο στη ρύθμιση των κυτταρικών αλληλεπιδράσεων και των αντιδράσεων στο περιβάλλον τους. Ωστόσο, σε πολλές περιπτώσεις, ο ακριβής μηχανισμός και το λειτουργικό αποτέλεσμα αυτών των ανταλλαγών παραμένει ακόμη να διασαφηνιστεί.

Η δυναμική και η κινητική της ανταλλαγής μεμβρανικών ενώσεων επηρεάζουν πολλές διαφορετικές βιολογικές δραστηριότητες σε κύτταρα, συμπεριλαμβανομένων της αναγνώρισης κυττάρου-κυττάρου, της παραγωγής ενέργειας, της μεταγωγής κυτταρικού σήματος, της προσκόλλησης των κυττάρων και της αναγνώρισης ξένων μορίων.

Στο **Κεφάλαιο 3** παρουσιάζεται μια προσαρμόσιμη στρατηγική που χρησιμοποιεί κυτταρομετρία ροής, στην οποία χρησιμοποιούνται επισημασμένα συστατικά μεμβράνης για να ποσοτικοποιήσουν τους ρυθμούς ανταλλαγής τους μεταξύ κυττάρων θηλαστικών σε συν-καλλιέργεια, να ανιχνεύσουν τις αλληλεπιδράσεις μεταξύ γλυκανών και λιπιδίων μεμβράνης και να κατανοήσουν τον μηχανισμό ανταλλαγής.

Χρησιμοποιώντας αυτή την προσέγγιση, η ταχύτητα της ανταλλαγής στερολών αποδείχθηκε ότι εξαρτάται σε μεγάλο βαθμό από τη γραμμή των κύτταρων και ο ρυθμός της ανταλλαγής συστατικών που περιέχουν σιαλικό οξύ είναι σημαντικά βραδύτερος από εκείνον των στερολικών λιπιδίων. Επιπρόσθετα, σε ένα διαφορετικό πείραμα μια μη-ανταλλασσόμενη κυτταρική γραμμή αναγκάστηκε να ανταλλάξει τόσο στερόλες όσο και υδατάνθρακες όταν εξαναγκάστηκε σε εκτεταμένη εγγύτητα χρησιμοποιώντας συμπληρωματικά σπειροειδή πεπτίδια.

Το **Κεφάλαιο 4** περιγράφει μελλοντικές επιπλοκές και κατευθύνσεις σχετικά με την ποσοτικοποίηση και την ταυτοποίηση της ανταλλαγής μεμβρανικών λιπιδίων μεταξύ ανοσοκυττάρων. Παρουσιάζει μια προσαρμόσιμη στρατηγική που βασίζεται σε δοκιμασίες τρογοκυττάρωσης στις οποίες χρησιμοποιούνται φθορίζοντα και κλικ- λιπίδια για την πρόκληση της ανταλλαγής των ενώσεων της μεμβράνης μεταξύ των αντιγονοπαρουσιαστικών και των Τ κυττάρων σε συν-καλλιέργεια. Μια σειρά στερολών και αλειφατικών οξέων υποβλήθηκαν σε διαλογή και προκλήθηκε η επίδρασή τους στην τρογοκυττάρωση. Είναι γενικά αποδεκτό ότι τα λιπίδια της κυτταρικής μεμβράνης ενδέχεται να μην μεταφέρονται ισομερώς κατά τη διάρκεια της επαφής κυττάρου-κυττάρου. Ωστόσο, φαίνεται πως υπάρχει ένας συγκεκριμένος ρυθμός επιλεκτικότητας στις κατηγορίες συστατικών κυτταρικής μεμβράνης τα οποία μεταφέρονται από κύτταρα που περιέχουν αντιγόνο σε κύτταρα Τ.

Ο ακριβής μηχανισμός ανταλλαγής μεταξύ ανοσοκυττάρων δεν έχει ακόμη ανακαλυφθεί, αλλά πιθανόν απαιτεί τον σχηματισμό μιας συνάψεως μετά από άμεση επαφή μεταξύ των κυττάρων δότη και δέκτη. Αυτά τα ευρήματα θα μπορούσαν να οδηγήσουν σε εναλλακτικές προσεγγίσεις στην ανταλλαγή λιπιδίων μεμβράνης στα ανοσοκύτταρα, εστιάζοντας στον χειρισμό είτε των στοχευμένων λιπιδίων για τον περιορισμό των ανεπιθύμητων διεργασιών είτε των επιδρώντων κυττάρων, προκειμένου να συμβιβαστούν και να κατανοηθούν οι ανοσοθεραπείες

Το **Κεφάλαιο 5** ασχολείται - για πρώτη φορά - με την τροποποίηση της επιφάνειας των ζωντανών βακτηρίων τα οποία έχουν ανεπαρκή κυτταρικά τοιχώματα (π.χ L-μορφής), ως ένα πρώτο βήμα για τη σύντηξη των βακτηρίων, χρησιμοποιώντας σπειροειδή πεπτίδια συμβατά με τα κύτταρα. Τα βακτήρια L-μορφής που χρησιμοποιούνται σε αυτήν τη μελέτη έχουν αναπαραχθεί από

ακτινομύκητα, αναστέλλοντας σημαντικά στάδια βιοσύνθεσης του κυτταρικού τοιχώματος. Αναπτύχθηκε μια υπερμοριακή μέθοδος, βασισμένη σε ένα ισορροπημένο ζεύγος πεπτιδίων που σχηματίζει περιστρεφόμενη σπείρα, προκειμένου να λειτουργήσει γρήγορα και αποτελεσματικά στην τροποποίηση των μεμβρανών των βακτηρίων μορφής L. Επίσης, αυτό το κεφάλαιο περιγράφει, εκτός από την τροποποίηση της μεμβράνης των βακτηρίων μορφής L, τη βιωσιμότητα των βακτηρίων, την λιποσωματική σύνδεση καθώς και την πιθανή σύντηξη της μεμβράνης.

Λόγω του μικρού μεγέθους των βακτηριδίων καθώς και των περιορισμών σκέδασης του φωτός, ήταν δύσκολο να γίνει διάκριση μεταξύ συσσωματωμένων και συντηγμένων κυττάρων. Για να ξεπεραστούν αυτοί οι περιορισμοί στην τρέχουσα πειραματική εγκατάσταση, θα μπορούσε να σχεδιαστεί ένας διπλός προσδιορισμός επιλογής αντιβιοτικού για τα συντηγμένα L-μορφής βακτήρια. Επιπροσθέτως, σπειροειδή πεπτίδια με διαφορετικούς διαχωριστές πολυαιθυλενογλυκόλης, διαφορετικά μήκη πεπτιδίων ή τμήματα λιπιδίων μπορεί να έχουν θετική επίδραση στη σύντηξη των L βακτηρίων . Αναμένεται ότι αυτή η μέθοδος θα είναι ικανή να διεγείρει τη σύντηξη μεταξύ L-κυττάρων ή διαφορετικών ειδών, όπου δύο κύτταρα να συγχωνεύονται σε ένα νέο κύτταρο. Η επιτυχής σύντηξη και αναγέννηση διαφορετικών στελεχών ακτινομύκητων με υψηλή συχνότητα θα διευκόλυνε την ανακάλυψη νέων αντιβιοτικών και τη βελτίωση των μικροβιακών στελεχών.

Το **Κεφάλαιο 6** παρουσιάζει τη σύνθεση ενός φθορίζοντος αλκυλο φωσφολιπιδικού αιθερικού αναλόγου και μια αρχική μελέτη σχετικά με το κατά πόσο αυτό το τροποποιημένο φωσφολιπίδιο είναι ένα πιθανό εργαλείο για τη στόχευση μεμβρανών καρκίνου του προστάτη.

Αυτό το φωσφολιπίδιο χρησιμοποιείται με τις τρέχουσες συσκευές απεικόνισης φθορισμού για την απεικόνιση του καρκίνου του προστάτη *in vitro*. Για *in vivo* μελέτες, χρησιμοποιήθηκε μοντέλο ξενομοσχευμάτων σε ζεβρόψαρα. Τα μοντέλα ξενομοσχευμάτων σε ζεβρόψαρα είναι κατάλληλα για απεικόνιση ζωντανών κυττάρων επιτρέποντας την εξέταση σε πραγματικό χρόνο της κυκλοφορίας και της κατανομής των σημασμένων ενώσεων. Ωστόσο, θα πρέπει να πραγματοποιηθούν περαιτέρω μελέτες, συμπεριλαμβανομένων διαφορετικών μοντέλων καρκίνου, καθώς και κινητικών πειραμάτων.

List of publications

1. *A flow cytometry assay to quantify intercellular exchange of membrane components.*
   Poulcharidis D, Belfor K, Kros A, van Kasteren SI**.**
   Chem Sci. **2017** Aug 1;8(8):5585-5590, DOI: 10.1039/c7sc00260b. Epub 2017 May 24.

2. *Quantification of Bioorthogonal Stability in Immune Phagocytes Using Flow Cytometry Reveals Rapid Degradation of Strained Alkynes.*
   Bakkum T, van Leeuwen T, Sarris AJC, van Elsland DM, **Poulcharidis D**, Overkleeft HS, van Kasteren SI. *ACS Chem Biol.* **2018** May 18;13(5):1173-1179. DOI: 10.1021/acschembio.8b00355. Epub 2018 Apr 30.

3. *Spatiotemporal Control of Doxorubicin Delivery from "Stealth-Like" Prodrug Micelles.*
   Kong L, **Poulcharidis D**, Schneider GF, Campbell F, Kros A. *Int J Mol Sci.* **2017** Sep 22;18(10). pii: E2033. DOI: 10.3390/ijms18102033.

Curriculum vitae

Dimitris Poulcharidis was born on the 7th of June 1989 in Thessaloniki, Greece. After taking the National University Entrance Examination in 2008, he entered the school of Chemistry at the Aristotle University of Thessaloniki. In 2012 he obtained his bachelor's degree in Chemistry first of his class, specialising in organic chemistry, biochemistry/biotechnology and food chemistry. Thereafter, he moved to the University of Leeds for his master's study in the field of chemical biology and drug design. In 2013, he obtained his master's degree with merit, with the thesis 'Identifying the molecular targets of TRPC inhibitors' under the supervision of Dr. Robin Bon.

From September 2013 to October 2017, Dimitris studied in the groups of Bio-organic Synthesis and Supramolecular & Biomaterials Chemistry in Leiden University as a PhD student under the supervision of Prof. Dr. Alexander Kros and Dr. Sander I. van Kasteren. The author conducted research at the interface of chemical biology and supramolecular chemistry. During his PhD study, he developed an assay to study cell-cell interactions and studied the supramolecular modification of L-form bacteria. Part of the research described in his thesis was conducted at the Max Planck Institute (Freiburg) in the department of Immunobiology and Epigenetics of Prof. Dr. Erika L. Pearce. He presented his work at several (inter)national conferences, including the Chemical Biology Symposium (London, United Kingdom, 2017) and CHAINS (Veldhoven, the Netherlands, 2017).

In November 2017 he joined Ortec Finance as a business consultant. Since October 2018 he has been working as a consultant for Deloitte.